

PRINCETON SOIL ENGINEERING

RESEARCH SERIES No. 3



THE DETERMINATION OF SOIL PROPERTIES  
IN SITU BY AN IMPACT PENETROMETER

by Werner E. Schmid

DEPARTMENT OF CIVIL ENGINEERING  
SCHOOL OF ENGINEERING AND APPLIED SCIENCE  
PRINCETON UNIVERSITY, PRINCETON, NEW JERSEY

CONTRACT NO. AF19(628) - 2427

PROJECT NO. 7628

TASK NO. 76280

SCIENTIFIC REPORT NO. 1

JANUARY 1966

*Code 1*

CLEARINGHOUSE FOR FEDERAL SCIENTIFIC AND TECHNICAL INFORMATION			
Hardcopy	Microfiche		
\$5.00	\$1.00	197	as
ARCHIVE COPY			

D D C  
RECEIVED  
JUN 21 1966  
B

Prepared  
for

AIR FORCE CAMBRIDGE RESEARCH LABORATORIES  
OFFICE OF AEROSPACE RESEARCH  
UNITED STATES AIR FORCE  
BEDFORD, MASSACHUSETTS

AD 634043

AD 634043

PRINCETON SOIL ENGINEERING  
RESEARCH SERIES NO. 3

The Determination of Soil Properties  
in Situ by an Impact Penetrometer

by Werner E. Schmid

Department of Civil Engineering  
School of Engineering and Applied Science  
Princeton University, Princeton, New Jersey

Contract No. AF 19 (628) - 2427

Project No. 7628

Task No. 76280

Scientific Report No. 1

January 1966

Prepared for

AIR FORCE CAMBRIDGE RESEARCH LABORATORIES  
OFFICE OF AEROSPACE RESEARCH  
UNITED STATES AIR FORCE  
BEDFORD, MASSACHUSETTS

DISTRIBUTION OF THIS  
DOCUMENT IS UNLIMITED

## Abstract

This report presents parts of the scientific investigations carried out under a task program related to the determination and assessment of surface dynamic soil properties by laboratory instrumentation. It first reviews the historical development of the hardness-penetrometer concept and presents a pilot model for a new aerial penetrometer. Basic theoretical considerations are then advanced regarding the stress-strain relationships in axial symmetry and the dynamic loads associated with a drop-impact penetrometer. The existing theory of elasticity solutions are then reviewed and the solutions for a sphere impacting on an ideally plastic and on an elasto-plastic semi-infinite solid are presented. The Hertz solution of an elastic sphere impacting on an elastic half-space is modified by using the elastic-viscoelastic analogy to find a solution for a sphere dropping onto a four parameter viscoelastic half-space.

The problem of energy transfer during impact by vibrations is discussed shortly. The data for fifteen test series carried out with the pilot model penetrometer on natural soils and on some artificial materials are presented and evaluated. It is concluded that the principle of the drop impact-penetrometer is applicable in experiments for assessing the mechanical properties of a natural soil surface. The proposed

modification of a prototype penetrometer should also increase its capability and reliability as a remote sensor for operational applications. The instrument, as envisaged, will not only permit determination of mechanical surface properties on terrestrial soils but should also be extremely useful for the exploration, by remote techniques, of lunar and other extraterrestrial surfaces.

Table of Contents

	<u>Page</u>
I. Introduction and Definition of Problem - - - - -	1
II. Historical Development - - - - -	5
Principle of Penetrometer Methods - - - - -	6
Hardness Measurements - - - - -	7
Hardness Measurement in Soil Mechanics - - - - -	11
1. The Steel Ball Test by Tsytoovich - - - - -	12
2. The Swedish Cone Test - - - - -	14
3. The Proctor Plasticity Needle - - - - -	15
4. The California Bearing Ratio Test (CBR) - - - - -	16
5. The Ram Penetrometer - - - - -	18
6. The U.S. Army Corps of Engineers Cone Penetrometer - - - - -	19
7. The Aerial Penetrometer - - - - -	20
The Princeton Impact Penetrometer - - - - -	22
III. The Drop Capsule Penetrometer - - - - -	24
1. Test Principle - - - - -	24
2. Instrument Capsule - - - - -	27
IV. Basic Theoretical Considerations - - - - -	32
1. States of Stress and Deformation with Axial Symmetry - - - - -	32
2. Surface Stresses on the Elastic Half-Space - - - - -	36
3. The Stress Distribution after Hertz - - - - -	41
4. Stresses and Deformations with Axial Symmetry in the Plastic Range - - - - -	43
V. Dynamics of Load Application for the Drop-Impact Penetrometer - - - - -	49
1. Stereoc-Mechanical Impact - - - - -	49
2. Ideally Elastic Impact (Hertz Theory) - - - - -	53
3. Impact on the Plastic Half-Space - - - - -	58
4. Elasto-Plastic Impact - - - - -	62
VI. Impact of a Sphere on a Viscoelastic Half-Space - - - - -	65
1. Principles of Rheology - - - - -	65
2. Solutions by the Elastic-Viscoelastic Analogy - - - - -	69
3. Impact of a Sphere on a Four-Parameter Half-Space - - - - -	71

	<u>Page</u>
VII. Vibrations of the Half-Space due to Impact - - - -	77
1. Basic Equations - - - - -	77
2. Propagation Velocities - - - - -	80
3. Vibrations due to a Point Load - - - - -	81
4. Damping, Dispersion and Distortion - - - - -	86
5. Group Velocity and Phase Velocity - - - - -	89
6. Impact with High (Ballistic) Velocities - - - -	92
VIII. Description of Test Series - - - - -	93
IX. Evaluation of Test Results - - - - -	99
1. General Discussion of Test Data - - - - -	99
2. Impact Velocity $V(\circ)$ - - - - -	102
3. Strength Properties of Target Materials - - - -	107
4. Wave Propagation Velocities - - - - -	115
5. Evaluation of Vibration Energy - - - - -	118
X. Summary and Conclusions - - - - -	121
Acknowledgment - - - - -	123
References - - - - -	124
Figures 1-27	
Appendix A	A-1 - A-32
Appendix B	B-1 - B-12

## I. Introduction and Definition of Problem

The determination of soil properties is one of the most important tasks of modern soil mechanics. For its successful solution one needs, first of all, a clear and rigorous definition and a thorough understanding of these properties. Next, it will be necessary to develop suitable methods and instruments for determining these properties and, finally, one will have to evaluate, interpret and apply the data that are obtained.

Historical progress in this field followed a more or less logical development. It began by measuring properties of disturbed soils in the laboratory (e.g. Atterberg consistency limits, friction angle in the shear box). But one soon recognized that certain soil properties were strongly influenced and adumbrated by the disturbance that is unavoidable in the normal soil sampling process. For this reason the measurement of properties in the laboratory on "undisturbed samples" found wider and wider acceptance (e.g. the consolidation test and the triaxial test). It is obvious that the term "undisturbed" must be understood relatively and merely designates generally accepted standard methods by which soils are being sampled to achieve reasonably undisturbed samples without undue expense. The actual method used for sampling and its applicability for the soil being sampled becomes very important.

Even these methods, however, do not yet constitute an ideal solution because first, a truly undisturbed sample cannot be obtained - even with the greatest care, and secondly, the transport of the sample to the laboratory, the assembly of the sample in the testing apparatus, the test itself as well as its evaluation always require a large amount of time and labor. Moreover, according to Burmister (1957) the soil properties depend also on the soil environment, particularly the system of stresses that exists "in situ" in the soil and this author is in complete agreement with this hypothesis.

For this reason it would be advantageous to develop methods that permit the measurement of soil properties "in situ," i.e., in place. The advantages of such methods could be listed as follows:

- 1) There is no need for sampling and, therefore, any disturbance during the sampling process, the transport of the sample and its assembly in the apparatus is eliminated.
- 2) The time lag between sampling and evaluation of the test results is eliminated.
- 3) The measured properties are available immediately on location.

For these reasons developments of new measuring techniques have been directed increasingly towards instruments and methods that measure soil properties "in situ." Among these instruments and methods are:

- a) The standard penetration test
- b) The shear vane
- c) The Menard-pressuremeter
- d) The static penetrometer (e.g. CBR)
- e) The drop penetrometer (e.g. aerial penetrometer)

The methods a), b) and c) are mainly concerned to measure the shearing strength of a soil in a bore hole whereas methods d) and e) have the purpose to determine the properties of the soil surface. The mechanical properties of the soil surface are of importance in the design of highway or airport pavements, or when it is necessary to judge the trafficability of a surface by a tractor, by construction equipment or by a military vehicle.

The latter problem is a tactical-logistical one of great military significance which normally is made more difficult still because often the soil surface to be judged is not accessible. From a purely scientific point of view this problem is of great interest also. For example, the design of the lunar exploratory module (LEM) being developed at the moment by the Grumman Aircraft Company requires a reliable indication of the surface properties of the moon.

In the fall of 1962 the author initiated a research project sponsored by the Terrestrial Sciences Laboratory, Air Force Cambridge Research Laboratories (OAR), Hanscom Field, Bedford, Massachusetts. A part of this project was to

investigate the principles which would permit the measurement of mechanical properties of a soil surface by remote methods, i.e. without requiring the physical presence of an operator at the surface. The aim was to determine the properties of a natural soil surface that might control modern aerospace operations on natural terrain such as landing and take-off of aircraft and recovery of space vehicles.

The problem then was to develop a method for measuring those properties of a soil surface which govern the operational possibilities of natural terrain sites for modern military aircraft and other aerospace vehicles. The problem was not entirely new.

## II. Historical Development

During 1950-1953 an aerial penetrometer was developed at New York University (Fig. 1; see also Molineaux, 1955, and Anonymous, 1953) that could be dropped from an airplane and, upon impact, would release signals in the form of flares, colored vanes or flags that would indicate the severity of the impact. The signals could be observed from the plane and would indicate the hardness of the impacted surface.

In its practical application, this aerial penetrometer had several flaws. One of the principal difficulties was that it required an impact with zero horizontal velocity component together with a perfect vertical alignment of the penetrometer axis.

In the normal operational case this was to be achieved by flying the airplane at a constant speed of 180 knots and ejecting the penetrometer rearwards and slightly downwards with a speed such that the net difference between the two horizontal velocity components would be zero. Because of wind and small variations in the forward speed of an airplane it is most difficult to achieve exactly this condition of  $V_h = 0$ . Even more important, if the longitudinal axis of this penetrometer is just slightly off the vertical at the instant of impact, part of its energy will be converted into a moment which tends to throw the penetrometer onto the surface broadside and thus a good part of the impact resistance will not

be transmitted through the point of the penetrometer. It was found rather difficult to stabilize the penetrometer aerodynamically in such a fashion that it would always hit vertically. Furthermore, this instrument, as developed, cannot make an absolute measurement. Rather, before being dropped an estimate must be made with respect to the expected impact resistance and the observed signal then merely indicates whether the actual resistance encountered was larger or smaller than the one previously estimated.

#### Principle of Penetrometer Methods

The development of the aerial penetrometer just discussed was not at all without precedent but followed in principle the "cone penetrometer" developed by the Waterways Experiment Station of the Corps of Engineers, U.S. Army, in Vicksburg, Mississippi (Fig. 2)(WES 1957) which is used to determine the trafficability of a natural soil surface.

This instrument is a rod with a standard conical tip at the lower end. This tip is pushed vertically into the soil surface by a force on the handle at the upper end and this force is measured by a dial through a proving ring.

The instrument and its operation is described in a Waterways Experiment Station manual and is discussed by Hechtl (1964) in the context of trafficability evaluation. Although the Vicksburg cone penetrometer is an original instrumentation

development, it is based on the same principle as other penetrometers. In the final analysis all penetrometer methods have their origin in the principles of hardness measurement of materials which can, according to Williams (1942), be traced back to an article by Reaumur in 1722. The more modern investigations, however, most probably were initiated as a consequence of the solution of the contact stresses of two elastic spheres by Hertz.

The idea to use the results of this solution for the determination of material properties was obvious and led to the various methods of measuring the surface hardness of a material.

#### Hardness Measurements

In measuring the well-known Brinell hardness, e.g., a steel sphere is pressed by a force  $P$  into the surface to be examined and the diameter of the resulting permanent deformation is measured. The Brinell hardness is then given by the ratio of the force  $P$  to the curved contact area of the deformation:

$$H_B = \frac{P}{\frac{\pi D}{2} (D - \sqrt{D^2 - d^2})} \quad (1)$$

where  $D$  is the diameter of the sphere and  $d$  the diameter of the permanent deformation.

In most cases the Brinell hardness is not a constant but a function of the load  $P$  and the diameter of the sphere. According to general physical principles one would expect that for geometrically similar deformations, the Brinell hardness number is constant and independent of their absolute magnitude. This was indeed found to be so.

If, for example, a sphere of diameter  $D_1$  causes a deformation  $d_1$  and a sphere of diameter  $D_2$  causes a deformation  $d_2$  then the Brinell hardness number will be the same provided that the deformations are geometrically similar, i.e. the central angle  $\phi$  (Fig. 3) is the same. This is the case if

$$\frac{d_1}{D_1} = \frac{d_2}{D_2}$$

According to Tabor (1950) the Brinell hardness is not a very satisfactory quantity because the ratio of the load  $P$  to the contact area does not give the average pressure over the contact surface.

If, on the other hand, we use the vertical projection of the contact pressure  $p$  only and apply the equilibrium condition we obtain:

$$P = 2\pi \int_0^a p \times dx = \pi p a^2$$

where  $a$  is the radius of the circular indentation at the surface and the projected pressure  $p$  is given by  $p = \frac{P}{\pi a^2}$ . This measure of hardness, namely:

$$H_M = \frac{4P}{\pi d^2} \quad (2)$$

was first proposed by Meyer and is generally known as Meyer hardness. Meyer also found an empirical relation between the load  $P$  and the diameter of the indentation as:

$$P = kd^n$$

where  $k$  and  $n$  are constants of the material. The exponent  $n$  usually being larger than 2.0 lying in the range  $2.0 < n < 2.5$ . If the load is applied by spheres of different diameters then the values  $k$  and  $n$  change also and we get

$$P = k_1 d_1^{n_1} = k_2 d_2^{n_2} = k_3 d_3^{n_3} = \dots \quad (3)$$

For a large number of tests Meyer found that the exponent  $n$  is independent of  $D$  but that  $k$  decreases with increasing sphere diameters such that

$$A = k_1 D_1^{n-2} = k_2 D_2^{n-2} = k_3 D_3^{n-2} = \dots \quad (4)$$

where  $A$  remains constant. Therefore we may write:

$$P = \frac{A}{D_1^{n-2}} d_1^n = \frac{A}{D_2^{n-2}} d_2^n = \frac{A}{D_3^{n-2}} d_3^n = \dots \quad (5)$$

from which follows that:

$$\frac{P}{d^2} = A \left(\frac{d}{D}\right)^{n-2} \quad (6a)$$

and

$$\frac{P}{D^2} = A \left(\frac{d}{D}\right)^n \quad (6b)$$

Equation (6a) states that for geometrically similar deformations ( $\phi$  constant) the hardness number must be constant

whereas (6b) indicates that for geometrically similar deformations the ratio  $\frac{P}{D^2}$  must be constant.

That is to say a static load of 3000 kg applied by a sphere of 10 mm causes a plastic indentation which is geometrically similar to that caused by a load of 750 kg applied through a sphere with  $D = 5$  mm or by a load of 30 kg with  $D = 1$  mm. In all these cases the hardness number must remain the same.

For the general case one may write:

$$\frac{P}{d^2} = F\left(\frac{d}{D}\right) \quad (5c)$$

where  $F$  is a suitable function expressing the similarity principle.

In order to avoid the problem of the different geometry for different penetration ratios  $\frac{d}{D}$  which presents itself when measuring the Brinell or Meyer hardness, P. Ludwik (1908) chose a conical indenter with an angle of  $90^\circ$  instead of a sphere. Thereby the penetration  $t$  is equal to the indentation radius  $\frac{d}{2}$ . The contact area is then given by  $A = \frac{\pi d^2}{4 \sin 45^\circ}$  and the Ludwik hardness number can be computed from:

$$H_L = \frac{4 P \sin 45^\circ}{\pi d^2} = 0.898 \frac{P}{d^2} \quad (7)$$

For a homogeneous material the hardness number of Ludwik is thus independent of the penetration ratio and geometric similarity obtains for any load  $P$  or any penetration depth  $t$ .

Ludwik used this hardness number mainly to investigate the internal friction of metals (Ludwik, 1916).

As a consequence of these investigations by Brinell, Meyer and Ludwik, a large number of methods for measuring hardness were developed which in detail vary mainly in the absolute magnitude and shape of the indenters and in the form in which the loads are applied (statically or dynamically). Here shall be mentioned only the methods of Vickers and Rockwell. For dynamic load application a series of methods were developed, e.g. the Shore scleroscope and the pendulum by Herbert and that by Kuznetsov. A detailed description of all these methods is given by Williams (1942).

We are particularly interested here in to what degree the principles of hardness measurement have been applied in the field of soil mechanics.

#### Hardness Measurement in Soil Mechanics

A surprising number of soil mechanics tests can be traced back either directly or at least indirectly to the principles of hardness measurements just discussed. For example, as direct descendants we may consider: the steel ball test by Tsytoovich, the Swedish cone test, the Proctor plasticity needle, the California bearing ratio test, the ram penetrometer for measuring the hardness of a snow surface developed by CRREL (Cold Regions Research & Engineering Laboratory) of

the U.S. Army, the Waterways Experiment Station cone penetrometer of the U.S. Army Corps of Engineers and the aerial penetrometer of the U.S. Air Force. As soil mechanics tests which have their origin at least indirectly in the principles of hardness measurement may be considered the U.S. standard penetrometer and the penetrometers used in the various countries, e.g. in Denmark, Holland, Sweden, Switzerland and Germany. The various penetrometer points are shown for example by Terzaghi and Peck (1948) and the experiences made with these various penetrometers are described in the literature. These latter methods have the purpose of measuring the shear or penetration resistance of a soil at some depth either in a bore hole or after the penetrometer has been pushed into the ground already some depth.

These methods are, therefore, of little interest here.

We are mainly interested in those methods and tests which we classified as direct descendants of the hardness measurement principles. In the following we shall give a short description and discussion of the various methods.

#### 1. The Steel Ball Test by Tsytovich

To investigate the consistency of cohesive soils, Tsytovich modified the Brinell test in the following manner. A steel ball of diameter  $D = 9.5$  mm is forced by a load  $P$  into the smoothed surface of the soil. The load is chosen

such that the penetration "t" is between 0.5 and 1.0 mm where t is measured with an accuracy of 0.01 mm. The apparatus is shown in Fig. 4. The penetration is read after a load period of 5, 10, 30, 60 and 300 seconds and the corresponding shear resistance is computed by the formula:

$$S = 0.057 \frac{P}{Dt} \quad (8)$$

where P is the load in kg, D the diameter of the sphere (cm) and t the penetration (cm). This formula was derived for ideal, plastic, i.e., frictionless materials, and is supposed to be usable for soils with a friction angle of up to 7°. For soils with a higher friction angle the results must be multiplied by a correction factor m according to Beresanzev

friction angle	correction factor m
10°	0.61
20°	0.28
30°	0.11

Since the penetration depth t is time-dependent and increases with increasing load duration this method yields a shear resistance that decreases logarithmically with the load duration.

This, indeed, also corresponds to actual clay soil behavior which exhibits a shear strength that tends asymptotically towards an ultimate value as the duration of the load is increased. It is interesting to note that this method is one of the few ones which is able to reveal the rheological properties of a soil.

Nevertheless, a certain amount of the penetration  $t$  may also be caused by consolidation which will introduce a small error; however, its magnitude can be determined fairly well, if it should be considered necessary.

## 2. The Swedish Cone Test

This test follows exactly the same principle as that of Tsytoevich except that the sphere is replaced by a cone with an angle of  $60^\circ$  or  $30^\circ$  respectively. The apparatus is shown in Fig. 5. The disturbed or undisturbed soil is placed in the container and the surface is leveled and smoothed. The cone is then adjusted by a screw such that its point just touches the soil surface. Then the cone is released and penetrates by its own weight into the soil. This penetration is measured by a micrometer and serves to determine the strength index  $H$  of the soil which is defined as one sixth of the load producing a penetration of 1 cm of the  $60^\circ$  cone.

From a large number of tests a table could be established giving the strength index for any penetration and load. The strength index  $H$  is a purely empirical value and serves mainly to determine the sensitivity of a clay and to compare the relative strength of various soil layers.

If  $H_1$  and  $H_2$  is the strength index in the undisturbed and disturbed state respectively, then the sensitivity is

$H_1/H_2$ . In the range of small indici an empirical relationship was found between H and the shear strength s, namely:

$$s \approx \frac{H}{400} \text{ (kg/cm}^2\text{)}$$

This relationship is supposed to be valid for  $H \leq 240$ .

Although the experiment is evaluated on a purely empirical basis it is claimed to be very useful.

Table 1

Strength Index for Swedish Cone Test

Penetration (mm)	Strength Index H			
	load P cone angle	100 grams 30°	60 grams 60°	10 grams 60°
2.0		1140	195	-
3.0		526	100	-
4.0		296	58	-
5.0		189	36.5	-
6.0		140	26.8	4.5
7.0		104	19.7	3.3
8.0		79	15.4	2.6
9.0		62	12.2	2.0
10.0		42	10.0	1.7
11.0			8.2	1.4
12.0			6.9	1.2
14.0			4.9	0.8
16.0			3.6	0.6
18.0			-	0.4
20.0			-	0.3

### 3. The Proctor Plasticity Needle

R. H. Proctor (1933) proposed to measure the force necessary to push a plane indenter of circular cross-section with a penetration rate of about 0.5 inch per second into the surface of a compacted soil. The apparatus used is shown in

Fig. 6. Exchangeable indenters with cross-sectional areas varying from 1.0 to 0.01 square inch are pressed by a rod and handle assembly through a spring into the soil and the necessary force is read off. The necessary force should be around 300 psi. at the optimum water content. Proctor proposed this test as a construction control test to determine whether the required compaction had been obtained at the permissible water content. He considered a penetration resistance from 200 to 300 psi. as acceptable. The test, however, has been replaced more and more by "in situ" density measurements and is hardly used any longer.

#### 4. The California Bearing Ratio Test (CBR)

In 1940 the U.S. Army Corps of Engineers was suddenly faced with the task to develop a method that would permit the quick and reliable design of airfield and highway pavements. After months of intensive research the conclusion was reached that the method developed by the California State Highway Department was the most suitable. It was therefore adopted for the design of asphalt pavements and it permitted to take advantage of the experience already gained with this test in California. The CBR test is, in principle, a penetration-shear test which determines a bearing strength modulus. This bearing strength modulus then determines, according to a purely empirical relationship, for a given wheel load the

required pavement thickness. For the design of airfield pavements the design curves of the California State Highway Department were extended and confirmed by measurements on existing airfield pavements. This method then was used extensively during and after the second world war and probably is one of the most successful methods of modern soil mechanics.

The equipment for the CBR test is shown in Fig. 7. In this test a circular steel cylinder of 1.954-inch diameter is pressed into the soil surface by a hydraulic piston and the load-penetration diagram is found. In the normal case the stress corresponding to the penetration of 0.1 inch divided by the stress corresponding to the same penetration (0.1 inch) for the standard material (crushed rock) is the CBR value:

$$\text{CBR} = \frac{\sigma_{\text{soil}}}{\sigma_{\text{standard}}}$$

Since the stress for the standard material at 0.1 inch penetration is 1000 psi., a soil stress of 300 psi. at 0.1 inch penetration would give a CBR value of 30%.

This method has found wide application in the western hemisphere and is being used with great success. A detailed investigation of the method was carried out in 1945 by the Waterways Experiment Station in which the soil deformation characteristics below the piston were carefully examined also (see Fig. 8). The CBR test is thus surely that test method in which the principle of hardness measurement has found its widest application in modern soil mechanics.

### 5. The Ram Penetrometer

This instrument is a steel rod with a conical point that is driven into a material surface by the repeated impacts of a falling weight and the penetration is then related to the impact energy. In principle this method is therefore related to the pile driving formulae. There are a number of ram penetrometers in existence and as a typical example we may just mention that developed by the U.S. Army Cold Regions Research and Engineering Laboratory.

The equipment is shown in Fig. 9. A steel block of weight  $W$  falls through a height  $H$  onto an anvil. The resulting impact drives the conical point of the rod into the material surface and causes a penetration  $s$ . A detail of the conical point is shown in Fig. 10.

The ram hardness  $R$  is then determined from:

$$R = \frac{WH}{s} + W + Q \quad (9a)$$

where  $Q$  is the weight of the penetrometer rod. Since it is often difficult to determine the penetration  $s$  for a single blow, one often determines the total set from a heat of  $n$  blows and finds

$$R = \frac{nWH}{s_n} + W + Q \quad (9b)$$

where  $s_n$  now is the penetration after  $n$  blows. The results obtained with the penetrometer shown were compared with unconfined compression tests which yielded a linear relationship between the unconfined compression test and the logarithm of  $R$  according to:

$$Q_u = 4.078 \ln R - 14.72 \text{ (kg/cm}^2\text{)} \quad (10)$$

A series of experiments and the scattering of the results are shown in Fig. 11.

It is interesting to note that in this case the load is applied by impact, i.e. dynamically. As one can see, equations (9a) and (9b) have the same structure as the various pile driving formulae and, therefore, are subject to the same criticisms and reservations that were made with respect to those by Cummings. Especially the assumption that the penetration resistance remains constant throughout the penetration process along the distance  $s$  is of questionable validity and the further assumption that the various energy losses may be neglected shows that these formulas at best have an approximate value.

#### 6. The U.S. Army Corps of Engineers Cone Penetrometer

This instrument was developed by the Waterways Experiment Station of the U.S. Army Corps of Engineers in Vicksburg,

Mississippi and has been used for several years to determine the shear strength or the trafficability of a soil surface for given cross-country type vehicles. The apparatus was already shown in Fig. 2 and consists mainly of a conical point having an opening angle of  $30^{\circ}$  and an area of  $0.5 \text{ in}^2$  connected by a steel rod and proving ring to a handle. The cone is forced by hand into the soil surface and the force required is read off from the proving ring dial. This dial is calibrated in such a fashion that one reads directly the ultimate bearing pressure. This figure is called the "cone index." Hechtl and Herbst (1963) described the application of this index in more detail.

#### 7. The Aerial Cone Penetrometer

As we have indicated earlier, this instrument is the logical follow on to the U.S. Army Corps of Engineers penetrometers. It was developed particularly for those situations where, for practical or military reasons, the Corps of Engineers penetrometer cannot be used. The instrument (see Fig. 1) essentially is a long aluminum tube having a conical point with a spike at the lower end. The cone is connected through a spring-firing pin assembly to a cartridge that sets off a smoke signal, flare or color vane when it is fired. If the impact of the penetrometer is hard enough the cartridge is

set off and the resulting signal may be observed visually from the air. An infrared bulb may also be lighted. As the spring of the firing pin can be varied, one can use stiffer and stiffer springs until one is found which no longer permits the firing pin to fire the cartridge.

The instrument has a number of limiting characteristics and disadvantages. For one, the severity of the impact will depend on the impact velocity. This velocity therefore must be measured independently or, at least, it must be estimated. Secondly, every impact only gives a relative indication, namely whether the resistance encountered by the penetrometer was greater or less than the one required by the chosen spring; thus a determination of the actual magnitude requires at least several, if not a large number, of impacts to bracket the true value with sufficient accuracy. One of the most severe disadvantages, however, in the practical application is the aerodynamic instability of the instrument and the geometric requirements for its perfect operation.

In order to give perfect results the aerial penetrometer should impact upon the horizontal soil surface not only in perfect vertical alignment but also without any horizontal velocity component. In practice, however, the aerial penetrometer would most likely have a small inclination  $\alpha$ . Such an inclination not only reduces any resisting force transmitted through the pin by the factor  $\cos \alpha$  but also causes

the impact energy to be transmitted to a small degree only through the conical point while most of it is converted into a moment causing the penetrometer to impact broadside. Even in a perfect vertical alignment impact such a moment may develop, namely if the penetrometer has a horizontal velocity component different from zero.

For the normal operational case it will be practically impossible to eliminate all these sources of error and achieve a perfectly vertical impact with zero horizontal velocity component and an accurately known vertical component.

#### The Princeton Impact Penetrometer

Because of these difficulties the author, in the fall of 1962, began a research project sponsored by the Terrestrial Sciences Laboratory of AFCRL to investigate the feasibility of methods measuring the soil properties of interest without the disadvantages cited above such that aircraft trafficability on a soil surface in terms of predictable deformations could be evaluated.

The important practical as well as theoretical considerations for developing such a method are discussed below. Also, a description of a laboratory instrument (Fig. 12) to check the design concept is given as well as the results of several series of tests that were carried out with the instrument.

The instrument itself was designed by the author and manufactured in the central machine shop of the School of Engineering and Applied Science of Princeton University. Mr. Christian Hechtel, research assistant, assembled and calibrated the electronic equipment and during the summer and fall 1963 carried out a first pilot test series mostly on disturbed, artificially prepared soils in the laboratory. These pilot tests had the purpose to confirm, in principle, whether the chosen concept and system was satisfactory, to find the most favorable shape of the nose for the drop capsule and to find the influence of water content and dry density on the test results. The results of these pilot tests were presented in February 1964 by Mr. Hechtel as his Ph.D. dissertation.

The bulk of the results presented in this report were carried out jointly by the author and Dr. Hechtel during the summer of 1964 mostly on natural, undisturbed soil.

It is the purpose of the remainder of this report to present first the basic, theoretical considerations for this type of remote testing and then analyze the test results and discuss the possible further improvement and development of the impact penetrometer and its operation.

### III. The Drop Capsule Penetrometer

#### 1. Test Principle

One of the main difficulties encountered with the aerial penetrometer is measuring, or at least estimating, the impact velocity since the square product of this quantity determines the impact energy. A small error in determining this velocity, therefore, causes a rather large error in the kinetic energy at impact.

An attempt, therefore, was made to consider techniques which would permit a direct measurement of the velocity. This would have been possible perhaps with microwave radar techniques using the Doppler principle. However, it was feared that this would lead to rather complicated electronic equipment. On the other hand modern solid state technology had developed a series of accelerometers using piezo-electric crystals (which had already found wide application in ordinance and rocket development) which were uniquely suited for our purposes.

If one attaches an accelerometer (measuring the deceleration as a function of time) to any instrument impacting on a target, one can apply Newton's law and write:

$$F(t) = ma(t) \quad (11)$$

and the accelerometer signal variation with time corresponds, except for the mass  $m$ , to the variation with time of the force exerted by the target material on the instrument which, however, due to a second law by Newton must be equal to the force exerted upon the target material. Moreover, since the final velocity of a missile after impact without rebound is equal to zero one can obtain from the acceleration-time signal  $a(t)$  not only the velocity  $v(t)$  but also the distance traveled  $s(t)$ . Because, according to an elementary rule of differential calculus:

$$v(t) = \int a(t) dt + c_1 \quad (12)$$

and

$$s(t) = \int v(t) dt + c_2 \quad (13)$$

If we designate the instant of initial contact as  $t = 0$ , the velocity at this instant with  $v(0)$  and the total period of the force exchange with  $T$ , then according to (12) we may write:

$$v(0) = \int_0^0 a(t) dt + c_1 = 0 + c_1 \quad (14a)$$

$$v(T) = \int_0^T a(t) dt + v(0) = 0 \quad (14b)$$

thus

$$v(0) = - \int_0^T a(t) dt = - A(T) \quad (14c)$$

That is to say the impact velocity can be obtained as the area under the acceleration-time diagram. Furthermore, we

observe that for  $t = 0$  the penetration  $s(0)$  must be zero, i.e.  $c_2 = 0$  and the final penetration  $s(T)$  must, hence, be:

$$s(T) = \int_0^T v(t) dt \quad (15)$$

Assuming, for the sake of argument, the acceleration-time signal could be represented by the first half of a sine-curve, then:

$$a(t) = a_m \sin \pi \frac{t}{T} \quad (16)$$

which would then yield:

$$v(0) = - a_m \int_0^T \sin \pi \frac{t}{T} dt = - \frac{2}{\pi} a_m T \quad (17)$$

and:

$$s(T) = - \frac{a_m T^2}{\pi} \quad (18)$$

Once the deceleration-time signal during impact is known one also knows the variation of the force with time. The impact velocity as well as the final penetration can then be easily obtained by integration of the signal.

The choice of an instrument that gives an electronic signal corresponding to the deceleration upon impact thus avoids all those difficulties which stem from the complicated measurement of the impact velocity or its erroneous estimate.

It was mainly for this reason that the piezo-electric accelerometer capsule was chosen. Here we have to mention,

however, one difficulty that presents itself, namely, that of the velocity components. A piezo-electric accelerometer, of course, gives only the acceleration along its piezo-electric axis. If, therefore, the instrument impacts with a velocity component normal to this axis, the deceleration in this direction does not give any signal. For the prototype of a piezo-electric penetrometer this problem can be easily solved by using a triple accelerometer with their respective axes mounted along the axes of a cartesian coordinate system. The maximum component can then be found by superposition:

$$a_{\max} = \sqrt{a_x^2 + a_y^2 + a_z^2} \quad (19)$$

Since, for our laboratory experiments, accelerometer axis and impact velocity component in most cases could easily be made to coincide we avoided the complication of using three accelerometers. This was also in the interest of economy since the instrumentation per channel cost about \$4,000-\$5,000. However, for the prototype of an aerial penetrometer a triple accelerometer or possibly a directional stabilization would be necessary.

## 2. Instrument Capsule

The instrument was designed as a hollow, circular chromium steel cylinder of 75 mm diameter having an

exchangeable tip which was either conical, hemi-spherical or flat. The accelerometer is attached by a thread to a small anvil inside the tip in such a fashion that the axis of the accelerometer and that of the cylinder coincide. The total weight was 1.573 kg. In Figs. 12 and 13 a photograph and a section of the instrument respectively are shown.

A shielded cable transmits the signal through an amplifier system to the screen of the oscilloscope. The horizontal beam velocity of the oscilloscope could be varied widely. Thus, the time axis of the signal could be arbitrarily extended or compressed which permitted a proper choice for the best readability of the signal.

For the test series used so far the signal was photographed by a polaroid camera which permitted to make a judgment within a few minutes whether a test had been successful. Of course, the signal could have also been stored on a magnetic tape which for a prototype operational penetrometer appears more suitable and practicable.

The first experiments with this instrumentation were carried out by Christian Hechtl under supervision of the author in the summer of 1963. They served above all to confirm the applicability of the testing principle, to calibrate the instrument, to test the equipment and collect first experience with it in the laboratory and to find the most important parameters that determine the target response. Above all, we

wanted to find the most suitable shape for the tip of the capsule.

The results were reported in detail by Hecht1 in his dissertation. They were summarized by the author in November 1963 in Status Report No. 4, Contract No. AF(19)-628-2427, submitted to the Terrestrial Science Laboratory, and the tentative conclusions were:

1. The drop penetrometer, in principle, is suitable for the determination of soil properties.
2. The magnitude of the maximum deceleration permits the determination of the strength of the soil in the range of the impact velocities used (up to 15 m/sec).
3. First tentative comparisons between the Hertz and the Meyer theories of impact showed that the results were closer to that by Meyer. This comparison was made by Hecht1 using rather severe simplifications.
4. The most important parameter for the laboratory tests appeared to be the dry density of the soil, a second one the water content.
5. For clay soils with a higher than Proctor optimum water content smooth curves resulted with a monotonously increasing and then decaying signal.

In very dry soils and in sand and gravel we observed certain vibrations of very high frequency which correspond to the eigen values of the vibration of the capsule and are

superimposed on the target response signal. In the normal case these superimposed high frequency oscillations have no influence on and do not prevent the evaluation of the response signal.

Over and above these characteristic frequencies excited by firm targets there also appear certain softening and rehardening phases during the impact period, especially in sands. These should be further investigated.

Later experiences with the drop penetrometer - especially outdoors - led to the conclusion that it will be impossible to stabilize the penetrometer against any lateral forces or movements in such a fashion that the instrument will always impact vertically and without any horizontal velocity components. To minimize any error due to these influences, we chose for all future tests the hemi-spherical tip.

Among the thirty test series reported by Hecht1 there were, however, only four carried out with hemi-spherical head, namely the series No. 12, 15, 19 and 22. The rest had mostly been carried out with a conical head because it gives a deformation that, as already observed by Ludwik, always maintains geometric similarity for any penetration depth. This initially appeared advantageous for the theoretical evaluation of the results.

The above mentioned experience and the consequent conclusions led to a second test series in which the hemi-spherical

head was used exclusively. Initially, the penetrometer was to be tested with various target materials which, in contrast to most natural soil deposits, had uniform, well defined properties that were either known or could be easily determined. For this purpose we chose two greases of varying consistency and two paraffins of different hardness.

Further tests were then carried out on natural soils.

Before we discuss these tests, however, it will be advantageous to consider theoretically the state of stress and deformation that occurs in the target material during the impact process.

We deal here with a typical case of central symmetry for which the use of a cylindrical coordinate system is most suitable. We will, starting from the theory of elasticity, consider the interplay of forces and the deformation using an ideal plasticity theory. Finally, we will derive relationships for a viscoelastic half-space under the influence of a dynamic load applied through a spherical surface.

#### IV. Basic Theoretical Considerations

##### 1. States of Stress and Deformation with Axial Symmetry

In any state of stress or strain being symmetrical to a rotational axis one uses, as is well-known, the cylindrical coordinates  $r$  and  $z$ . We follow here essentially a notation and treatment given by Nadai and consider a volume element with the sides  $r d\phi$ ,  $dr$ ,  $dz$  (Fig. 14) and designate the displacement components of the point  $P$  in the radial and vertical direction with  $u$  and  $w$  respectively. The resulting normal strains can then be expressed as follows:

$$\epsilon_r = \frac{\partial u}{\partial r} ; \epsilon_t = \frac{u}{r} ; \epsilon_z = \frac{\partial w}{\partial z} \quad (20)$$

and the shear strain in any vertical plane is given by:

$$\gamma_{rz} = \frac{\partial u}{\partial z} + \frac{\partial w}{\partial r} \quad (21)$$

The volume change (dilatation) is then:

$$\epsilon = \epsilon_r + \epsilon_t + \epsilon_z = \frac{\partial u}{\partial r} + \frac{u}{r} + \frac{\partial w}{\partial z} \quad (22)$$

If we designate the stress components in the radial, tangential and axial direction with  $\sigma_r$ ,  $\sigma_t$  and  $\sigma_z$  respectively and the corresponding shear stress with  $\tau_{rz} = \tau$  the equilibrium conditions for the volume element of Fig. 14 may be stated (ignoring body forces):

$$\frac{\partial \sigma_r}{\partial r} + \frac{\sigma_r - \sigma_t}{r} + \frac{\partial \tau}{\partial z} = 0 \quad (23a)$$

$$\frac{\partial \sigma_z}{\partial z} + \frac{\partial \tau}{\partial r} + \frac{\tau}{r} = 0 \quad (23b)$$

For an elastic material the stresses can be computed from the strains using Hooke's stress-strain relationships:

$$\sigma_r = 2 G \left( \frac{\partial u}{\partial r} + \frac{\nu \epsilon}{1 - 2\nu} \right) \quad (24a)$$

$$\sigma_t = 2 G \left( \frac{u}{r} + \frac{\nu \epsilon}{1 - 2\nu} \right) \quad (24b)$$

$$\sigma_z = 2 G \left( \frac{\partial w}{\partial z} + \frac{\nu \epsilon}{1 - 2\nu} \right) \quad (24c)$$

$$\tau = G \left( \frac{\partial u}{\partial z} + \frac{\partial w}{\partial r} \right) = G \gamma_{rz} \quad (24d)$$

where  $G$  is the shear modulus and  $\nu$  is Poisson's ratio. If we introduce the stress-strain relations of equations (24) into the equilibrium conditions (equations 23), we get:

$$(1 - 2\nu) \left( \Delta u - \frac{u}{r^2} \right) + \frac{\partial \epsilon}{\partial r} = 0 \quad (25a)$$

and

$$(1 - 2\nu) \Delta w + \frac{\partial \epsilon}{\partial z} = 0 \quad (25b)$$

where  $\Delta = \frac{\partial^2}{\partial r^2} + \frac{\partial}{r \partial r} + \frac{\partial^2}{\partial z^2}$  is the Laplace operator. Accordingly the volume change

$$\epsilon = \frac{1-2\nu}{2(1+\nu)G} (\sigma_r + \sigma_t + \sigma_z) = \frac{1-2\nu}{E} (\sigma_r + \sigma_t + \sigma_z) \quad (26)$$

must automatically satisfy the Laplace equation

$$\Delta \epsilon = \frac{\partial^2 \epsilon}{\partial r^2} + \frac{\partial \epsilon}{r \partial r} + \frac{\partial^2 \epsilon}{\partial z^2} = 0 \quad (27)$$

By using the relationship (27), the equations (25) can be transformed into the differential equations of the displacement components  $u$  and  $w$ :

$$\left(\Delta - \frac{1}{r^2}\right)\left(\Delta u - \frac{u}{r^2}\right) = 0 \quad (28)$$

$$\Delta \Delta w = 0 \quad (29)$$

Let us consider now the problem of an elastic half-space  $z \geq 0$  which has on its surface  $z = 0$  a given distribution of the normal and shear stresses or of the deformation components  $u$  and  $w$ . We restrict our considerations to the case of symmetry with respect to a vertical axis. A problem of this type can be solved by various methods especially by using potential theory. General solutions are given, e.g., by Riemann-Weber (1910). However, we consider here only some partial integrals of equations (28) and (29) which can be used to express arbitrary functions of  $r$ , either as infinite series or as definite integrals. These functions can be made to satisfy the prescribed boundary conditions on the surface of the half-space  $z = 0$  as it is often done analogously with trigonometric series or Fourier integrals.

A double pair for each partial integral of (28) and (29) for  $u$  and  $w$  respectively would be:

$$u_1 = e^{\pm\alpha z} J_1(\alpha r), \quad u_2 = z e^{\pm\alpha z} J_1(\alpha r) \quad (30)$$

$$u_1 = e^{\pm\beta z} J_0(\beta r), \quad u_2 = z e^{\pm\beta z} J_1(\beta r) \quad (31)$$

where  $J_0(\beta r)$  and  $J_1(\alpha r)$  are Bessel functions of the first kind and of order zero and one respectively for a real variable,  $\alpha$  and  $\beta$  being real constants. These functions  $J_0(x)$  and  $J_1(x)$  as is well-known are the solutions of the differential equation.

$$x^2 \frac{d^2 y}{dx^2} + x \frac{dy}{dx} + (x^2 - n^2) y = 0 \quad (32)$$

for  $n = 0$  and  $n = 1$  respectively which are regular at the origin  $x = 0$ .

They may also be expressed as infinite series which are convergent for any value of  $x$ :

$$J_0(x) = 1 - \frac{(x/2)^2}{(1!)^2} + \frac{(x/2)^4}{(2!)^2} - \frac{(x/2)^6}{(3!)^2} + \dots$$

$$J_1(x) = \frac{x}{2} - \frac{(x/2)^3}{1!2!} + \frac{(x/2)^5}{2!3!} - \frac{(x/2)^7}{3!4!} + \dots$$

for very large values of  $x$ , i.e. for  $x \rightarrow \infty$ , these series converge asymptotically to:

$$J_0(x) = \sqrt{\frac{2}{\pi \cdot x}} \sin \left( x + \frac{\pi}{4} \right) \quad (33)$$

$$J_1(x) = \sqrt{\frac{2}{\pi \cdot x}} \sin \left( x - \frac{\pi}{4} \right) \quad (34)$$

whereby the following rules of integration and differentiation apply:

$$\frac{dJ_0}{dx} = J_0' = -J_1 \quad ;$$

$$\frac{dJ_1}{dx} = J_1' = J_0 - \frac{J_1}{x} ;$$

$$\int J_1 dx = -J_0 ;$$

$$\int xJ_0 dx = xJ_1 ;$$

$$\int_0^{\infty} J_0(x) dx = \int_0^{\infty} J_1(x) dx = 1 ;$$

$$\int_0^{\infty} \frac{1}{x} J_1(x) dx = 1$$

## 2. Surface Stresses on the Elastic Half-Space

We consider the half-space  $z > 0$  having stresses  $\sigma_z = p(r)$  applied on its surface  $z = 0$  which are symmetrical with respect to the vertical axis  $r = 0$  with the shear stresses at  $z = 0$  being zero.

This includes also the case where the normal pressures  $p(r)$  act within the circle  $r \leq a$  and vanish for  $r > a$ .

For such a case the stress components  $\sigma_r$ ,  $\sigma_t$ ,  $\sigma_z$  and  $\tau$  must all decay to zero for large values of  $z$ . Therefore, the values in the vicinity of the loaded circle would be of main interest.

We introduce the displacement components of the half-space:

$$u = (A + Baz) e^{-\alpha z} J_1(\alpha r) \quad (36a)$$

$$w = (C + Daz) e^{-\alpha z} J_0(\alpha r) \quad (36b)$$

where the values A-D are constants of integration and u and w are solutions for (28) and (29) respectively. The constants A-D are, however, not independent of each other but must be chosen in such a way that the conditions (25) are satisfied simultaneously. Besides these conditions the shear stresses on the surface must also vanish which means that for  $z = 0$

$$\frac{\partial u}{\partial z} + \frac{\partial w}{\partial r} = 0 \quad (37)$$

If we carry out the differentiation of the displacements (36) according to (37) we obtain

$$C = -A + B \quad (38)$$

If we further carry out the operations with u and w which are required by equations (25) we obtain

$$B = D = -\frac{A}{1 - 2\nu} ; \quad (39a)$$

$$C = -\frac{2(1 - \nu)}{1 - 2\nu} A \quad (39b)$$

This means that except for the constant A all other constants are determined and the displacement components (36) can be given as:

$$u = A (1 - 2\nu - \alpha z) e^{-\alpha z} J_1(\alpha r) \quad (40a)$$

$$w = -A 2(1 - \nu) + \alpha z e^{-\alpha z} J_0(\alpha r) \quad (40b)$$

The constant A must now be found by a second boundary condition, namely either by prescribing the distribution of the normal stresses or that of the displacements u and w at the surface. Let us assume that A is a function of a parameter  $\alpha$ :  $A(\alpha)$ . If we multiply the right-hand side of equations (40) by  $d\alpha$  and integrate from  $\alpha = 0$  to  $\alpha = \infty$  we can express the displacements by the definite integrals:

$$u = \int_0^{\infty} A(\alpha) (1 - 2\nu - \alpha z) e^{-\alpha z} J_1(\alpha r) d\alpha \quad (41a)$$

$$w = \int_0^{\infty} A(\alpha) [2(1 - \nu) + \alpha z] e^{-\alpha z} J_0(\alpha r) d\alpha \quad (41b)$$

which yields the displacements at the surface  $z = 0$ :

$$u = (1 - 2\nu) \int_0^{\infty} A(\alpha) J_1(\alpha r) d\alpha \quad (42a)$$

$$w = -2(1 - \nu) \int_0^{\infty} A(\alpha) J_0(\alpha r) d\alpha \quad (42b)$$

By using the expressions (41) we can again compute the volume change:

$$\epsilon = \frac{\partial u}{\partial r} + \frac{u}{r} + \frac{\partial w}{\partial z} = 2(1 - 2\nu) \int_0^{\infty} A(\alpha) e^{-\alpha z} J_0(\alpha r) \alpha d\alpha \quad (43a)$$

which for  $z = 0$  yields:

$$\epsilon = 2(1 - 2\nu) \int_0^{\infty} A(\alpha) J_0(\alpha r) \alpha d\alpha \quad (43b)$$

To evaluate  $A(\alpha)$  we consider the case where the normal stresses  $\sigma_z$  are a prescribed function of  $r$  and apply the boundary conditions for  $z = 0$ .

According to Hooke's law:

$$\sigma_z = 2G \left( \frac{\partial w}{\partial z} + \frac{\nu \epsilon}{1 - 2\nu} \right) \quad (24c)$$

we get:

$$\sigma_z = -p = f(r) - 2G \int_0^\infty A(\alpha) J_0(\alpha r) \alpha d\alpha \quad (44)$$

A comparison of (43b) and (44) shows that:

$$\epsilon = - \frac{1 - 2\nu}{G} p \quad (45)$$

This means that the volume change is directly proportional to the pressure  $p$ . According to the theory of Bessel functions an arbitrary function  $f(r)$  may be expressed as a Fourier integral:

$$f(r) = \int_0^\infty J_0(\alpha r) \alpha d\alpha \int_0^\infty f(\lambda) J_0(\alpha \lambda) \lambda d\lambda \quad (46)$$

By comparing equations (44) and (46) we see that the function  $A(\alpha)$  is determined by the definite integral:

$$A(\alpha) = - \frac{1}{2G} \int_0^\infty p(\lambda) J_0(\alpha \lambda) \lambda d\lambda \quad (47)$$

accordingly the displacements  $u$  and  $w$  of the surface of the half-space are given by:

$$u = - \frac{1 - 2\nu}{2G} \int_0^{\infty} p(\lambda) \lambda d\lambda \int_0^{\infty} J_1(\alpha r) J_0(\alpha \lambda) d\alpha \quad (48)$$

$$w = \frac{1 - \nu}{G} \int_0^{\infty} p(\lambda) \lambda d\lambda \int_0^{\infty} J_0(\alpha r) J_0(\alpha \lambda) d\alpha \quad (49)$$

The interior integral of (48) is nothing but a discontinuity function of the variable  $\lambda$  which may be omitted if we replace the upper limit of  $\infty$  by  $r$  and hence we get:

$$u = - \frac{1 - 2\nu}{2G r} \int_0^r p(\lambda) \lambda d\lambda \quad (50)$$

Because:

$$\begin{aligned} \int_0^{\infty} J_1(\alpha r) J_0(\alpha \lambda) d\alpha &= \frac{1}{r} \quad \text{for } 0 < \lambda < r \\ &= 0 \quad \text{for } r < \lambda < \infty \end{aligned} \quad (51)$$

We introduce an average pressure  $\bar{p}$  of the pressure  $p(r)$  within the circle of variable radius ( $0 < r < \infty$ )

$$\bar{p} = \frac{2}{r^2} \int_0^r p(\lambda) \lambda d\lambda \quad (52)$$

The displacements of the surface  $z = 0$  becomes:

$$u = - \frac{1 - 2\nu}{4G} \bar{p} r \quad (53)$$

The displacements  $w$ , however, cannot be determined so easily.

At the origin  $r = z = 0$  we get, according to (49):

$$w_0 = \frac{1 - \nu}{G} \int_0^{\infty} p(\lambda) \lambda d\lambda \int_0^{\infty} J_0(\alpha \lambda) d\alpha \quad (54)$$

But from:

$$\int_0^{\infty} J_0(\alpha\lambda) d\alpha = \frac{1}{\lambda}$$

we get:

$$w_0 = \frac{1-\nu}{G} \int_0^{\infty} p(\lambda) d\lambda \quad (55)$$

Thus, on the surface the displacements  $u$  and the volume change are known. According to (24) we may, therefore, compute the surface stresses and get:

$$\sigma_z = -p(r) \quad (56a)$$

$$\sigma_r = -p(r) + \frac{1}{2} (1 - 2\nu) \bar{p} \quad (56b)$$

$$\sigma_t = -2\nu p(r) - \frac{1}{2} (1 - 2\nu) \bar{p} \quad (56c)$$

which are valid for every point of the surface. At the origin  $z = r = 0$  we get:

$$\sigma_z = -p(0) \quad (56d)$$

$$\sigma_r = \sigma_t = -\frac{1}{2} (1 + 2\nu) p(0) \quad (56e)$$

### 3. The Stress Distribution after Hertz

Hertz investigated the distribution of stresses and displacements of two elastic spheres which are pressed together by a force  $P$  whose line of action intersects the

centers of both spheres. If the radius  $R_2$  of the second sphere approaches very large values, we get the problem of a sphere pressed upon the half-space. The pressure on the surface is then given by:

$$\sigma_z = -p = -p_0 \sqrt{1 - (r/a)^2} \quad (57)$$

That is to say within the circle of contact with radius  $a$ , the pressure is given by (57) for all values of  $r < a$  the pressure on the surface vanishes. If we would plot these pressures as ordinates above the corresponding radii, we would get an ellipsoid of revolution. The resultant force  $P$  which is equal to the volume of this ellipsoid would be:

$$P = \frac{2\pi}{3} p_0 a^2 \quad (58)$$

According to (52) the average pressure is:

$$\bar{p} = \frac{2}{r^2} \int_0^r p r dr \quad (59)$$

hence:

$$\bar{p} = \frac{2p_0 a^2}{3r^2} \left[ 1 - \left( 1 - \frac{r^2}{a^2} \right)^{3/2} \right] \text{ for } 0 \leq r \leq a \quad (60)$$

and

$$\bar{p} = \frac{2p_0 a^2}{3r^2} \quad \text{for } r > a \quad (61)$$

The vertical displacements according to Föeppi (1920) will be:

$$w = \frac{1 - \nu}{G} \frac{3}{8} \frac{P}{a^2} \left( a - \frac{r^2}{2a} \right) \quad (62)$$

The highest indentation occurs at the central axis  $r = 0$ :

$$w_0 = \frac{1 - \nu}{G} \frac{3}{8} \frac{P}{a} \quad (63)$$

and at the edge where  $r = a$ :  $w_a = \frac{1}{2} w_0$

The radius of the circle of contact is given by:

$$a = \left( \frac{3}{8} PR_1 \frac{1 - \nu}{G} \right)^{1/3} \quad (64)$$

The direct application of these results is not possible because practically in all experiments with the penetrometer the elastic limit is exceeded. However, as will be shown later, the Hertz solutions can be used when applying the elastic-viscoelastic analogy and it is for this reason that the elastic solutions are discussed in such detail.

#### 4. Stresses and Deformation with Axial Symmetry in the Plastic Range

As already indicated, the main part of the deformation of the soil surface during the penetrometer test takes place in the plastic range. Therefore, an investigation of the deformations due to a sphere penetrating into a plastic body is necessary.

The plane strain problem of a plastic deformation of a half-space by a punch was investigated by Prandtl (1921) and

Hencky (1923). Hencky also considered an approximate solution for the penetration problem with a symmetrical axis and noted that the radii of the slip lines varied only by 12.5% from those for the problem of plane strain.

In his considerations Hencky used the assumption of Karman-Haar, namely, that in the plastic range two of the three principal stresses are equal and that the third principal stress is different from the two first ones by the amount  $2k$ . That is to say, it differs by an amount corresponding to the yield stress. He thus used a statically determined system of stress as follows:

$$\sigma_1 = 2k + \sigma_2 = 2k + \sigma_3$$

Prandtl gives an ultimate bearing pressure of  $p_s = 2k(1 + \theta)$  which for the half space with  $\theta = \pi/2$  gives  $p_s = 2k \times 2.57$ . The considerations of Hencky yield a variable pressure (see Fig. 15) with a value of  $2k \times 3.33$  in the center and  $2k \times 2.52$  at the edge of the punch. The average pressure is  $2k \times 2.83$ .

Because the investigations by Prandtl and Hencky were made for a rectangular punch, one might assume that for a spherical penetrometer they are not applicable. However, if we compare Figures 16a and 16b which show the slip line patterns for a rectangular and for a spherical punch respectively, we recognize that this assumption is not justified.

It happens that in both cases a conical wedge directly below the punch is forced into the material and the angle at the apex of this cone must be  $90^\circ$  in both cases. This wedge of material is practically in a hydrostatic state of stress and may be considered as being part of the penetrometer thus making the actual body penetrating into the material identical. The only difference is that for the cylindrical punch the loaded surface remains constant while for the spherical indenter the loaded surface increases with increasing penetration. Iterson (1947) analyzed the spherical indenter for the hardness test in detail. Using the same assumptions as Prandtl he came to the result that the ultimate bearing pressure for a spherical penetrometer is also  $p_s = 2k \times 2.57$  as found by Prandtl for the cylindrical punch. Iterson also carried out experiments to check Hencky's observation that the radii of the slip lines for the three-dimensional problem differ only by 12.5% from those of the plane problem (see Fig. 15). He found that the plastified zone D at the surface of the material (Fig. 17) in the plane strain problem was equal to three punch diameters:  $D = 3d$ . For the three-dimensional problem he found, from several series of tests with different loads, different sphere diameters and penetration, an average  $D/d = 2.76$ .

An exact, theoretical analysis using the hypothesis of Karman-Haar was carried out by Ishlinsky (1944). He utilized

some mathematical results obtained earlier by Sokolowsky which differs from that shown in Fig. 15 only by the fact that the straight lines have a very small curvature. Moreover, Ishlinsky comes to the same result, namely, that the yield stress is approximately 0.34 to 0.36 times the average pressure. This observation agrees also with the statement of Hencky who gives the yield stress as  $0.35 p_{av}$ .

The solutions by Hencky and Ishlinsky have been criticized by Symonds (1948) who claims that the hypothesis of the two principal stresses being equal have neither a physical nor a mathematical justification. This may be formally correct, however the application of the Mises yield criterion carried out by Symonds shows that real solutions exist only in a few special cases and for the problem of plane strain the solution is identical with that of Prandtl-Hencky.

In summary we may state that according to the theory of plasticity, a relationship can be established between the statical hardness test value and the yield stress or the shearing strength of a material. Hence, a spherical penetrometer can be used, in principle, to evaluate the strength of a material. Accordingly, a number of authors have investigated the relationship between Brinell hardness and the yield stress or tensile strength. For example, Foster (1936) gives the empirical relationship between tensile strength  $\sigma_t$  and Brinell hardness  $H_B$  for non-ferrous metals as:

$$\sigma_t = \frac{H_B}{4} - 1 \quad (\text{in tons per square inch})$$

For steel and steel alloys the same author gives the yield stress as:

$$\sigma_y = 0.21 \text{ to } 0.23 H_B$$

The value  $0.22 H_B$  is also cited by Hencky as the one found from experiments that correlates yield stress and Brinell hardness. The discrepancy from the theoretical value ( $0.35 H_B$ ) is explained by Hencky as follows: "According to the Brinell hardness test, the yield stress would be 0.22 times the average bearing pressure. According to our calculations it should be 0.35 times the average pressure. However, we can hope to find agreement with the Brinell test only if we assume the penetrated surface of radius  $A_0$  ... exactly as it results after plastic equilibrium obtains. We, therefore, have to solve first for different penetrations of the sphere, the equations (14a) and (14b) as well as equation (12). Only then a comparison with the experimental results will be possible.

"If we assume the penetrating punch is bounded by a conical surface, we see from equation (15) that the pressure below the tip increases logarithmically toward infinity. Furthermore, we note that from the sector OBC the part from  $\phi = -45^\circ$  to  $\phi = 0^\circ$  is vanishing more and more whereby the integral  $\int \frac{dz}{r}$  changes its sign and yields a positive contribution to the exterior (negative) compressive stress.

"The relationship between yield stress and average bearing pressure (based on the projected surface), therefore, cannot be constant but depends on the penetration and the shape of the penetrating body. According to equations (12) and (14) one could, at least approximately, determine the relationship between yield stress and average bearing pressure for any penetration and any penetrometer shape and would then have to compare this with the experimental results. By such a comparison one should also be able to determine the influence of strain hardening which at present cannot be taken into account theoretically...."

How far these statements suffice to explain the rather considerable discrepancy between theory and experiment we may leave open at this time. It is obvious, however, that if a significant strain hardening of the material takes place during the plastic penetration, the resulting hardness number  $H_B$  or, according to Hencky, the average bearing pressure  $p_{av}$  will be larger than it would be without strain hardening. This means that the value  $\frac{\sigma_y}{H_B}$  will become bigger if no strain hardening occurs and may well approach the theoretical value.

Experiments with materials that closely approximate the stress-strain relationship of an ideal plastic body could clarify this point.

V. Dynamics of Load Application for the Drop-Impact Penetrometer

All considerations so far were made for static or quasi-static loads. However, the drop penetrometer has a basically different load application because the exchange of energy between the penetrometer and the target material takes place during a very short time interval. The loads are therefore applied very rapidly and decay in the same fashion, i.e. we deal here with a dynamic, impact type of load.

1. Stereo-Mechanical Impact

The classical theory of impact is principally based on the conservation of momentum theorem for rigid body and leads to a simple mathematical formulation. The application of this theorem, however, does not permit the determination of any stresses or forces during the impact process. One can merely determine the initial and final velocity components and compare them with the applied linear or angular momentum. Also, the classical theory is unable to describe any local deformations at the point of impact and, moreover, assumes the part of the kinetic energy that is transformed into vibrations to be negligible. This assumption is said to be valid for the impact of two spheres (Raleigh, 1906) or for that of a sphere with a huge rigid mass (Hunter, 1957). For an

ideally elastic impact a second condition can be found by using the conservation of energy theorem which permits the determination of the final velocities.

If the impact is not completely elastic and permanent deformations do occur, one introduces a coefficient of restitution "e." This coefficient describes the degree of energy exchange such that for  $e = 1.0$  the impact is ideal elastic, for  $e = 0$  it is fully plastic. The value  $e$  may also be found as the ratio of the velocity components normal to the contact surface before and after impact:

$$e = \frac{V_{\text{final}}}{V_{\text{initial}}}$$

Frictional forces that may appear on the contact surface can be taken into consideration by a dynamic friction factor  $f$ . This factor is usually assumed purely on an empirical basis.

Let us consider a mass point of mass  $m$  moving with the velocity  $\bar{v}$  along a path that may be described by the radius  $\bar{r}$ . The equation of the motion can then be written as:

$$m \ddot{\bar{r}} = m \dot{\bar{v}} = \bar{F} \quad (65)$$

where  $\bar{F}$  is the force causing a change in velocity. After integrating once with respect to time for the time interval  $T$  we get:

$$m(\bar{v} - \bar{v}_0) = \int_0^T \bar{F} dt = \bar{Q} \quad (66)$$

where the product  $m\bar{v}$  is the momentum. The time integral of the force  $\int_0^T \bar{F} dt = \bar{Q}$  is called the impulse. A further integration yields:

$$m(\bar{r} - \bar{r}_0 - \bar{v}_0 T) = \int_0^T \bar{Q} dt = \bar{G}r \quad (67)$$

where  $\bar{G}$  is the mean value of the integral  $\bar{Q} dt$ . Equation (66) is the impulse-momentum theorem. If we determine the scalar product of  $\frac{1}{2}(\bar{v} + \bar{v}_0)$  with both sides of equation (66) we get:

$$\frac{1}{2} m (\bar{v}^2 - \bar{v}_0^2) = \bar{Q} \frac{\bar{v} + \bar{v}_0}{2} \quad (68)$$

This means that the change in kinetic energy is equal to the scalar product between the impulse and the average velocity before and after the impact.

If we multiply equation (66) scalarly with  $\bar{v}$  and note that:

$$\bar{v}(\bar{v} - \bar{v}_0) = \frac{1}{2} (\bar{v}^2 - \bar{v}_0^2) + \frac{1}{2} (\bar{v} - \bar{v}_0)^2 \quad (69a)$$

it follows that:

$$\frac{1}{2} m (\bar{v}_0^2 - \bar{v}^2) = \frac{1}{2} m (\bar{v} - \bar{v}_0)^2 - \bar{Q}\bar{v} \quad (69b)$$

For a rigid body the last term of equation (69b) is usually zero if there is no friction and no external forces, i.e.:

$$\frac{1}{2} m (\bar{v}_0^2 - \bar{v}^2) = \frac{1}{2} m (\bar{v} - \bar{v}_0)^2 \quad (70)$$

This is the well-known theorem of Carnot.

If we designate  $\mathbf{v}_i$  and  $\mathbf{v}'_i$  the velocity of the particle  $m_i$  before and after impact respectively then the principal equations of the classical theory of impact for perfectly elastic conditions are:

$$\sum m_i \mathbf{v}_i = \sum m_i \mathbf{v}'_i \quad (71a)$$

and

$$\sum m_i (\mathbf{r}_i \times \mathbf{v}_i) = \sum m_i (\mathbf{r}_i \times \mathbf{v}'_i) \quad (71b)$$

Equation (71a) postulates the conservation of momentum and (71b) that of the moment of momentum. Hence, for the normal impact of two bodies the following equations apply:

$$m_1 v'_1 + m_2 v'_2 = m_1 v_1 + m_2 v_2 \quad (71c)$$

$$m_1 (v'_1)^2 + m_2 (v'_2)^2 = m_1 v_1^2 + m_2 v_2^2 \quad (71d)$$

The terminal velocities may thus be determined from:

$$v'_1 = v_1 - \frac{2m_2}{m_1+m_2} (v_1 - v_2); \quad v'_2 = v_2 + \frac{2m_1}{m_1+m_2} (v_1 - v_2) \quad (71e)$$

while the magnitude of the force at impact according to (66) will be:

$$\begin{aligned} P &= m_1 (v'_1 - v_1) = -m_2 (v'_2 - v_2) = -\frac{2m_1 m_2}{m_1 + m_2} (v_1 - v_2) \\ &= \frac{2m_1 m_2}{m_1 + m_2} (v'_1 - v'_2) \end{aligned} \quad (71f)$$

## 2. Ideally Elastic Impact (Hertz Theory)

The consideration of the contact stresses between two elastic spheres were extended by Hertz also to the case of a dynamic load. He made the assumption that all the energy during impact is being exchanged twice, i.e., that the energy which is transformed into vibrations of the impacting bodies may be neglected.

For the impact of an elastic sphere impinging vertically on an elastic half-space we combine equations (58) and (64) and instead of the radius of the contact circle we introduce the approach of the two masses  $\alpha$ . Then the load deformation relationship yields:

$$P = k_2 \alpha^{3/2} \quad (72)$$

where  $\alpha$  is the sum of the elastic deformation of the surface of the half-space  $w_1$  and the shortening of the sphere radius  $w_2$  and  $k_2$  expresses the elastic properties of the sphere and the half-space. Thus:

$$\alpha = w_1 + w_2 \quad (73)$$

If, instead of the half-space, we first consider the impact of two spheres with the radii  $R_1$  and  $R_2$  and the masses  $m_1$  and  $m_2$  respectively then the equation of motion can be written as follows:

$$P = -m_1 \ddot{w}_1 = -m_2 \ddot{w}_2 = \frac{m_1 m_2}{w_1 w_2} \ddot{\alpha} \quad (74)$$

From (66) follows that:

$$\ddot{\alpha} = \ddot{w}_1 + \ddot{w}_2 \quad \left| \begin{array}{l} r = 0 \\ x = 0 \end{array} \right. \quad (75)$$

By combining equations (72) and (74) and integrating using the initial conditions  $\dot{\alpha}(0) = v(0)$ ;  $\alpha(0) = 0$  where  $v(0)$  is the relative impact velocity at the beginning of contact, i.e., the sum of the velocities of the two spheres:  $v(0) = v_1(0) + v_2(0)$ , one obtains:

$$\ddot{\alpha} = - \frac{m_1+m_2}{m_1m_2} k_2 \alpha^{3/2} = k_1k_2 \alpha^{3/2} \quad (76)$$

and

$$\frac{1}{2} [\dot{\alpha}^2 - v(0)^2] = - \frac{2}{5} k_1k_2 \alpha^{5/2} \quad (77)$$

The maximum approach occurs when  $\alpha = 0$ , consequently:

$$\alpha_m = \left[ \frac{5}{4} \frac{v(0)^2}{k_1k_2} \right]^{2/5} \quad (78)$$

The approach  $\alpha$  at any time  $t$  is given by:

$$t = \int_0^{\alpha} \frac{d\alpha}{v(0)^2 - \frac{4}{5} k_1k_2 \alpha^{5/2}} \quad (79)$$

Since the deformation process is assumed to be perfectly reversible the maximum approach occurs exactly at the midpoint of the contact period. This contact period may be found by integrating equation (77). For this purpose we introduce a dimensionless variable  $Z = \frac{\alpha}{\alpha_m}$  and obtain:

$$\begin{aligned}
 T &= 2 \int_0^{1/2T} dt = 2 \int_0^{\alpha_m} \frac{d\alpha}{\sqrt{v(0)^2 - \frac{4}{5} k_1 k_2 \alpha^{5/2}}} \\
 &= \frac{2 \alpha_m}{v(0)} \int_0^1 \frac{dz}{\sqrt{1 - z^{5/2}}}
 \end{aligned} \tag{80}$$

The solution of the integral yields:

$$\begin{aligned}
 T &= \frac{4}{5} \sqrt{\pi} \frac{\Gamma(\frac{2}{5})}{\Gamma(\frac{9}{10})} \frac{\alpha_m}{v(0)} = 2.943 \frac{\alpha_m}{v(0)} \\
 &= \frac{2.943}{v(0)^{1/5}} \left[ \frac{5}{4 k_1 k_2} \right]^{2/5}
 \end{aligned} \tag{81}$$

where  $\Gamma$  is the gamma function.

Hunter (1957) gives a simplified approximation for the relation expressed in equation (79) as:

$$\alpha = \alpha_m \sin \frac{1.068 v(0)t}{\alpha_m} \tag{82}$$

Thereby the force  $P$  becomes a function varying with time according to a sine-curve:

$$\begin{aligned}
 P &= \frac{1.140 v(0)^2}{k_1 \alpha_m} \sin \frac{1.068 v(0)t}{\alpha_m} ; 0 < t < \frac{\pi \alpha_m}{1.068 v(0)} \\
 P &= 0 ; t > \frac{\pi \alpha_m}{1.068 v(0)}
 \end{aligned} \tag{83}$$

If we let the radius of the second sphere  $R_2$  become infinitely large, we have the impact of a sphere on a half-space instead of the impact of two spheres.

The equations (73) through (83) do not change except that the impact parameters  $k_1$ ,  $k_2$ ,  $a$ ,  $\alpha$ ,  $\alpha_m$ , and  $T$  are simplified considerably. A tabulation of these parameters for the two cases in question yields the following values (Goldsmith, 1960).

Table 2  
Elastic Parameters for the Hertz Impact Theory

impact parameter	centric impact of two elastic spheres with radii $R_1$ and $R_2$	normal impact of an elastic sphere with radius $R_1$ on the elastic half-space
$k_1$	$\frac{m_1 + m_2}{m_1 m_2}$	$\frac{1}{m_1} = \frac{3}{4\pi \rho_1 R_1^3}$
$k_2$	$\frac{4}{3} \left( \frac{1}{\delta_1 + \delta_2} \right) \sqrt{\frac{R_1 R_2}{R_1 + R_2}}$	$\frac{4}{3\pi} \frac{1}{\delta_1 + \delta_2} \sqrt{R_1}$
$a^2$	$\frac{3\pi}{4} \frac{R_1 R_2}{R_1 + R_2} (\delta_1 + \delta_2) P$	$\frac{3\pi}{4} R_1 (\delta_1 + \delta_2) P$
$\alpha$	$a^2 \frac{R_1 + R_2}{R_1 R_2} = \frac{3\pi}{4a} (\delta_1 + \delta_2) P$	$\frac{a^2}{R_1} = \frac{3\pi}{4a} (\delta_1 + \delta_2) P$
$\alpha_m$	$\left[ \frac{15\pi v(o)^2 (\delta_1 + \delta_2) m_1 m_2}{16(m_1 + m_2)} \right]^{2/5} \left[ \frac{R_1 + R_2}{R_1 R_2} \right]^{1/5}$	$\left[ \frac{15\pi v(o)^2 (\delta_1 + \delta_2) m_1}{16 \sqrt{R_1}} \right]^{2/5}$
$T$	$4.53 \left[ \frac{(\delta_1 + \delta_2) m_1 m_2}{m_1 + m_2} \right]^{2/5} \left[ \frac{R_1 + R_2}{v(o) R_1 R_2} \right]^{1/5}$	$4.53 \left[ \frac{(\delta_1 + \delta_2) m_1}{\sqrt{R_1} v(o)} \right]^{2/5}$

The values  $\delta_1$  and  $\delta_2$  designate the elastic constants for the spheres 1 and 2 respectively for the Hertz impact problem and are determined by:

$$\delta = \frac{1 - \nu^2}{E} \quad (84)$$

where  $E = Y$  or  $G$ 's modulus,  $\nu =$  Poisson's ratio.

As stated initially these relationships are valid if the vibration energy is negligible. According to Hunter (1957) the ratio of vibrational energy  $E_v$  to total energy  $E_0$  for the impact of a sphere on the half-space according to (83) is given by:

$$\frac{E_v}{E_0} = \frac{2.7}{gc^3} \left[ \frac{3v(0)^3}{4\pi \rho_1 g} \right]^{1/5} \quad (85)$$

where  $g$  is the gravitational acceleration and  $c$  the velocity of sound in the half-space. The vibrational energy, hence, is very small as long as the impact velocity is smaller than  $c$ .

The second basic assumption for the Hertz impact problem, namely complete elasticity and reversibility of the deformation, is much farther off the mark. If we compute e.g. the resulting impact force according to (72) with the corresponding values of Table 2, we get:

$$\frac{P}{\pi a^2} = \frac{4}{3\pi^2} \frac{1}{\delta_1 + \delta_2} \sqrt{\frac{\alpha}{R_1}} \quad (86)$$

which according to (78) gives the maximum value of the resulting stresses:

$$P_m = \frac{F_{\max}}{\pi a^2} = \frac{1}{3\pi^2} (\delta_1 + \delta_2)^{-3} R_1^{-1} [30\pi(\delta_1 + \delta_2)m_1 v(o)^2]^{1/5} \quad (87)$$

If we let a sphere drop on the half-space and introduce e.g. the values of a steel sphere of 10 mm diameter and compute the height of drop which is possible without the yield stress being exceeded in the half-space material, we get the following values:

Table 3

Critical Drop Height for Elastic Impact

half-space material	Brinell hardness $H_B$	critical height plastic deformation (mm)
soft copper	55	0.0033
A-7 carbon steel	125	0.182
high strength steel alloy	320	3.5

It is thus obvious that for most practical cases the assumption of complete elasticity and reversibility of the deformations is far from realistic.

### 3. Impact on the Plastic Half-Space

Because of the limited applicability of the Hertz theory and equation (72) an attempt was made to formulate

relationships that would hold in the plastic range. As in the case of the Hertz theory we begin again with the static load-deformation relationship and return to the results obtained by Meyer who found empirically:

$$P = \bar{k} a^{\bar{n}} \quad (3a)$$

where  $a$  is again the radius of the permanent crater and  $\bar{k}$  as well as  $\bar{n}$  are constants of the half-space material which, however, as we remember, are also dependent upon the radius  $R_1$  of the impacting sphere. If the crater is sufficiently shallow, i.e., for penetration depths  $\alpha < R/2$ , we may replace the crater radius by the crater depth according to the approximation (see Fig. 3b):

$$a^2 = 2R\alpha \quad (88)$$

Then equation (3b) may be rewritten:

$$P = k\alpha^n \quad (89)$$

where  $k$  and  $n$  are now different quantities. Equation (89) is valid until the process of restitution starts. The latter is assumed to be elastic and the relationship between the force and the deformation during this restitution process is given by

$$P = P_m \left[ \frac{\alpha - \alpha_r}{\alpha_m - \alpha_r} \right]^s ; \alpha_m \geq \alpha \geq \alpha_r \quad (90)$$

where  $\alpha_r$  is the permanent crater depth and  $\alpha_m$  the maximum

penetration. If the restitution is assumed to proceed according to Hertz, the exponent  $s$  assumes the value  $3/2$ .

Equation (89) may be assumed exact if the elastic deformation is negligible and if, moreover, the plastic flow pressure  $p_0$  is acting uniformly over the entire contact surface and remains constant throughout the penetration process (no strain hardening occurs). For this case

$$k = 2 \pi R p_0 \quad \text{and} \quad n = 1.0 \quad (91)$$

This means the load-deformation relation corresponds to that predicted by the theory of plasticity. In the general case, however, these idealizations are not satisfied because of strain hardening, the flow of the displaced material during the impact process and, finally, because of the particular stress-strain relations that obtain for the high strain velocities during impact. For these reasons the values  $k$  and  $n$  of equation (89) will in general also depend on the penetration velocity  $\dot{\alpha}$ .

For the plastic penetration of a rigid sphere with radius  $R$  into a soft target material as shown in Fig. 3b, one can establish the following simple relationship:

$$P = \pi p_0 a^2 = 2 \pi p_0 R \alpha = - m \frac{d^2 \alpha}{dt^2} \quad (92a)$$

or:

$$\ddot{\alpha} + \frac{2\pi R p_0}{m} \alpha = 0 \quad (92b)$$

The solution of this simple differential equation with the assumption that the flow pressure  $p_0$  is constant and independent of  $\alpha$  yields:

$$\alpha = v(0) \sqrt{\frac{m}{2\pi R p_0}} \sin \sqrt{\frac{2\pi R p_0}{m}} t \quad (92c)$$

The maximum crater depth occurs at the end of the impact period, namely when:

$$\dot{\alpha} = \pm v(0) \cos \sqrt{\frac{2\pi R p_0}{m}} t = 0 \quad (93a)$$

i.e. for:

$$\sqrt{\frac{2\pi R p_0}{m}} T = \frac{\pi}{2}; \quad T = \frac{\pi}{2} \sqrt{\frac{m}{2\pi R p_0}} \quad (93b)$$

Thus the maximum crater depth becomes:

$$\alpha_{\max} = v(0) \sqrt{\frac{m}{2\pi R p_0}} \quad (94)$$

Introducing (94) into (93b) yields:

$$T = \frac{\pi}{2} \frac{\alpha_m}{v(0)} = 1.57 \frac{\alpha_m}{v(0)} \quad (95)$$

As a comparison the Hertz theory gives a contact period of:

$$T = 2.943 \frac{\alpha_m}{v(0)} \quad (81)$$

and a maximum approach of:

$$\alpha_{\max} = \left[ \frac{5v(0)^2}{4k_1 k_2} \right]^{2/5} \quad (78)$$

The formulations of equations (92) to (95) assume that the dynamic flow pressure  $p_0$  is a constant. They are therefore subject to the same reservations that were made already earlier.

#### 4. Elastic-Plastic Impact

Tabor (1951) considered the impact of a rigid sphere on an elastic-plastic half-space. Assuming that the sphere of mass  $m$  falls through a height  $h_1$  onto the half-space and, after impact, rebounds to the height  $h_2$  leaving a permanent crater with radius  $a$ , one can calculate the total energy as  $E_1 = mgh_1$  and the energy of restitution  $E_2 = mgh_2$ . If one assumes, as before, the vibration energy to be negligible, the energy used to form the crater  $E_3$  must be:

$$E_3 = E_1 - E_2 = mg (h_1 - h_2) \quad (96)$$

But the energy of restitution can be computed also from the theory of elasticity because it describes a purely elastic process and one may write:

$$E_2 = mgh_2 = \frac{3}{10} \frac{P^2}{a} \pi (\delta_1 + \delta_2) \quad (97)$$

The volume of the crater, in first approximation, is given by:

$$V = \frac{\pi a^4}{4R_2} \quad (98)$$

$R_2$  is here the radius of curvature of the permanent crater which because of restitution is larger than the sphere radius  $R_1$ . If the flow pressure is again assumed constant the energy  $E_3$  is given by:

$$E_3 = p_0 V = p \frac{\pi a^4}{4R_2} = mg (h_1 - h_2) \quad (99)$$

Expressing  $R_2$  as a function of  $R_1$  by using the Hertz relations one gets:

$$\frac{1}{R_2} = \frac{1}{R_1} - \frac{3}{4} \frac{p\pi}{a^3} (\delta_1 + \delta_2) \quad (100)$$

which gives:

$$E_3 = p_0 \frac{a^4}{4R_1} - \frac{3}{16} \frac{p^2}{a} \pi (\delta_1 + \delta_2) \quad (101a)$$

The first term is simply  $p_0 V_s$  where  $V_s$  is the apparent volume of the crater which would result if the crater had the same radius  $R_1$  as the sphere. The second term is nothing else but  $\frac{5}{8} E_2$  as a comparison with (97) reveals at once. Therefore:

$$E_3 = p_0 V_s - \frac{5}{8} E_2 \quad (101b)$$

from which one gets for the flow pressure:

$$p_0 = \frac{mg (h_1 - \frac{3}{8} h_2)}{V_s} \quad (102)$$

It is obvious that for small values of  $h_2$

$$p_0 = \frac{mgh_1}{V_s} \quad (103)$$

This result was already observed experimentally by Markel (1895).

For the derivation of equations (96) through (103) again a constant flow pressure was assumed. For the case of a variable flow pressure one can again return to the relation obtained by Meyer:

$$p = \frac{P}{d^2} = K d^{n-2} \quad (6a)$$

where  $n$  is a value between 2.2 and 2.5. Then the energy of plastic deformation would be:

$$E_3 = \frac{4}{n+2} pV \quad (104)$$

where now  $p$  is the average flow pressure at the end of the deformation process.

$$p = \frac{n+2}{4} mg \frac{h_1 - \frac{2n-1}{2(n+2)} h_2}{v_a} \quad (105)$$

This formula yields values about 10 to 12% larger than those computed from equation (102).

## VI. Impact of a Sphere on a Viscoelastic Half-Space

### 1. Principles of Rheology

The theory of elasticity and that of plasticity determine the solution of problems of stress or deformation by assuming idealized stress-strain laws. However, most engineering materials follow these laws only approximately. Moreover, these solutions have an additional deficiency, namely they completely ignore an additional dimension - time.

These theories assume that upon load application a state of strain is attained instantaneously and, thereafter, without a change of the load no change of stress or strain can take place. Unfortunately, real materials do not behave that way. Time-dependent deformation (creep) and, often combined with it, changes in stress (relaxation) do take place and these occur in every material under any state of stress. In some cases, fortunately, stress relaxation and creep are negligible (as for example, for steel at normal loads and temperatures). For softer materials as e.g. asphalt, plastics and especially for soils these time-dependent deformations however make up the major portion of the total deformation. For this reason a consideration of these time-dependent processes becomes necessary.

The relatively young branch of mechanics that deals with the time-dependent deformation of solid bodies is rheology.

As the theory of elasticity rheology formulates idealized stress-strain-time laws. With these idealized laws of material behavior solutions for a given problem are found which now are time-dependent.

To visualize the conditions prevailing one often works with rheological models which are built in such a way that the equations describing their deformations have the same mathematical structure as the stress-strain-time laws of the material under consideration. As building blocks for these models the following elements are used:

<u>element</u>	<u>symbol</u>	<u>deformation equation</u>	<u>description</u>
Hooke	G	$\tau_{ij} = G \gamma_{ij}$	elastic body
Newton	$\eta$	$\tau_{ij} = \eta \dot{\gamma}_{ij}$	viscous fluid
St. Venant		$\gamma_{ij} = 0 ; \tau_{ij} < k$ $(\tau_{ij} - k) = \eta \dot{\gamma}_{ij} \quad \tau_{ij} > k$	rigid plastic body

Combination of the Hooke and Newton elements in parallel yields the Kelvin model with the deformation equation:

$$\tau_{ij} = G \gamma_{ij} + \eta \dot{\gamma}_{ij} \quad (106)$$

combination in series on the other hand yields the Maxwell model with the deformation equation:

$$\dot{\gamma}_{ij} = 1/\eta \tau_{ij} + 1/G \dot{\tau}_{ij} \quad (107)$$

By combining Kelvin or Maxwell models in parallel or in series very complicated material behavior can be described (see Fig. 18). The corresponding deformation equations can be found by the proper combination of equations (106) and (107). In general form the deformation equation of these various models can be given as:

$$\begin{aligned} & (p_n \frac{d^n}{dt^n} + p_{n-1} \frac{d^{n-1}}{dt^{n-1}} + \dots + p_1 \frac{d}{dt} + p_0) \tau = \\ & (q_{n+1} \frac{d^{n+1}}{dt^{n+1}} + q_n \frac{d^n}{dt^n} + \dots + q_1 \frac{d}{dt} + q_0) \end{aligned} \quad (108a)$$

or

$$R(\tau) = S(\gamma) \quad (108b)$$

where R and S are polynomials of the operator d/dt with constant coefficients. As can be seen, derivatives with respect to time appear in the deformation law which means that in the solution of a problem partial derivatives with respect to the time as well as with respect to the coordinates x, y, z will appear.

For certain special problems, namely if the time-dependence is linear, the problems may be solved by introducing a Laplace or Fourier transformation. By this method the problem is "translated" into a simpler problem in the Laplace or Fourier domain which is now time-independent. The solution is then carried out in this domain and is generally

much simpler but the results later have to be translated back into the real domain and in this translation the time-dependence reappears. This method is used frequently for the simplification of complex mathematical problems (Doetsch, 1937) and was applied by Lee (1955) to the determination of the stresses and deformations of viscoelastic bodies.

In doing this Lee found that the viscoelastic problem in the real domain always was reduced to the purely elastic problem in the Laplace domain. This means that problems solved by the theory of elasticity can be retranslated into viscoelastic problems provided the method of Lee is applicable in principle. This requires that the stress-strain law be linear and permit superposition as follows:

If the stress  $\sigma_1(t)$  yields the strain  $\epsilon_1(t)$  and  $\sigma_2(t)$  the strain  $\epsilon_2(t)$  respectively, then the stress-strain law is said to be linear if and only if upon application of  $\sigma_1(t) + \sigma_2(t)$  the strain at any time will be  $\epsilon_1(t) + \epsilon_2(t)$ .

As in the case of the linearity postulated by Hooke's law in the theory of elasticity real materials will probably satisfy this linearity condition only approximately. Nevertheless, the elastic-viscoelastic analogy has been found to be a versatile and powerful tool in recent years for the solution of viscoelastic problems.

## 2. Solutions by the Elastic-Viscoelastic Analogy

In 1957 Lee himself applied his method to the contact problem of Hertz and found for the contact stresses of a sphere on a half-space subject to a sudden force  $Q$  according to (108a):

$$R [p(r,t)] = \frac{4}{R_1} S [\sqrt{a^2 - r^2}] \quad (109a)$$

and

$$R [p(t)] = \frac{8}{3R_1} S(a^3) \quad (109b)$$

As one can see, the operators  $R$  and  $S$  act on the load and on the deformation respectively. For a body behaving like a Maxwell model equation (108a) yields:

$$R = p_0 + p_1 \frac{\partial}{\partial t} ; \quad S = \frac{\partial}{\partial t} \quad (110)$$

A comparison with (107) shows that  $p_0 = \frac{1}{\eta}$  and  $p_1 = G$ .

For a suddenly applied load  $Q$  which thereafter remains constant, equations (109) yield:

$$a^3 = \frac{3}{8} R_1 Q (p_1 + p_0 t) \quad (111)$$

The solution follows after the translation back into the real domain which is very simple in this case:

$$p(r,t) = \frac{4}{\pi R_1 G} \left[ \sqrt{a^2 - r^2} - \frac{\eta}{G} \int_0^t e^{-\frac{\eta}{G}(t-\tau)} \sqrt{a^2 - r^2} d\tau \right] \quad (112)$$

The resulting stress distribution is compared with that of Hertz in Fig. 19.

For the half-space behaving like a Kelvin model the relationship was found in a similar manner and gave:

$$a^3 = \frac{3}{8} \frac{R_1 Q}{G} \left( 1 - e^{-\frac{G}{\eta} t} \right) \quad (113)$$

The solutions just found still have some important deficiencies which do not permit their application to the drop penetrometer problem. First, the Maxwell or Kelvin models are still too simple to describe a somewhat complex material behavior and, secondly, Lee assumed for his solution that the load  $Q$  was applied according to a unit step function and remained constant thereafter. Both these conditions are different in the drop penetrometer experiment, although one might consider the results (112) and (113) as rather elementary and rough approximations.

Below we will derive a solution for a more complete rheological model for the half-space and for a force that increases and decays monotonously with time, i.e. one that varies as a sine curve according to equation (83).

### 3. Impact of a Sphere on the Four-Parameter Half-Space

Inspection of equations (106) and (107) shows at once that for a constant load on a Maxwell model, e.g. the deformations increase linearly with time without any limit. Upon unloading there is an immediate elastic rebound which corresponds to the instantaneous deformation exhibited when the load was first applied. The Kelvin model on the other hand does not have any permanent deformation upon unloading and merely exhibits delayed elasticity. The Kelvin body requires, however, a certain time until all the deformations are recovered.

Since the mathematical difficulties increase very rapidly with an increasing number of model elements - as we shall see shortly - it is advantageous to choose the simplest model that still is able to represent the material behavior adequately and with sufficient accuracy. The simplest model that satisfactorily expresses the mechanical behavior of a soil is the four-parameter model (Fig. 20). It may be considered as a combination of a Maxwell and a Kelvin model in series or a model according to Fig. 18c with Kelvin elements in series and  $n = 3$  where the first and last element are degenerated.

The differential equation of the four-parameter model is:

$$D^2\tau + \left(\frac{G_1}{\eta_1} + \frac{G_1}{\eta_2} + \frac{G_2}{\eta_2}\right) D\tau + \frac{G_1}{\eta_1} \frac{G_2}{\eta_2} = G_1 D^2\gamma + G_1 \frac{G_2}{\eta_2} D\gamma \quad (114)$$

and its Laplace transformation is given by:

$$\begin{aligned} s^2 \bar{\tau} - s\tau(0) - \dot{\tau}(0) + \left( \frac{G_1}{\eta_1} + \frac{G_1}{\eta_2} + \frac{G_2}{\eta_2} \right) [s\bar{\tau} - \tau(0)] + \frac{G_1}{\eta_1} \frac{G_2}{\eta_2} \bar{\tau} \\ = G_1 [s^2 \bar{\gamma} - s\dot{\gamma}(0) - \ddot{\gamma}(0)] + G_1 \frac{G_2}{\eta_2} [s\bar{\gamma} - \dot{\gamma}(0)] \end{aligned} \quad (115)$$

If we introduce the initial conditions:

$$\tau(0) = \dot{\tau}(0) = 0; \text{ hence, also } \dot{\gamma}(0) = \ddot{\gamma}(0) = 0$$

we get:

$$\left[ s^2 + \left( \frac{G_1}{\eta_1} + \frac{G_1}{\eta_2} + \frac{G_2}{\eta_2} \right) s + \frac{G_1}{\eta_1} \frac{G_2}{\eta_2} \right] \bar{\tau} = \left[ G_1 s^2 + \frac{G_1 G_2}{\eta_2} s \right] \bar{\gamma} \quad (116)$$

Then the viscoelastic analogy yields:

$$\bar{\tau} = 2 \mu \bar{\gamma} \quad (117)$$

where the viscoelastic analogy modulus  $\mu$  is given by:

$$\mu = \frac{G_1}{2} \frac{s^2 + \frac{G_2}{\eta_2} s}{s^2 + \left( \frac{G_1}{\eta_1} + \frac{G_1}{\eta_2} + \frac{G_2}{\eta_2} \right) s + \frac{G_1}{\eta_1} \frac{G_2}{\eta_2}} \quad (118)$$

We now return to the elastic problem of Hertz and rewrite equation (62) as follows:

$$w = \frac{3}{8} (1 - \nu) \frac{P}{Ga} - \frac{3}{16} (1 - \nu) \frac{Pr^2}{Ga^3} \quad (119)$$

By introducing Lamé's constants  $\lambda$  and  $\mu$ :

$$G = \mu$$

$$\nu = \frac{\lambda}{2(\lambda + \mu)}$$

equation (119) is rewritten as

$$w = \frac{3}{16} \frac{\lambda + 2\mu}{\mu(\lambda + \mu)} \frac{P}{a^2} \left( a - \frac{r^2}{2a} \right) \quad (120)$$

At  $r = 0$ , the total penetration of the drop capsule can be obtained as

$$w = \frac{3}{16} \frac{\lambda + 2\mu}{\mu(\lambda + \mu)} \frac{P}{a} \quad (121)$$

For a spherical shaped head of the drop capsule

$$a = \sqrt{w(R - \frac{w}{4})} \quad (122)$$

It is thus obvious that a non-linear relationship exists between  $w$  and  $P$  such that the Laplace transform cannot be applied directly. However, we can introduce a quantity, say  $b = wa$ , which varies linearly with the force  $P$ :

$$b = wa = \frac{3}{16} \frac{\lambda + 2\mu}{\mu(\lambda + \mu)} P \quad (123)$$

If  $P$  varies with time as indicated by (83),  $P = P_m \sin \omega t$ , we have:

$$b = \frac{3}{16} \frac{\lambda + 2\mu}{\mu(\lambda + \mu)} P_m \sin \omega t \quad (124)$$

Then the viscoelastic solution in the Laplace transform domain is

$$\bar{b}(s) = \frac{3P_m}{16} \frac{\bar{\lambda} + 2\bar{\mu}}{\bar{\mu}(\bar{\lambda} + \bar{\mu})} \{ \overline{\sin \omega t} \} \quad (125)$$

Letting

$$\bar{\phi} = \frac{\bar{\lambda} + 2\bar{\mu}}{\bar{\mu}(\bar{\lambda} + \bar{\mu})} \quad (126)$$

and introducing

$$\lambda = K - \frac{2}{3} \mu \quad (127)$$

we obtain

$$\begin{aligned} \bar{\phi}(s) &= \frac{\bar{\lambda} + 2\bar{\mu}}{\bar{\mu}(\bar{\lambda} + \bar{\mu})} \\ &= \frac{2}{G_1} \frac{1}{1+\Gamma} \left\{ (1+4\Gamma) - \frac{3\Gamma}{1+\Gamma} \frac{(\omega_1+k\omega_2)s + \omega_1\omega_2}{s^2 + \left(\frac{\omega_1+k\omega_2}{1+\Gamma} + \omega_2\right)s + \frac{\omega_1\omega_2}{1+\Gamma}} \right. \\ &\quad \left. + \frac{[(\omega_1+k\omega_2)s+\omega_1\omega_2][((1+4\Gamma)s^2+(\omega_1+\omega_2+k\omega_2+4\Gamma\omega_2)s+\omega_1\omega_2)]}{s(s+\omega_2)[s^2 + \left(\frac{\omega_1+k\omega_2}{1+\Gamma} + \omega_2\right)s + \frac{\omega_1\omega_2}{1+\Gamma}]} \right\} \end{aligned} \quad (128)$$

where

$$\Gamma = \frac{G_1}{6K}, \quad k = \frac{G_1}{G_2}, \quad \omega_1 = \frac{G_1}{\eta_1}, \quad \omega_2 = \frac{G_2}{\eta_2}$$

and K is the bulk modulus introduced earlier instead of  $\lambda$ .

The inverse Laplace transform yields:

$$\phi(t) = \frac{2}{G_1} \frac{1}{1+\Gamma} \left\{ (1+4\Gamma)\delta(t) + (1+\Gamma)(\omega_1+k\omega_2 e^{-\omega_2 t} + \beta_1 e^{-\omega_3 t} + \beta_2 e^{-\omega_4 t}) \right\} \quad (129)$$

where

$$\omega_3 = \frac{1}{2} \left\{ \omega_2 + \frac{1}{1+\Gamma}(\omega_1+k\omega_2) \right\} \pm \frac{1}{2} \left\{ \left[ \omega_2 + \frac{1}{1+\Gamma}(\omega_1+k\omega_2) \right]^2 - \frac{4}{1+\Gamma} \omega_1\omega_2 \right\}^{\frac{1}{2}}$$

$$\beta_1 = \frac{1}{1+\Gamma} \alpha_1 \left\{ \frac{1+2\Gamma+4\Gamma^2}{1+\Gamma} + \frac{k\omega_2}{\omega_2-\omega_3} - \frac{\omega_1}{\omega_3} \right\}$$

$$\beta_2 = \frac{1}{1+\Gamma} \alpha_2 \left\{ \frac{1+2\Gamma+4\Gamma^2}{1+\Gamma} + \frac{k\omega_2}{\omega_2-\omega_4} - \frac{\omega_1}{\omega_4} \right\}$$

$$\alpha_1 = \frac{\omega_1\omega_2 - \omega_1\omega_3 - k\omega_2\omega_3}{\omega_4 - \omega_3}$$

$$\alpha_2 = \frac{\omega_1\omega_2 - \omega_1\omega_4 - k\omega_2\omega_4}{\omega_3 - \omega_4}$$

By using the convolution theorem, the inverse Laplace transform of equation (125) gives the viscoelastic solution in the real domain:

$$\begin{aligned} b(t) &= \frac{3P_m}{16} \int_0^t \phi(t-\tau) \sin \omega \tau d\tau \\ &= \frac{3P_m}{8G_1} \left\{ \left[ \frac{1+4\Gamma}{1+\Gamma} + \frac{k\omega_2^2}{\omega^2 + \omega_2^2} + \frac{\beta_1\omega_3}{\omega^2 + \omega_3^2} + \frac{\beta_2\omega_4}{\omega^2 + \omega_4^2} \right] \sin \omega t \right. \\ &\quad - \left[ \frac{\omega_1}{\omega} + \frac{k\omega\omega_2}{\omega^2 + \omega_2^2} + \frac{\beta_1\omega}{\omega^2 + \omega_3^2} + \frac{\beta_2\omega}{\omega^2 + \omega_4^2} \right] \cos \omega t \\ &\quad \left. + \frac{\omega_1}{\omega} + \frac{k\omega\omega_2}{\omega^2 + \omega_2^2} e^{-\omega_2 t} + \frac{\beta_1\omega}{\omega^2 + \omega_3^2} e^{-\omega_3 t} + \frac{\beta_2\omega}{\omega^2 + \omega_4^2} e^{-\omega_4 t} \right\} \end{aligned} \quad (130)$$

From equations (122) and (130), the viscoelastic deformation  $w(t)$  can be calculated. Since the equation (130) involves a complex combination of the elementary model parameters  $G_1$ ,  $G_2$ ,  $\eta_1$ ,  $\eta_2$ ,  $K$ , it has to be calculated by an electronic computer.

The principal difficulty is that the material parameters do not appear in linear form or combinations only. Thus it is not at all certain that a unique, real solution exists and it is possible that several different sets of parameters will satisfy the experimental data with sufficient accuracy.

## VII. The Vibrations of the Half-Space due to Impact

### 1. Basic Equations

For an isotropic, homogeneous and ideally elastic body the equations of motion for the propagation of an impact wave can be given by the equations of motion (131) below. For a soil the first two conditions are satisfied frequently, at least in a statistical sense, whereas the latter (ideal elasticity) surely is an approximation only. These equations are:

$$(\lambda + \mu) \frac{\partial \epsilon}{\partial x} + \mu \nabla^2 u + X = \rho \frac{\partial^2 u}{\partial t^2} \quad (131a)$$

$$(\lambda + \mu) \frac{\partial \epsilon}{\partial y} + \mu \nabla^2 v + Y = \rho \frac{\partial^2 v}{\partial t^2} \quad (131b)$$

$$(\lambda + \mu) \frac{\partial \epsilon}{\partial z} + \mu \nabla^2 w + Z = \rho \frac{\partial^2 w}{\partial t^2} \quad (131c)$$

where  $u$ ,  $v$ , and  $w$  are the elastic displacement components in the cartesian coordinate system  $x$ ,  $y$ ,  $z$ ; and  $\epsilon$  being the volume change as in equation (22):

$$\epsilon = \frac{\partial u}{\partial x} + \frac{\partial v}{\partial y} + \frac{\partial w}{\partial z} \quad (132)$$

$$\nabla^2 = \frac{\partial^2}{\partial x^2} + \frac{\partial^2}{\partial y^2} + \frac{\partial^2}{\partial z^2} \quad (133)$$

is the Laplace Operator,  $\rho$  the density;  $X$ ,  $Y$ ,  $Z$  are the components of the body forces while  $\lambda$  and  $\mu$ , as before, are the Lamé constants related as follows:

$$\lambda = \frac{\nu}{(1+\nu)(1-2\nu)} ; \quad E = K - \frac{2}{3} G ; \quad \mu = \frac{1}{2(1+\nu)} E = G \quad (134)$$

In an elastic material with infinite dimensions in all directions a dynamic disturbance causes two types of waves independent of each other such that the total displacement of any point may be considered as the sum of the two independent displacements:

$$u = u_1 + u_2 ; \quad v = v_1 + v_2 ; \quad w = w_1 + w_2 \quad (135)$$

The components of the first wave are irrotational, i.e., satisfy the conditions:

$$\frac{\partial w_1}{\partial y} - \frac{\partial v_1}{\partial z} = \frac{\partial u_1}{\partial z} - \frac{\partial w_1}{\partial x} = \frac{\partial v_1}{\partial x} - \frac{\partial u_1}{\partial y} = 0 \quad (136)$$

which means that they are determined by potential functions:

$$u_1 = \frac{\partial \phi}{\partial x} ; \quad v_1 = \frac{\partial \phi}{\partial y} ; \quad w_1 = \frac{\partial \phi}{\partial z} \quad (137)$$

The components of the second wave are without dilation, i.e., they satisfy the condition:

$$\epsilon_2 = \frac{\partial u_2}{\partial x} + \frac{\partial v_2}{\partial y} + \frac{\partial w_2}{\partial z} = 0 \quad (138)$$

Thus the total displacements become:

$$u = \frac{\partial \phi}{\partial x} + u_2 ; \quad v = \frac{\partial \phi}{\partial y} + v_2 ; \quad w = \frac{\partial \phi}{\partial z} + w_2 \quad (139)$$

Substituting these values into the equations of motion (131) yields:

$$\frac{\partial^2 \phi}{\partial t^2} = a^2 \nabla^2 \phi \quad (140)$$

$$\frac{\partial^2 u_2}{\partial t^2} = b^2 \nabla^2 u_2 \quad (141a)$$

$$\frac{\partial^2 v_2}{\partial t^2} = b^2 \nabla^2 v_2 \quad (141b)$$

$$\frac{\partial^2 w_2}{\partial t^2} = b^2 \nabla^2 w_2 \quad (141c)$$

where

$$a^2 = \frac{\lambda + 2\mu}{\rho} ; \quad b^2 = \frac{\mu}{\rho}$$

The deformations according to equation (140) are pure volume changes according to

$$\varepsilon_1 = \nabla^2 \phi \quad (142)$$

For this reason the wave given by equation (140) is often called dilatational or longitudinal wave. The second type of wave because of equation (138) is free of any dilatation.

The propagation of this wave yields only relative displacements whose components are given by:

$$2 u_2 = \frac{\partial w_2}{\partial y} - \frac{\partial v_2}{\partial z} \quad (143a)$$

$$2 v_2 = \frac{\partial u_2}{\partial z} - \frac{\partial w_2}{\partial x} \quad (143b)$$

$$2 w_2 = \frac{\partial v_2}{\partial x} - \frac{\partial u_2}{\partial y} \quad (143c)$$

For this reason the wave given by equations (141) is called a shear wave. In a dilatational wave the movement of a point is in the direction of wave propagation, in a shear wave it is normal to it. The equations (140) and (141) are not coupled which means that the two motions are entirely independent from each other.

## 2. Propagation Velocities

Integrals of equations (140) and (141) can be written in the following form:

$$\frac{1}{r} F \left( t - \frac{r}{c} \right) \quad (144)$$

where  $r$  is the radius vector of the point under consideration,  $F$  is an arbitrary function which satisfies the initial and the boundary conditions. The propagation velocity  $c = a$  for the longitudinal waves and  $c = b$  for the shear waves. Using equation (134) these can be computed from:

$$a = \sqrt{\frac{1-\nu}{(1+\rho)(1-2\nu)} \frac{E}{\rho}} = \sqrt{\frac{2(1-\nu)G}{(1-2\nu)}} \quad (145)$$

$$b = \sqrt{\frac{1}{2(1+\nu)} \frac{E}{\rho}} = \sqrt{\frac{G}{\rho}} \quad (146)$$

from which follows that the propagation velocities depend only upon the elastic constants.

The ratio of the velocities

$$\frac{a}{b} = \sqrt{\frac{2(1-\nu)}{1-2\nu}}$$

is, hence, always larger than unity. Barkan (1948) gives the following values for these velocities:

Table 4  
Wave Propagation Velocities in Soils

Soil Type	density kg sec <sup>2</sup> /cm <sup>4</sup> 10 <sup>-6</sup>	a m/sec	b m/sec
Moist Clay	1.80	1500	150
Loess (nat. water cont.)	1.67	800	260
Dense Sand & Gravel	1.70	480	250
Fine Sand	1.65	300	110
Medium Sand	1.65	550	160
Medium Gravel	1.80	750	180

### 3. Vibrations Due to a Point Load

Assuming that we deal with simple harmonic waves originating from a point source we will attempt to find solutions of equations (140) and (141) by introducing the following functions:

$$\varphi = e^{i\omega t} \phi(x,y,z) \quad (147)$$

and

$$u_2 = e^{i\omega t} U ; \quad v_2 = e^{i\omega t} V ; \quad w_2 = e^{i\omega t} Z \quad (148)$$

where  $\omega$  is the exciter frequency. Introducing these functions into the wave equation the following conditions must obtain:

$$(\nabla^2 + h^2) \phi = 0 \quad (149)$$

and

$$(\nabla^2 + k^2) U = (\nabla^2 + k^2) V = (\nabla^2 + k^2) W = 0 \quad (150)$$

Moreover, because of (138) the functions  $U$ ,  $V$ , and  $W$  must also satisfy:

$$\frac{\partial U}{\partial x} + \frac{\partial V}{\partial y} + \frac{\partial W}{\partial z} = 0 \quad (151)$$

The solutions for equations (150) can be found by the substitutions:

$$U = \frac{\partial^2 \psi}{\partial x \partial y} ; \quad V = \frac{\partial^2 \psi}{\partial y \partial z} ; \quad W = \frac{\partial^2 \psi}{\partial z^2} + k^2 \psi \quad (152)$$

Introducing these values into (150) reveals that  $\psi$  must satisfy:

$$(\nabla^2 + k^2) \psi = 0 \quad (153)$$

Let us now consider a cylindrical coordinate system for the half-space with its origin at the surface such that:

$$x = r \cos \theta ; \quad y = r \sin \theta ; \quad z = z$$

for which the Laplace operator becomes

$$\nabla^2 = \frac{\partial^2}{\partial r^2} + \frac{1}{r} \frac{\partial}{\partial r} + \frac{\partial^2}{\partial z^2} \quad (154)$$

and designate the displacement in the direction of the radius vector  $r$  by  $q$ , then

$$u = \frac{x}{r} q ; \quad v = \frac{y}{r} q \quad (155)$$

Thus, according to (139) and (152), we get:

$$q = \frac{\partial \phi}{\partial r} + \frac{\partial^2 \psi}{\partial r \partial z} ; \quad w = \frac{\partial \phi}{\partial z} + \frac{\partial^2 \psi}{\partial z^2} + k^2 \psi \quad (156)$$

We now introduce a dynamic load  $P_z$ :

$$P_z = - P J_0(\alpha r) \quad (157)$$

$$(\tau_{rz} = 0)$$

which is applied at the surface  $z = 0$ .  $J_0(\alpha r)$  is, as before, a Bessel Function.

Again we assume a solution for (149) and (150) analogously to (36):

$$\phi = A e^{-\alpha z} J_0(\alpha r) ; \quad \psi = B e^{-\beta z} J_0(\xi, r) \quad (158)$$

where  $A$ ,  $B$  and  $\xi$  are arbitrary constants which can be determined from the boundary conditions:

$$\frac{\sigma_z}{\mu} = - k^2 \phi - 2 \frac{\partial^2 \phi}{\partial r^2} - 2 \frac{\partial^2 \psi}{\partial r \partial z} \quad (159a)$$

$$\frac{\tau_{rz}}{\mu} = 2 \frac{\partial^2 \phi}{\partial r \partial z} - k^2 \psi - 2 \frac{\partial^2 \psi}{\partial z^2} \quad (159b)$$

which yield:

$$A = \frac{2\xi^2 - k^2}{F(\xi)} \frac{P}{\mu} ; \quad B = \frac{2}{F(\xi)} \frac{P}{\mu} \quad (160)$$

$$F(\xi) = (2\xi^2 - k)^2 - 4\xi^2 \alpha\beta \quad (161)$$

Hence, the displacement components at the surface ( $z = 0$ ) can be computed from (156):

$$g_0 = \frac{-\xi(2\xi^2 - k^2 - 2\alpha\beta)}{F(\xi)} J_1(\xi, r) \frac{P}{\mu} \quad (162a)$$

$$w_0 = \frac{k^2}{F(\xi)} J_0(\xi, r) \frac{P}{\mu} \quad (162b)$$

Let us now examine the case that  $P$  have the form:

$$F_v e^{i\omega t} \quad \text{i.e.}$$

$$P = - \frac{P_v}{2\pi} \xi d\xi$$

Introducing this value into (162) and integrating we obtain the displacements of the surface of the half-space:

$$g_0 = \frac{P_v}{2\pi\mu} \int_0^\infty \frac{\xi^2(2\xi^2 - k^2 - 2\alpha\beta)}{F(\xi)} J_0(\xi, r) d\xi \quad (163a)$$

and

$$w_0 = - \frac{P_v}{2\pi\mu} \int_0^\infty \frac{k^2 \xi \alpha}{F(\xi)} J_0(\xi, r) d\xi \quad (163b)$$

The integrals (163) cannot be evaluated directly because  $F(\xi)$  is zero for certain values, e.g., for  $\xi = \pm \frac{\omega}{c}$ .

By introducing a new variable, rearranging and using a series approximation Shekhter (1948) succeeded in finding a solution for small values of  $\rho = kr$ :

$$w_0 = \frac{Pk}{\mu} e^{i\omega t} (f_1 + i f_2) \quad (164)$$

where the functions  $f_1$  and  $f_2$  depend on Poisson's ratio. For  $\nu = 0.5$  Shekhter obtained:

$$f_1 = -1.00196 \frac{1}{\rho} + 0.0598 \rho - 0.00607 \rho^3 + 0.000243 \rho^5 - \dots$$

$$f_2 = 0.0571 J_0(1.047) + 0.0474 - 0.00647 \rho^2 + 0.000264 \rho^4 - \dots$$

and for  $\nu = 0.25$ :

$$f_1 = -0.119 \frac{1}{\rho} + 0.0895 \rho - 0.0104 \rho^3 + 0.00466 \rho^5 - \dots$$

$$f_2 = 0.0998 J_0(1.08777) + 0.0484 - 0.00595 \rho^2 + 0.00240 \rho^4$$

In general the vertical component in the vicinity of the exciter force can be given in simplified form from (164):

$$w = -A_0 \psi(\rho) \sin(\omega t - \gamma) \quad (165a)$$

where

$$A_0 = \frac{P}{b\mu} \quad (165b)$$

$$\psi(\rho) = \sqrt{f_1^2 + f_2^2} \quad (165c)$$

and

$$\tan \gamma = \frac{f_1}{f_2} \quad (165d)$$

The function  $\psi(\rho)$  for Poisson's ratios of  $\nu = 0, 0.25$  and  $0.5$  are shown in Fig. 21.

Sauter (1950) evaluated the integrals of the displacement components for the surface of the half-space due to an

aperiodic impact and obtained the following result for a purely normal impact:

$$w_0 = - \frac{1}{2\pi\rho b^2 \left(1 - \frac{b^2}{a^2}\right)t} \sigma_1 \quad (166)$$

where  $\sigma_1$  is the impact stress.

If we introduce the values given by Barkan for dense sand ( $\rho = 1.70$ ,  $a = 480$  m/sec,  $b = 250$  m/sec) and for moist clay ( $\rho = 1.80$ ,  $a = 1500$  m/sec,  $b = 150$  m/sec), then we get:

$$w_0 = 0.0002 \frac{\delta_1}{t} \text{ for sand} \quad (167a)$$

$$w_0 = 0.0004 \frac{\delta_1}{t} \text{ for clay} \quad (167b)$$

#### 4. Damping, Dispersion and Distortion

If there are also frictional forces active in the half-space in addition to the elastic forces that tend to return the body to its original shape, then damped vibrations result. If these frictional forces are assumed to be proportional to the point velocity, the following equation describes this type of vibration:

$$\frac{\partial^2 \psi}{\partial t^2} = a^2 \nabla^2 \psi + 2\delta \frac{\partial \psi}{\partial t} \quad (168)$$

where  $\delta$  is the damping factor which is always negative. For the sake of simplicity we may consider a one-dimensional

vibration according to (168). It is advantageous to exchange the variables by substituting:

$$\varphi = Ue^{rt} \quad (169)$$

Introducing this into (168), we obtain:

$$\frac{\partial^2 U}{\partial t^2} + 2r \frac{\partial U}{\partial t} + r^2 U = a^2 \frac{\partial^2 U}{\partial x^2} + 2r \delta U + 2\delta \frac{\partial U}{\partial t} \quad (170)$$

If we introduce  $r = \delta$ , the terms with the first derivative vanish and we get:

$$\frac{\partial^2 U}{\partial t^2} = a^2 \frac{\partial^2 U}{\partial x^2} + \delta^2 U \quad (171)$$

As one can see, the solution of this equation is given by:

$$U = A \sin (rx - st) \quad (172)$$

provided that:

$$s^2 = a^2 r^2 - \delta^2 \quad (173)$$

This means that the damping factor is a function of the frequency from which follows that different frequencies are damped in a different way. This phenomenon is called distortion. Thus the wave front is changing as it progresses.

Let us consider the solution:

$$u = U e^{-i\omega t} \quad (174)$$

where  $U$  is a function of  $x$  only. Then, according to equation (168), we have:

$$\frac{\partial^2 U}{\partial x^2} = -U \left( \frac{w^2 - 2iw\delta}{a^2} \right) \quad (175)$$

This equation has two solutions of which, however, only one has a practical significance, namely, the one that does not yield infinite values for  $u$  for large values of  $x$ . If we put:

$$\frac{w^2 - 2iw\delta}{a^2} = (\alpha + i\beta)^2 \quad (176)$$

the solution becomes:

$$U = B e^{i(\alpha + i\beta)x} \quad (177)$$

which, according to equation (174), yields:

$$u = B e^{-\beta x} e^{i(\alpha x - wt)} \quad (178)$$

Since  $\beta$  is also related to the damping factor, both  $\alpha$  as well as  $\beta$  are functions of the frequency and are related by:

$$\alpha^2 - \beta^2 = \left(\frac{w}{a}\right)^2; \quad \text{and} \quad \alpha\beta = -\frac{w\delta}{a^2} \quad (179)$$

When  $\alpha$  is a function of the frequency, the phenomenon is called dispersion, when  $\beta$  is dependent on  $w$ , it is called distortion. When both phenomena occur simultaneously, the wave energy is slowly dispersed while the shape of the wave front is continuously changing.

### 5. Group Velocity and Phase Velocity

Considering two wave trains determined by:

$$\frac{\partial^2 u}{\partial t^2} = a_1^2 \frac{\partial^2 u}{\partial x^2} \quad (180a)$$

$$\frac{\partial^2 u}{\partial t^2} = a_2^2 \frac{\partial^2 u}{\partial x^2} \quad (180b)$$

where  $a_1$  and  $a_2$  are two different propagation velocities, then these trains may be considered to be of the form:

$$u_1 = A \cos \left[ p_1 \left( \frac{x}{a_1} - t \right) + E_1 \right] \quad (181a)$$

$$u_2 = A \cos \left[ p_2 \left( \frac{x}{a_2} - t \right) + E_2 \right] \quad (181b)$$

where  $f_1 = \frac{p_1}{2\pi}$ ,  $f_2 = \frac{p_2}{2\pi}$  are two different frequencies. Superposition of the two frequencies yields:

$$u = u_1 + u_2 = 2 A \cos \left[ \pi x \left( \frac{f_1}{a_2} + \frac{f_1}{a_2} \right) - \pi t (f_1 + f_2) + \frac{E_1 + E_2}{2} \right] \\ \cdot \cos \left[ \pi x \left( \frac{f_1}{a_2} - \frac{f_2}{a_2} \right) - \pi t (f_1 - f_2) + \frac{E_1 - E_2}{2} \right] \quad (182)$$

This equation describes two harmonic motions, one with a frequency and propagation velocity of:

$$f = \frac{f_1 - f_2}{2} \quad (183)$$

and

$$a = \frac{a_1 a_2 (f_1 + f_2)}{f_1 a_2 + f_2 a_1} \quad (184)$$

respectively, and the second with:

$$f' = \frac{f_1 - f_2}{2} \quad (185)$$

and

$$a' = \frac{a_1 a_2 (f_1 - f_2)}{f_1 a_2 - f_2 a_1} \quad (186)$$

We note that for the case of  $f_1 = f_2$ , equation (182) gives a harmonic motion that slowly changes amplitudes. If the maximum displacement of the point  $x = 0$  occurs at time  $t$ , then that of the point  $x$  occurs at time  $t + \frac{x}{a'}$  and returns with a period  $\frac{1}{f'}$ . An interesting characteristic of this motion is the continuously changing wave front and the recurrence of the maximum amplitudes in certain intervals.

If we consider two motions with frequencies that lie within a narrow band, say within  $f$  and  $f + \Delta f$ , we have the phenomenon of dispersion. The value of  $a'$  of equation (186) is the so-called group velocity, while the "a" given by (184) is the wave- or phase-velocity. To determine the former we introduce into (186):  $a_2 = a$ ,  $a_1 = a + \Delta a$ ,  $f_2 = f$  and  $f_1 = f + \Delta f$ , and determine  $a'$  in the limit as  $\Delta f$  approaches zero. Then:

$$a' = \frac{a}{1 - f/a \frac{da}{df}} \quad (187)$$

According to the binomial theorem and neglecting higher order terms, we get:

$$a' = a \left( 1 + f/a \frac{da}{df} \right) \quad (188)$$

If we introduce also the corresponding periods,  $T$ , and  $T + \Delta T$  and the wave lengths  $L$  and  $L + \Delta L$ , one can easily deduce from (188) that:

$$a' = \frac{\Delta(\frac{1}{T})}{\Delta(\frac{1}{L})} \quad (189)$$

The group velocity is of primary technical interest because it determines the propagation of the maximum displacements. The situation is demonstrated in Fig. 23. There a train of waves is propagated like an energy packet traveling with its group velocity without essentially changing its shape.

However, because of dampening and dispersion the amplitudes gradually become smaller and the frequencies lower. The velocities  $a$  and  $a'$  thus become also dependent upon frequency or wave length. In water, for example, long waves travel faster than short ones and the group velocity  $a'$  is half the phase velocity  $a$ . In elastic rods, on the other hand, short waves run faster than long ones and the group velocity is twice the phase velocity. The group velocity can thus be larger as well as smaller than the wave velocity. Moreover, Lamp (1904) has shown that the two velocities  $a$  and  $a'$  need not run in the same sense: the wave trains may be running toward the right with such a velocity that the center of the group moves toward the left.

## 6. Impact with High (Ballistic) Velocities

If a projectile impacts on a body with very high (ballistic) velocities, a crater develops whose volume depends on the kinetic energy of the projectile and the properties of projectile and target. This is a classic problem of ordinance research that has been investigated extensively for some time. The impact of a meteorite is a problem of a similar nature. Some recent results that especially also discuss the penetration of projectiles into sand, rock and sod are reported by Rinehart (1954), Goldsmith (1960), McCarthy and Carden (1962), and Kornhauser (1964).

Since our experiments were carried out at relatively low velocities (maximum 15 m/sec), the phenomena encountered at high velocity impact fall outside the scope of our considerations.

### VIII. Description of Test Series

The idea of measuring the deceleration upon impact of an instrumented capsule by a piezo-electric accelerometer was proposed by several people independently at about the same time. Hecht1 (1964), for example, states in his dissertation that such experiments were carried out on sand and rock at the Jet Propulsion Laboratory of the California Institute of Technology. Their instrument was to be used to explore the soil conditions of the lunar surface.

However, Hecht1 based his remarks on a preprint of a paper by Dr. Thormann which gave idealized response data. He learned during a personal visit in July 1964 that actual tests had not yet been carried out.

On the other hand, McCarthy and Carden (1962) carried out tests shooting an instrumented cylinder through a "pneumatic gun" of 20 feet in length and 6 inches in diameter against various target materials such as sod, moss, wood, sand, lead, and concrete with velocities up to 300 m/sec. At the same time the author proposed independently to use a similar capsule as a new version of an aerial penetrometer. The capsule has been described above (Chapter III, 2 and Figs. 12 and 13).

The first experiments were carried out by Dr. Hecht1 in the Soil Mechanics Laboratory of Princeton University. Hecht1

ran thirty different series of tests varying such experimental parameters as target soil, soil moisture content and density and shape of impact head.

The tests were carried out by attaching the drop capsule to an electrical release mechanism which was brought to the desired height above the soil target by a pulley-cable system. Upon impact the piezo-electric signal was transmitted through a trailing, calibrated and isolated cable, and a cathode follower to a Textronic oscilloscope. The oscilloscope screen was photographed upon arrival of the signal by a Polaroid camera. Thus a permanent record of the signal was obtained that could be evaluated later. The ordinate of the resulting photograph gives the deceleration (to some scale depending upon the amplification of the scope) as a function of the time (shown on the abscissa). A schematic sketch is shown in Fig. 22. The description of the measuring components and their calibration is given by Hechtl in his dissertation and need not be repeated here.

The first experiments showed that a perfectly centric impact occurred rarely with a conical impact head which led us to use a semispherical head for all later tests. Also, the difficulty of keeping an oblong capsule in a vertical position until impact under field conditions led us to believe that the proper shape of a prototype capsule should be a

sphere. This will avoid any problem of directional stabilization.

The instrument was tested outdoors under field conditions impacting on natural undisturbed soils and performed well. The field measurements were then carried out with the experimental setup shown in Fig. 22 except that the container with the soil target material used in the laboratory is replaced by the half-space in the field.

To measure wave propagation velocities of the target soils in the field experiments one, two or (in test series 41) even three accelerometers were buried in the soil at various distances from the impact point. They were placed with their sensitive axis parallel to the soil surface and directed toward the impact point. Since the accelerometers respond only to normal accelerations, the resulting signals are from waves of the type described by equation (140). The distances from the impact point were determined by direct chain measurement after impact and are designated by  $r_1$ ,  $r_2$  and  $r_3$ .

Since according to Newton actio equals reactio  $w$ , the penetrometer signal gives not only the force exerted by the target material on the penetrometer but also that exerted by the penetrometer on the target. Thus, the signals of those buried accelerometers show the decay and dispersion of the stress waves resulting from an aperiodic, dynamic disturbance. The signals from the buried accelerometers were usually taken

by a second camera on a second oscilloscope screen that was triggered by the penetrometer impact signal.

An attempt was also made to test the penetrometer on target materials that had clearly defined and easily determined mechanical or rheological properties. This was tried with water, soils of different viscosities, greases of different consistency, wax and paraffin. Not all of these experiments were successful. Dropping the penetrometer into water was tried, e.g., in the swimming pool in the basement of Dillor Gymnasium. Because of the extreme magnification of the signal required with the very low impact, a basic 60 cps frequency signal from the house current was somehow induced and superimposed and made the impact signal unrecognizable. This experiment was therefore abandoned. Oils as a target material also produced difficulties. The impact was often so weak that the electron beam of the oscilloscope cathode tube was not triggered.

The experiments were numbered consecutively. Continuing with the sequence begun by Hecht1 (30), thus they began with No. 31 and ended with No. 45. Table 5 lists the various experiments.

The experiments were carried out jointly by the author and his assistant, Dr. Christian Hecht1, during 1963-1964. Reproductions of the original Polaroid photographs of the oscilloscope signals are shown in the appendix (pp. A-1 to

Table 5

## List of Experiments

Series No.	Target Material	Location	Remarks
31	Wax: Cambar M-348 at 31°C	Princeton Soil Mechanics Lab.	Humble Oil Specs. Data Sheet DG-36
32	Lubricating grease Estan 3 (28°C)	" "	" " "
33	Estan 1	" "	Failed, too soft
34	Paraffin (at 28°C)	" "	
35	Water (failed)		
36	Failed		
37	Silty sand at soil surface	grass field behind Princeton Soil Mechanics Lab.	natural soil
38	Silty sand, 20" below surface	" "	" "
39	Uniform beach sand	beach at Sea- side Heights, N.J.	natural beach
40	Failed		
41	Sandy silt and clay	McCosh Circle Princeton, N.J.	natural soil
42	Sandy clay	field off U.S. 1, 2 mi. south of Princeton	field plowed & harrowed
43	Crushed rock ½-1"	Lambertville, N.J.	compacted
44	Fine sand	Sheppard's Mill Dam, Bridgeton, N.J.	natural soil
45	Swamp	Bridgeton, N.J.	

A-32). The necessary calibration constants for evaluating these data are also shown. The most important results and evaluations carried out so far are offered in the following chapter.

We have also appended those four test series carried out by Hecht1 which were conducted with a semispherical head, namely his series No. 12, 15, 19 and 22 (Appendix B-1 to B-12).

Whenever possible standard reference tests were carried out on all target materials for comparison. For natural soil surfaces this was the field CBR test. For the laboratory soils we also carried out CBR tests as well as unconfined compression tests. For the wax, paraffin and grease the values supplied by the manufacturer's data sheets were compared. Figs. 24 to 27 show some of the experimental details. For example, Fig. 24 shows the penetrometer before impact on the paraffin (Series 34); Fig. 25 shows the penetration into Estan 3 (Series 32); Fig. 26 shows the permanent, plastic deformation caused in Cambar wax; and Fig. 27 shows the test setup for Series No. 41.

## IX. Evaluation of Test Results

### 1. General Discussion of Test Data

The polaroid oscilloscope photographs in many cases (for example, in test series 12, 22, 31, 37, 38, 41, 42 and 44) give monotonously rising and falling curves which can be approximated by a sine wave. The variation of the impact force in these cases can very well be described by a formulation according to equation (83). In those cases where the curves show a significant variation from a sine curve this fact can be explained by the particular test condition. In test series 32, for example, the signal is rather constant over a considerable time interval. This was caused by the fact that in this series the depth of penetration was always larger than  $D/2$ . Thus, after an initial rise the penetration resistance remains constant because the area of penetration remains constant also and the resistance encountered is that of a viscous flow around a cylinder with a semispherical head. The last photo of that series, moreover, shows clearly the penetration of the penetrometer through the entire pail of grease (see Appendix A-5, photo 2).

In series 34 the brittleness of the target material is very clearly demonstrated. While the overall curve still follows a sine curve, successive brittle fractures cause local deviations.

A significantly different signal from that of a sine curve is revealed for all coarse grained target materials (test series 15, 19, 39, 43). First, the electron beam is broadly diffused (compare, for example, Appendix pages A-15 to A-18, B-4 to B-9). Upon increasing the sweep speed of the electron beam as done in series 43 (Appendix pages A-26 to A-28) one can observe that this diffusion of the signal is nothing but the superposition of a high frequency vibration upon the basic impact signal similar to the formulation of equation (182). This high frequency wave signal can only originate either from the natural frequency vibrations of the penetrometer or those of the piezo-electric crystal induced by a very hard impact. If one considers, however, that these vibrations do not affect the basic impact signal and are merely superimposed, the correct impact signal may be considered to be the average value within the diffuse band (see page A-28).

The superimposed natural frequency vibrations can also be detected on less hard target materials (e.g., series 12, 22, 38, 42 and 44) although to a much smaller extent and only at the beginning.

Even more surprising than the diffusion is the general shape of the signal when the target material is sand, gravel or crushed stone. There exists a definite peak force which drops off rapidly, after which comes again an increase

followed by a logarithmic decay. This can only be explained in such a way that in these materials a "temporary liquefaction" takes place at the beginning of the impact period. Since very few grains are affected initially, the specific energy per grain is very large and one can perhaps rationalize that during this short duration the grains partially lose their frictional support and behave like a quasi-fluid. Upon further penetration, however, the number of soil grains affected by the impact becomes quite large and the available energy is not sufficient to "liquefy" all these particles. Thus a stabilization of the penetration resistance occurs with a corresponding dropping off of the signal in the final phase of the impact period.

In any event, from the variation of the signals obtained it is clear that for the number of tests performed so far a fairly definite distinction can be made whether the target material was a granular, "liquefied-stabilized" soil or whether it was a plastic-cohesive soil, and whether the impact was hard or relatively soft depending on the magnitude and extent of the natural-frequency vibrations superimposed on the basic impact signal.

## 2. Impact Velocity $V(o)$

If the deceleration  $a(t)$  is known, the impact velocity can be determined from equation (14) by integrating  $a(t)$  over the impact period.

Since the oscilloscope photos - except for some constant - are nothing else but  $a(t)$  we only have to carry out the integration. Here a small technical difficulty is encountered: the sweep of the electron beam must be adjusted in such a way that a good resolution of the signal appears on the oscilloscope screen. If the beam velocity is relatively small, a high curve with a narrow base results (e.g., photos of test series 41 with a beam velocity of  $V_h = 0.2$  cm/millisecond). There the signal can be followed over a long period of time. Thus the end of the impact period can be clearly established. In the limiting case of zero horizontal beam velocity the signal, of course, would be only a vertical line. Thus it is easily possible that for a small beam velocity the signal is not sufficiently resolved along the time axis to permit integration with sufficient accuracy.

If the beam velocity, on the other hand, is relatively large (as for example in test series 42 with  $V_h = 0.5$  cm/millisecond), the signal has an excellent resolution with respect to time but the end of the impact period does no longer appear on the oscilloscope screen.

The technical solution of this dilemma is best solved by recording the signal on magnetic tape rather than by photographing an oscilloscope screen. The tape can later be run at any speed desirable and no part will be lost. For an operational penetrometer magnetic recording of the signal is probably essential. Even though such recording systems are standard items, their price is relatively high and for our pilot tests the oscilloscope photos were considered sufficient.

The evaluation of the impact velocities from the test data is, for this reason, not nearly as accurate as would be possible using the latest technology. Nevertheless, the integration of the oscilloscope curves using a planimeter yields a rather good agreement with the theoretical computed values. These were computed by assuming the frictional resistance of the penetrometer falling in air to be negligible. This assumption appeared justified because of the low velocities and small drop heights. Table 6 shows a comparison of these results.

The last column in Table 6 shows the per cent difference between the theoretically computed impact velocity and the one obtained by integrating the penetrometer signal. The mean discrepancy  $d_m$  calculated from:

$$d_m = \sqrt{\frac{\sum d_i^2}{n}} \quad (190)$$

Table 6

## Comparison of Measured and Computed Impact Velocities

Test Series	Drop Height cm	$v(o)_1 = \int a(t)dt$ cm/sec.	$v(o)_2 = \sqrt{2gh}$ cm/sec.	$v(o)_1/v(o)_2$	Discrepancy %
31	61	294	346	0.848	-15.2
	122	463	490	0.945	- 5.5
	183	533	600	0.890	-11.0
	305	798	773	1.030	+ 3.0
	425	900	918	0.982	- 1.8
32	61	312	346	0.905	- 9.5
	122	459	490	0.938	- 6.2
	183	713	600	1.190	+19.0
34	61	341	346	0.985	- 1.5
	122	456	490	0.930	- 7.0
	183	588	600	0.980	- 2.0
	305	779	773	1.003	+ 3.0
37	275	441	522	0.842	-15.8
	275	588	522	1.122	+12.2
	520	808	1010	0.800	-20.0
38	275	617	522	1.178	+17.8
	275	573	522	1.100	+10.0
	520	926	1010	0.918	- 8.2
39	275	515	522	0.985	- 1.5
	520	470	1010	0.465	-53.5
	520	559	1010	0.552	-44.8
41	275	643	522	1.230	+23.0
	275	441	522	0.842	-15.8
	275	404	522	0.772	-22.8
	520	937	1010	0.928	- 7.2
42	275	612	522	1.170	+17.0
	275	614	522	1.175	+17.5
	520	904	1010	0.900	-10.0
43	520	808	1010	0.800	-20.0

Table 6 (continued)

Test Series	Drop Height cm	$v(o)_1 = \int a(t) dt$ cm/sec.	$v(o)_2 = \sqrt{2gh}$ cm/sec.	$v(o)_1/v(o)_2$	Discrepancy %
44	275	556	522	1.061	+ 6.1
	520	786	1010	0.778	-22.2
	520	713	1010	0.708	-29.2
12	61	309	346	0.894	-10.6
	122	426	490	0.870	-13.0
	183	529	600	0.882	-11.8
	305	655	773	0.845	-15.5
	425	713	911	0.782	-21.8
	700	643	1175	0.548	-45.2
15	61	250	346	0.722	-27.8
	122	331	490	0.677	-32.3
	183	368	600	0.614	-38.6
	305	441	773	0.570	-43.0
	425	573	918	0.626	-37.4
19	61	233	346	0.672	-32.8
	122	316	490	0.644	-35.6
	183	279	600	0.465	-53.5
	305	537	773	0.693	-30.7
	425	662	918	0.724	-27.6
	700	662	1175	0.562	-43.8
22	61	357	346	1.080	+ 8.0
	122	422	490	0.860	-14.0
	183	515	600	0.836	-16.4
	305	537	773	0.693	-30.7
	425	654	911	0.718	-28.2

was found to be 13.8% for the test series 30 to 45. This discrepancy has several components. First, the direction of impact and the axis of the accelerometers are not always in perfect alignment. This error can be eliminated as was discussed earlier by using three accelerometers with mutually perpendicular axes and superposition of the signals according to the Pythagorean theorem. Secondly, the drop height could only be maintained with an accuracy of  $\pm 2\%$ . This was due to slack and elastic extension of the supporting cables.

The accelerometer has a guaranteed accuracy of 0.5%; however, due to the signal amplification this is magnified several times. In addition, of course, the theoretical value with which the experimental values are compared are not the exact and true ones because of air friction. Finally, there occurs a relatively large error in the evaluation especially when either, because of the sweep being too fast, the end of the impact signal does not appear any more on the photograph or, because of the sweep being too slow, the signal is not resolved sufficiently to permit accurate integration. These possible errors can be avoided by recording the signal on magnetic tape.

Increasing use and experience is certain to lead to progressive elimination or reduction of various sources of error so that the measurements will be sufficiently accurate and reliable for scientific purposes. Here it is perhaps

interesting to note that the mean discrepancy for the four test series by Hecht1 (No. 12, 15, 19, 22) computed in the same manner still have a discrepancy of 31.3% while those of our tests have only 13.8%.

The author believes that this is sufficient improvement so that one may judge the technical feasibility of the method as positive. We believe that the mean error can be easily brought within the range of 3% to 5%. This is judged to be entirely satisfactory considering the natural scattering of soil properties and the general nature of the problem.

### 3. Strength Properties of Target Materials

As shown in Table 3, the critical drop height for purely elastic impact is 3.5 mm. even for the hardest steels. Thus it is superfluous to attempt to evaluate elastic constants from the impact data.

The evaluation of the plastic flow pressure  $p_0$ , however, should give one of the critical material constants.

According to equation (92a) the penetration during plastic impact in a simplified form is given by:

$$\alpha = \frac{v(0)}{b} \sin bt \quad (92c)$$

where

$$b^2 = \frac{2\pi R}{m} p_0$$

The end of the impact period is determined by the fact that the penetration velocity  $\dot{\alpha}$  has decayed to zero:

$$\dot{\alpha} = v(o) \cos bT = 0 \quad \text{or}$$

$$bT = \frac{\pi}{2} \quad (93b)$$

Thus, the plastic flow pressure can be found:

$$p_o = \frac{m\pi}{8R T^2} \quad (191)$$

T signifies the duration of the impact. The flow pressure, however, can also be obtained from the maximum deceleration. If we differentiate, for example, equation (92d) twice with respect to time, we obtain:

$$\ddot{\alpha} = -v(o)b \sin bt \quad (192)$$

the maximum deceleration then is:

$$\ddot{\alpha}_{\max} = -v(o)b = -v(o) \left[ \frac{2\pi R}{m} p_o \right]^{\frac{1}{2}} \quad (193)$$

solving for  $p_o$  we get:

$$p_o = \frac{m}{2\pi R} \left[ \frac{\ddot{\alpha}_{\max}}{v(o)} \right]^2 \quad (194)$$

Thus the yield stress can be evaluated from the test data either by equation (191) or by (194). If we introduce the dimension of the penetrometer model as given in Chapter III, 2 into these equations we get:

$$m = \frac{W}{g} = \frac{1573}{981} = 1.6 \frac{\text{g sec}^2}{\text{cm}}$$

and

$$p_o = 0.168 \frac{1}{T^2} \quad \text{g/cm}^2 \quad (191a)$$

as well as

$$p_o = 0.068 \left[ \frac{\alpha_{\max}''}{v(o)} \right]^2 \quad \text{g/cm}^2 \quad (194a)$$

It is interesting to note that according to equation (191) the yield stress is independent of the drop height, the impact velocity or the maximum deceleration and depends only upon the impact duration  $T$ . The observed values do indeed show a surprising constancy of  $T$  for a given target material. Table 7 shows the evaluation of the  $p_o$  values by both methods. For a better comparison the average values  $\sum p_o / n$  for the individual target materials are compiled in Table 8 and are compared with the standard control test results of CBR or the equivalent unconfined compression strength  $q_u$ .

The values for the flow pressure have an average scattering of 25.5% for  $p_o$  computed from equation (191) and of 41% for  $p_o$  computed from equation (194). This is not too surprising, because equation (191) uses only one experimentally determined value while (194) requires  $\alpha_{\max}$  as well as  $v(o)$ . Thus, errors are being multiplied. Furthermore, not all the scattering is to be blamed on insufficient accuracy of the test method. A certain scattering is to be expected because the very properties being measured are not unique quantities

Table 7  
Determination of the Plastic Flow Pressure

Test Series	Drop Height H cm.	Impact Duration T m.sec.	$\frac{1}{T^2}$ $10^{-6} \text{sec.}^{-2}$	$P_o$ (eq.191a) $\text{kg/cm}^2$	$\alpha_{\text{max}}$ $\text{m/sec.}^2$	$v(o)$ $\text{cm/sec.}$	$\left[ \frac{\ddot{\alpha}_m}{v(o)} \right]^2$	$P_o$ (eq.194a) $\text{kg/cm}^2$
31	61	18	0.00309	0.52	570	346	26900	1.83
	122	19	0.00277	0.46	730	490	22200	1.50
	183	20	0.0025	0.42	970	600	26200	1.78
	305	22.5	0.00198	0.33	1140	773	21800	1.48
	425	21.0	0.00227	0.37	1350	918	21800	1.48
32	61	80	0.000153	0.026	114	346	1090	0.074
	122	85	0.000138	0.023	148	490	900	0.061
	183	90	0.000124	0.021	160	600	713	0.043
34	61	1.2	0.69	116.0	5920	346	2950000	201
	122	1.14	0.77	129.0	8550	490	3020000	205
	183	1.12	0.79	132.5	10250	600	2920000	198
	305	1.12	0.79	132.5	13150	773	2900000	197
37	275	8.0	0.0156	2.62	2170	522	172000	11.7
	275	8.0	0.0156	2.62	2170	522	190000	12.9
	520	8.0	0.0156	2.62	2850	1010	80000	5.4
38	275	8.8	0.0129	2.17	1600	522	94000	6.4
	275	9.2	0.0118	1.98	1550	522	87500	5.9
	520	8.8	0.0129	2.17	2850	1010	79500	5.4
39	275	45	0.000495	0.083	456	522	7600	0.52
	520	42	0.00057	0.096	548	1010	2900	0.20
	520	40	0.000625	0.105	502	1010	2480	0.17
41	275	7.0	0.0204	3.44	2530	522	230000	15.8
	275	6.5	0.0236	4.14	2450	522	220000	15.0
	275	7.0	0.0204	3.44	2740	522	270000	18.5
	520	8.0	0.0156	2.62	3540	1010	122500	8.3

Table 7 (continued)

Test Series	Drop Height H cm.	Impact Duration T m.sec.	$\frac{1}{T^2}$ $10^{-6} \text{sec.}^{-2}$	$P_0$ (eq.191a) kg/cm <sup>2</sup>	$a_{\text{max}}$ m/sec. <sup>2</sup>	$v(0)$ cm/sec.	$\left[ \frac{\ddot{\alpha}_m}{v(0)} \right]^2$	$P_0$ (eq.194a) kg/cm <sup>2</sup>
42	27	17.2	0.00338	0.57	820	522	24500	1.66
	27	12.8	0.0061	1.02	1185	522	51000	3.46
	520	13.2	0.00575	0.97	1510	1010	22500	1.52
43	275	10	0.0100	1.68	1715	522	19700	7.3
	520	11	0.0086	1.44	2000	1010	39200	2.7
	520	7	0.0200	3.36	2960	1010	86000	5.82
44	275	15	0.00444	0.75	1095	522	43800	2.98
	520	14	0.0051	0.86	1540	1010	23200	1.58
	520	11	0.0083	1.39	1770	1010	30900	2.10
45	200	172	0.0000338	0.0057	239			
12	61	18	0.00309	0.52	513	346	22000	1.50
	122	18	0.00309	0.52	685	490	19600	1.33
	183	16	0.0039	0.65	800	600	17800	1.21
	305	18	0.00309	0.52	1025	773	17500	1.19
	425	18	0.00309	0.52	800	911	7700	0.52
	700	16	0.0039	0.65	1540	1175	17500	1.19
15	61	38	0.00069	0.116	217	346	3700	0.25
	122	38	0.00069	0.116	331	490	4560	0.31
	183	38	0.00069	0.116	376	600	3940	0.27
	305	38	0.00069	0.116	548	773	5000	0.34
	425	38	0.00069	0.116	640	918	4900	0.33
19	122	48	0.000435	0.073	228	490	2170	0.15
	183	46	0.000475	0.008	388	600	4180	0.28
	425	39	0.000658	0.011	662	918	5220	0.35
	700	39	0.000658	0.011	800	1175	4650	0.32
22	61	16.4	0.0037	0.62	388	357	11800	0.80
	122	16.0	0.0039	0.65	502	490	10600	0.72
	305	13.8	0.00522	0.88	800	700	13000	0.89
	425	13.4	0.00555	0.93	970	918	11200	0.76

Table 8

## Comparison of Plastic Flow Stress with Control Tests

Series No. & Target Material	Average $P_0$ (eq.191) kg/cm <sup>2</sup>	$S_{max}$ %	$(S_{max})^2$	Average $P_0$ (eq.194) kg/cm <sup>2</sup>	$S_{max}$ %	$(S_{max})^2$	Con- trol CBR %	Tests $q_u$ kg/cm <sup>2</sup>
31 Cambar wax M-348 (at 31°C)	0.43	-23	528	1.62	+13	169	-	0.51 <sup>1</sup>
32 Estar 3 grease (at 28°C)	0.023	+13	169	0.061	+21	441	-	0.045 <sup>1</sup>
34 paraffin (at 29°C)	127.0	- 7	81	200.0	+ 3	9	-	134.0 <sup>2</sup>
37 clay	2.62	± 0		10.0	-46	2120	2.1	2.2
38 clayey sand silt	2.11	- 6	36	5.9	± 9	81	4.3	3.0
39 beach sand	0.089	+18	324	0.30	+73	5320	-	-
41 Princeton clay	3.41	-23	528	14.4	-42	1760	6.3	4.4
42 sandy clay	0.85	-33	1085	2.21	+57	3240	4.0	2.8
43 crushed rock	2.13	+59	3480	5.27	+49	24 7	18.5	-
44 fine sand	1.00	+39	1520	2.22	+34	1155	5.8	-
12 Princeton red clay	0.56	+16	256	1.14	-54	2905	2.8	2.1
15 Ottawa sand (dry)	0.12	- 0	0	0.30	-17	289	-	-
19 beach sand w=1.34 g/cm	0.009	-26	675	0.25	-60	3600	-	-
22 Princeton clay (w=2.65%)	0.76	+22	485	0.91	-11	121	1.9	1.4

$$\sum S^2 = 9167$$

$$\sum S^2/n = 652$$

$$\text{mean scatter: } S_m = 25.5\%$$

$$\sum S^2 = 23610$$

$$\sum S^2/n = 1685$$

$$S_m = 41\%$$

<sup>1</sup>Hardnes number computed from the penetration number N.

<sup>2</sup>Failure stress computed from the tensile stress at 23°C.

by themselves and, particularly with a rather extensive test program, they must be expected to have a certain scattering.

This is particularly so if one considers the great variability of the properties of natural soils from point to point. Thus, perhaps a major part of the scattering might be traceable to actual local variation of the soil properties in situ.

If, for example, we disregard the values for the scattering of  $p_0$  from (191) of test series No. 43 (i.e. impact on crushed rock which very much depends on the surface configuration at the exact impact point), the average scattering is reduced immediately to 20%. For a material such as crushed rock especially, it is surely important whether the impact energy is directly conducted away by a rigid grain skeleton or whether the impact is a resilient and elastic one.

The standard control test like CBR and unconfined compression test were not carried out on clean sands. The former is very difficult to do because the exact depth of penetration is difficult to establish and the latter is not possible at all in a non-cohesive material.

For the target materials of series 31, 32 and 34, i.e. for the cambar wax, the Estan 3 grease and the paraffin, the mechanical properties furnished by the manufacturer were accepted.

The penetration number  $N$  for a grease or wax is the penetration (in tenths of a millimeter) that occurs after five seconds when a  $90^\circ$  cone weighing 250 grams is applied to the grease at  $25^\circ$  centigrade.

For these materials one can thus determine a hardness number using equation (7) giving:

(a) for the Cambar wax

$$H_L = 0.898 \frac{P}{d^2} = 0.898 \frac{0.250}{(0.7)^2} = 0.51 \text{ (kg/cm}^2\text{)}$$

(b) for the Estan 3 grease:

$$H_L = 0.898 \frac{0.250}{(2.35)^2} = 0.045 \text{ kg/cm}^2$$

For the paraffin (Essowax 5010) the manufacturer gives a tensile strength (at  $23^\circ\text{C}$ ) of  $26 \text{ kg/cm}^2$ . If one uses this value to calculate the shear strength and applies the corresponding value to the Prandtl bearing capacity problem, one obtains a value of  $p_0 = 134 \text{ kg/cm}^2$  which is close enough to the experimentally found value of about  $200 \text{ kg/cm}^2$  particularly if one considers that the calculated value is based on a static strength and test whereas, for the case of the dynamic loads during the penetrometer impact, the observed values should be higher.

In general, the values for the plastic flow pressure  $p_0$  evaluated with equation (191) are more consistent and are in surprisingly good agreement with the standard control test

values, i.e. with the unconfined compression tests or the corresponding equivalent CBR values. The  $p_0$  values evaluated by equation (194) give in almost all cases two to three times higher values. The author has not been able to find an explanation so far for this fact, except, as was mentioned before, when calculating  $p_0$  from (194) two experimental values have to be introduced which may lead to a multiplication of any errors. However, the values from (194) are at least in agreement as far as the order of magnitude for  $p_0$  is concerned and they are also more or less consistent within any test series.

#### 4. Wave Propagation Velocities

The instrumenting of the target soils with accelerometers had one main purpose: to measure the elastic properties of these target materials. They all were built in at such a distance from the point of impact that in their vicinity the resulting stresses and deformations would remain within the elastic range. Furthermore, they were to check the validity of the assumption made generally that the energy carried away by vibrations may be neglected. The following values were evaluated from the vibration signals:

(a) for the propagation velocity:  $a_i = \frac{v_i}{A_i}$

(b) for the period of vibration  $T = \frac{t_n}{n}$

(c) maximum amplitude of

the acceleration: 
$$b_{i \max} = \frac{B_i}{K_i g}$$

where  $g = 981 \text{ cm/sec.}^2$  is the gravitational acceleration.

The next page demonstrates the evaluation of these quantities from the test data. The values obtained are listed in Table 9. From the average values for "a" the corresponding E moduli were found according to equation (145) which are shown in Table 10. According to this equation (145) they can be determined by:

$$\begin{aligned} E &= \frac{(1 + \nu)(1 - 2\nu)}{1 - \nu} f a^2 && (145a) \\ &= f a^2 && (\text{for } \nu = 0) \\ &= 0.83 f a^2 && (\text{for } \nu = 0.25) \end{aligned}$$

The values found are in very good agreement with those given by Barkan. Their scattering is relatively small.

The photographs of series 41 which have the least distortion and interference show clearly that the signals in the soil have the form given by equation (178). If we take the displacement:

$$u = B e^{-\beta x} e^{i(\alpha x - \omega t)}$$

and find the acceleration by double differentiation with respect to time, one gets:

Table 9  
Evaluation of the Vibration Signals

Test Series & page	Drop Height H cm	r <sub>1</sub> cm	r <sub>2</sub> cm	a <sub>1</sub> m/sec	a <sub>2</sub> m/sec	Period T <sub>1</sub> m.sec.	Period T <sub>2</sub> m.sec.	b <sub>1</sub> max cm/sec. <sup>2</sup>	b <sub>2</sub> max cm/sec. <sup>2</sup>
37 - A 8	275	283	482	113	105	16.3	12.9	26.0	8.8
A 9	520	290	510	151	159	13.5	14.0	28.9	11.4
38 - A 10	275	680	1000	400	357	14.6	12.8	63.2	29.0
A 11	275	680	1000	314	323	15.2	13.5	23.8	8.8
A 12	275	680	1000	400	454	13.5	13.0	82.2	36.0
A 14	520	680	1000	272	278	13.6	14.6	27.0	10.4
39 - A 15	275	140	280	200	200	12.0	11.0	38.0	17.4
A 17	520	140	280	188	200	13.0	12.0	50.8	17.3
A 18	520	140	280	165	170	12.0	6.5	108.0	28.9
41 - A 19	275	244	490	244	340	7.7	7.5	40.5	159.0
A 20	275	242	488	242	296	5.4	7.0	39.0	121.5
A 22	520	244	491	244	280	6.5	8.0	57.8	232.0
42 - A 24	275	178	396	170	208	9.6	12.5	57.8	17.9
43 - A 26	275	112	233	124	123	4.5	6.1	202.0	95.4
A 27	520	107	238	153	164	6.0	6.0	179.0	55.0
44 - A 29	275	151	375	-	417	-	10.0	98.1	21.7
A 31	520	166	394	-	329	7.5	10.0	188.0	41.9
		r <sub>3</sub>		a <sub>3</sub>		T <sub>3</sub>		b <sub>3</sub>	
41 - A 19		850		283		6.1		3.35	
A 20		825		275		7.25		3.00	
A 22		830		258		6.25		5.00	

$$\ddot{u} = B \omega^2 e^{ix(\alpha + i\beta)} e^{-i\omega t} \quad (195)$$

i.e. except for the factor  $\omega^2$  nothing has changed.

Table 10

## Determination of E-modulus

Test Series No.	Target Material	$\rho$ cm <sup>2</sup> /sec <sup>4</sup>	$a$ m/sec	$a^2$ m <sup>2</sup> /sec <sup>2</sup>	$E(\nu = 0)$ kg/cm <sup>2</sup>	$E(\nu = 1/4)$ kg/cm <sup>2</sup>
37	Clay soil	0.00126	135	18,200	230,000	190,000
38	Clayey sand - silt	0.00138	350	122,000	1,680,000	1,390,000
39	Beach sand	0.00137	188	35,200	480,000	400,000
41	Princeton clay	0.00156	274	45,000	1,117,000	970,000
42	Sandy clay	0.00141	189	36,000	510,000	422,000
43	Crushed rock	0.0230	141	20,000	460,000	380,000
44	Fine sand	0.00153	373	139,000	2,100,000	1,740,000

5. Evaluation of Vibration Energy

The energy furnished by a force  $P$  moving through a distance  $s$  is given by:

$$W = \int_0^s P ds = \int_0^s m \ddot{u} ds \quad (196)$$

If we determine an average value  $P$  through the integral interval from the test data, then the total vibration energy could be:

$$W = P_{av} \cdot s$$

Considering a half-period  $1/2 T$  with a sinusoidal change of the acceleration from zero to a maximum amplitude  $b$  and back to zero, we may write for the velocity change:

$$v \Big|_0^{1/2 T} = \frac{2}{\pi} \cdot \frac{1}{2} b \frac{1}{2} T = \frac{1}{2} \frac{bT}{\pi} \quad (197)$$

Analogously the distance traveled during the half-period is:

$$s = \frac{2}{\pi} v \frac{1}{2} T = \frac{1}{2} \frac{bT^2}{\pi^2} \quad (198)$$

and the average force becomes:

$$P_m = m \frac{b}{\pi} \quad (199)$$

where  $m$  designates the accelerated mass.

The total energy thus is determined by:

$$W = \frac{m b^2 T^2}{2\pi^3} \quad (200)$$

If one assumes the waves propagate spherically, the accelerated mass is:

$$m = \frac{2}{3} \pi r^3 \quad (201)$$

and the total energy then is:

$$W = \frac{1}{3\pi^2} r^3 b^2 T^2 \quad (202)$$

According to this formulation the maximum energy of vibration evaluated for all test series was found for series 38 (page A-10). Using the corresponding values from Tables 9 and 10, we found for this case:

$$W_v = \frac{1}{29.5} \cdot 680^3 \cdot 82.2^2 \cdot 13.5^2 \cdot 0.00138 = 18,500 \text{ cm.gm.}$$

The total impact energy however for this test was:

$$W_o = 1573 \cdot 275 = 433,000 \text{ cm.gm.}$$

giving a ratio N of vibration energy to impact energy:

$$N = \frac{W_v}{W_o} = \frac{18,500}{433,000} = 4.3\%$$

Since this was by far the largest value found, most other values being a significant amount below this ratio, we concluded that for our experiments the energy dissipated by the vibrations of the half-space is indeed negligible.

## X. Summary and Conclusions

The purpose of this investigation was to explore a method that would permit the reliable assessment of surface soil properties for the prediction of deformations during and after aircraft operations. After the historical development of the penetrometer concept is briefly traced, we present the basic theoretical aspects of the problem. A penetrometer with a piezo-electric accelerometer as the main feature was designed. This penetrometer was tested and for laboratory experimentation purposes evaluated. While the instrument as designed certainly should not yet be considered an ultimate version of a new operational penetrometer, the principle tested and the methods employed were found valid and useful. The modifications suggested are to make the penetrometer a complete sphere, use three mutually perpendicular accelerometers, record the signal on magnetic tape and eliminate the cable by telemetering the signal through a built-in transmitter to a receiver, the surface of the sphere acting as an antenna. With these modifications it is believed that a system will be achieved which will permit the remote determination of the mechanical strength of a soil surface with a reliability sufficient for engineering purposes.

The values found for the flow pressure were in reasonable agreement with the control test values and were consistent

among themselves. The solution for a sphere impacting on a four parameter half-space was developed which gives, however, a rather complicated, non-linear result that must yet be evaluated numerically. Finally, it was shown that the energy dissipated by vibrations when a body impacts on a half-space for the velocities and material investigated is indeed negligible.

### Acknowledgment

The author gratefully acknowledges the assistance given during various or all phases of the investigation by a number of people, especially:

Major Donald Klick, Terrestrial Science Laboratory, AFCRL, Contract Monitor, who always cooperated, asked questions and offered advice freely;

Dr. Christian Hechtel who as assistant of the author helped with all the experiments and calibrated the equipment;

Mr. Kuei-Wu Tsai who carried out and checked the mathematical inversion of the problem of Chapter VI, 3;

Mr. P. Salan, engineering representative of Endevco Corporation, who gave most valuable advice regarding the electronic instrumentation and often also loaned equipment needed rapidly;

Mr. L. Banning of the machine shop of the School of Engineering and Applied Science, Princeton University, who is responsible for the manufacture of the penetrometer.

Werner E. Schmid

Princeton  
January 1966

References

- Andrews, J. P. (1930) "Theory of Collision of Spheres of Soft Metal," Phil. Mag. Ser. 7, Vol. 9, p. 593.
- Andrews, J. P. (1931) "Experiments of Impact," Proceedings Physical Society of London, Vol. 43, p. 8.
- American Society for Testing Material (1955) Special Technical Publication No. 176, Philadelphia, ASTM, 1956.
- Barkan, D. D. (1948) "Dynamika Osnovaniy I Fundamentor" Strgyvoenmcrizdat, Moskau.
- Berger, F. (1924) Das Gesetz des Knaftverlaufes beim Stoss, F. Vieweg & Sohn, Braunschweig.
- Boltzmann, L. (1881) "Einige Experimente über den Stoss von Zylindern," Sitzungsberichte, Akad. d. Wissensch., Wien Mathem.-naturwissensch. Klasse Bd. 84, 1882 S. 1225.
- Brinell, J. A. (1900) II. Cong. Int. Méthodos d'Essai, Paris, Lehrbuch der Ballistik, Bd. 1 Aussere Ballistik, J. Springer, Berlin.
- Crook, A. W. (1952) "A Study of Some Impacts between Metal Bodies by a Piezoelectric Method," Proceedings, Royal Soc. London A212, p. 377.
- Doetsch, G. (1937) Theorie und Anwendung der Laplace Transformationen, Dover Verlag, New York, 1943.
- Ewing, W. M. (1957) Elastic Waves in Layered Media, McGraw-Hill Book Co., New York.
- Föppl, A., Föppl L. (1944) Drang und Zwang, Bd. II, R. Oldenburg, München, p. 385.
- Föppl, L. (1949) "Slow Motion Pictures of Impact Tests by means of Photoelasticity," Journ. Applied Mechanics, Vol. 16, p. 173.
- Goldsmith, W. (1960) Impact, the Theory and Physical Behaviour of Colliding Solids, Edward Arnold Publishers Ltd., London, p. 379.
- Grammel, R. (1928) "Mechanik der elastischen Körper," Handbuch der Physik, Vol. IV, Springer, Berlin, p. 632.

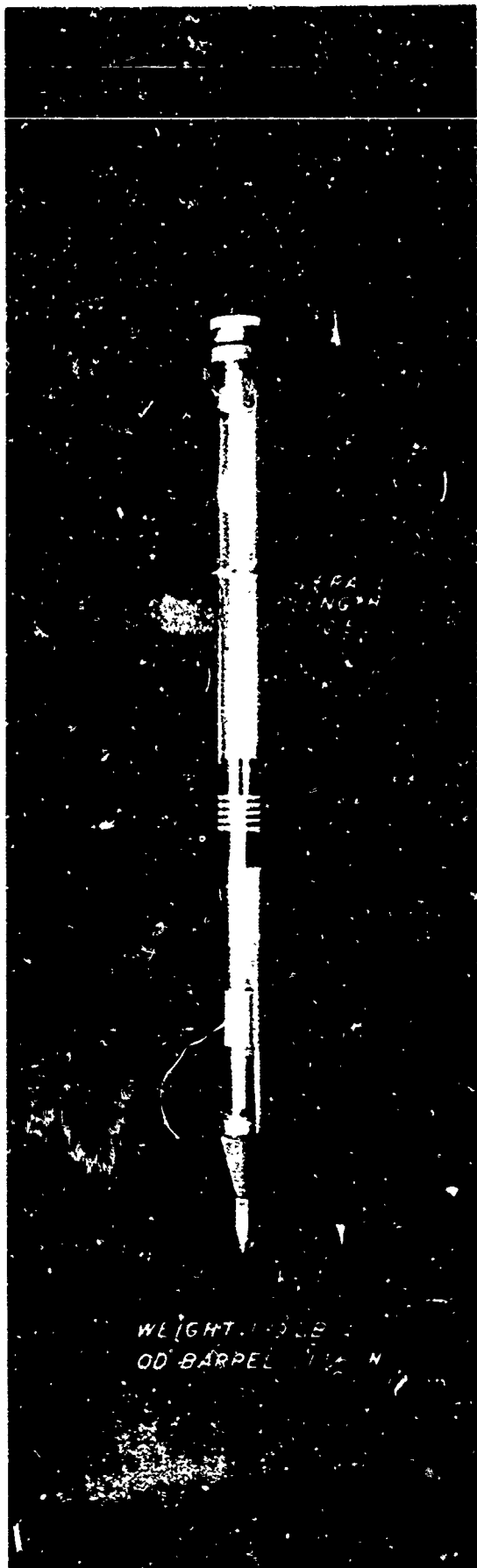
- Gunars, A. (1963) "Correlation of Unconfined Compressive Strength and Ram Hardness of Processed Snow," Technical Report 85, U.S. Army Cold Regions Research and Engineering Laboratory, Hanover, N.H., p. 14.
- Haefeli, R., Amberg, G., von Moos, A. (1951) "Eine leichte Rammsonde für geotechnische Untersuchungen, Schweiz. Bauzeitung, Nr. 36.
- Hecht1, H. und Herbst, T. (1963) "Trends in the Development of Trafficability," Internal Report, Dept. of Civil Engg., Princeton University, 44 pp.
- Hecht1, H. (1964) "Impact Tests on Soil and their Significance of Trafficability," Ph.D. Dissertation, Dept. of Civil Engineering, Princeton University, 135 pp.
- Hencky, H. (1923) "Über einige statisch bestimmte Fülle des Gleichgewichts in plastischen Körpern," Zeitschr. f. angewandte Mathematik und Mechanik, (Z.A.M.M.), Vol. III, pp. 241-251.
- Hill, R., Lee, E. H. and Tupper, S. J. (1947) "The Theory of Wedge Indentation of ductile Materials," Proceeding of the Royal Society of London, Serie A. Bd. 188, pp. 273-291.
- Holm, E., Holm, R. und Shobert, E. I. (1949) "Theory of Hardness and Measurements Applicable to Contact Problems," Journ. Appl. Physics, Vol. 20, p. 319.
- Hunter, S. C. (1957) "Energy Absorbed by Elastic Waves during Impact," Journ. Mech. Phys. Solids, Vol. 5, p. 162.
- Hvorslev, M. J. (1953) "Cone Penetrometer Operated by Rotary Drilling Rig," Proc. 3rd International Conference, ISSMFE, Vol. 1, p. 236.
- Ishlinsky, A. J. (1944) "The Problem of Plasticity with the Axial Symmetry and Brinell's Test," Frikladnaia Matematika i Mekhanika, Vol. VIII, Akademika Nauk. S.S.S.R., pp. 201-224.
- Iterson, van F. K. Th (1949) Plasticity in Engineering, Hafner Publishing Co. Inc., New York, 174 pp.
- Kolsky, H. (1953, Stress Waves in Solids, Oxford, Clarendon Press.

- Kornhauser, M. (1964) Structural Effects of Impact, Spartan Books, Inc., Baltimore, Md., 205 pp.
- Lamb, H. (1904) Proc. Lond. Math. Soc., Vol. I, p. 473.
- Lee, E. H. (1955) "Stress Analysis in Viscoelastic Bodies," Quarterly Applied Mathematics, XIII, pp. 183-190.
- Lee, E. H. (1957) "Stress Analysis for Visco-elastic Materials," Proc. of the Conf. on the Properties of Materials at High Rate of Strain, The Institution of Mechanical Engineers, London, pp. 164-172.
- Levy, Ezra C. (1958) A New Table of Laplace-Transform Pairs, Space Techn. Laboratory, Pasadena, Calif., 104 pp.
- Martel, R. (1895) Commission des Méthodes d'Essai des Matériaux, Paris, Vol. 3, p. 261.
- McCarthy, J. L., Carden, M. D. (1962) "Impact Characteristics of Various Materials Obtained by an Acceleration-Time History Technique Applicable to Remote Targets," Nasa Techn. Note D-1269, Langley Research Center, Hampton, Va., 61 pp.
- Meyer, E. (1908) "Untersuchungen über die Härteprüfung und Härte," Zeitschr. V.D. I, Vol. 52, p. 645.
- Mintrop, H. (1939) "Die Stossdauer beim Stoss einer Kugel gegen eine ebene Platte," Zeitschr. techn. Physik, Vol. 20, p. 314.
- Mintrop, H. (1942) "Der Einfluss der Masse der Stossplatte beim Stoss einer Kugel," Forschungsh. Geb. Ingenieurwiss, V.D.I., Vol. 13, p. 87.
- Mintrop, H. (1941) "Untersuchungen über den Stoss einer Kugel gegen eine ebene Platte," Forschungsh. Geb. Ingenieurwiss, V.D.I., Vol. 12, p. 127.
- Mises, R. von, Karman, Th. von (1953) Advances in Applied Mechanics, Academic Press Inc., N.Y., Vol. III, p. 324.
- Molineaux, C. E. (1955) "Remote Determination of Soil Trafficability by the Aerial Penetrometer," AFCKC Report No. 77, October 1955.

- Müller, W. (1914) "Zur Kenntnis der Stossdauer elastischer Körper," Sitzungsber. Akad. Wiss. Wien, Math.-naturw. Kl., Vol. 123, p. 2157.
- Müller, W. (1952) "Zur Theorie des Reibungsstosses einer Kugel gegen eine ebene Wand und gg. eine zweite Kugel," Ost. Ing. Arch., Vol. 6, p. 196.
- Nadai, A. (1921) "Versuche über die plastischen Formänderungen von keilförmigen Körpern aus Flusseisen," Z.A.M.M., V. 1, pp. 20-28.
- Nadai, A. (1963) Theory of Flow and Fracture of Solids, McGraw-Hill Book Co. Inc., Vol. II, 705 pp.
- Palmer, D. J. and Stuart, J. G. (1957) "Some Observations on the Standard Penetration Test and a Correlation of the Test with a new Penetrometer," Proc. 4th International Conf. ISSMFE, Butterworths Scientific Publications, London.
- Pao, Y. P. (1955) "Extension of the Hertz Theory of Impact to the Visco-elastic Case," Journ. Appl. Physics, Vol. 26, p. 1083.
- Pöschl, T. (1926) "Der Stoss," Handbuch der Physik, Vol. 6, Chapt. 7, J. Springer, Berlin.
- Prandtl, L. (1921) "Über die Eindringfestigkeit (Härte) plastisch. Baustoffe und die Festigkeit von Schneiden," Z.A.M.M., Vol. III, pp. 401-406.
- Proctor, R. R. (1933) Four articles on "Soil Compaction," Engineering News Record, Vol. 59.
- Rayleigh, J. W. S. (1906) "On the Production of Vibrations by Forces of Relatively Long Duration with Applications to the Theory of Collisions," Phil. Mag. Ser. 6, Vol. II, p. 283.
- Raman, C. V. (1920) "On Some Applications for Hertz' Theory of Impact," Phys. Review, Vol. 15, p. 277.
- Ramsauer, C. (1909) "Experimentelle und theoretische Grundlagen des elastischen und mechanischen Stosses," Ann. d. Phys. Chem. (Poggendorf), Ser. 7, Vol. 30, p. 417.
- Rinehart, J. S., Pearson, J. (1954) Behaviour of Metals under Impulsive Loads, The American Society for Metals, Cleveland, Ohio, 256 pp.

- Sauter, F. (1950) "Der elastische Halbraum bei mechanischer Beeinflussung der Oberfläche," Z.A.M.M., Vol. 30, No. 7, pp. 203-215.
- Schmid, W. E. (1963) Status Report No. 4 to the Terrestrial Science Laboratory, Office of Aerospace Research, Princeton University, 14 pp.
- Schneebeli, H. (1886) "Experimentaluntersuchungen über den Stoss elastischer Körper," Reportorium d. Physik, München (Exner), Vol. 22, p. 183.
- Sternglass, E. J. and Stuart, D. A. (1953) "An Experimental Study of the Propagation of Transient Deformation in Elastoplastic Media," Journ. Appl. Mech., Vol. 20, p. 427.
- Symonds, F. S. (1948) "On the General Equations of Problems of Axial Symmetry in the Theory of Plasticity," Quarterly of Applied Mathematics, Vol. VI, pp. 448-452.
- Tabor, D. (1951) The Hardness of Metals, Oxford, the Clarendon Press, 175 pp.
- Terzaghi, K. (1953) "Fifty Years of Subsoil Exploration," Proceedings, 3rd Int. Conf. ISSMFE, Vol. 3, p. 277. X
- Tillet, J. P. A. (1954) "A Study of the Impact of Spheres on Plates," Proc. Phys. Soc. London, Vol. 67, p. 677.
- Warlam, A. (1956) Determination of Snow Characteristics from Aircraft, Report to the AFCRC and U.S. Army Engineer Snow, Ice and Permafrost Establishment (SIPRE), April 1956.
- Weber, H. (1910) Die partiellen Differentialgleichungen der mathematischen Physik nach Riemanns Vorlesungen, 5. Ausg., Bd. 2, Vieweg Verl. Braunschweig pp. 184-198.
- Williams, S. R. (1942) Hardness and Hardness Measurements, American Society for Metals, Cleveland, Ohio, 558 pp.
- U.S. Waterways Experiment Station, Vicksburg, Miss. (1945) "The California Bearing Ratio Test as Applied to the Design of Flexible Pavement for Airports," Technical Memorandum No. 213-1, 38 pp.

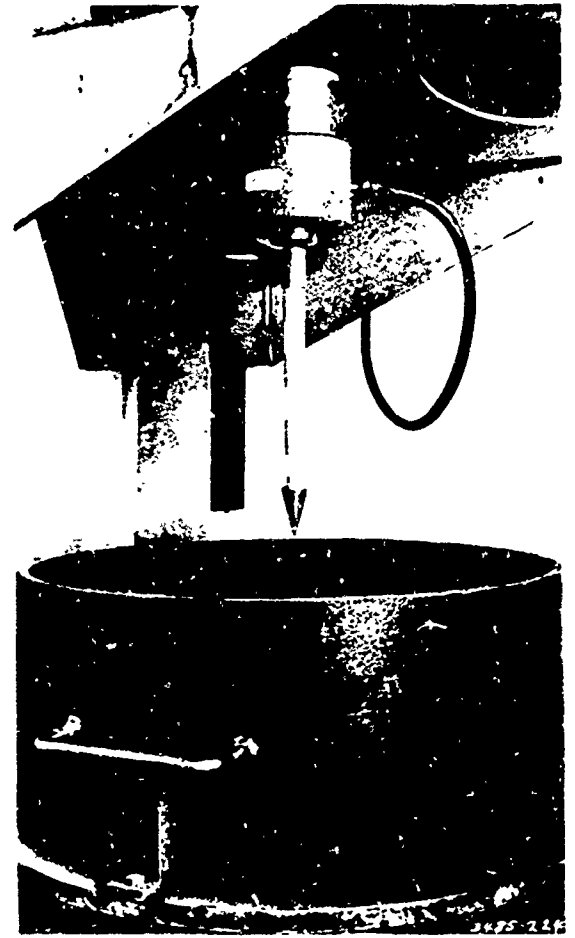
- U.S. Army Engineer Waterways Experiment Station, Corps of Engineers, Vicksburg, Miss. (1957) Laboratory Study of Mechanical Principles, "Studies of Aerial Cone Penetrometer," Technical Report No. 3-462, Report I, 27 pp.
- U.S. Army Engineer Waterways Experiment Station, Vicksburg, Miss. (1964) "Strength-Moisture-Density Relations of Fine-Grained Soils in Vehicle Mobility Research," Technical Report No. 3-639.
- Anonymous (1953) "Determination of Ground Trafficability from Aircraft," N.Y.U. Final Report No. 156.7, April 1, 1953.
- Anonymous (1955) "Development of a Ground Launched Penetrometer," Report No. 325.01, N.Y.U., December 1955.



The Aerial Penetrometer  
(U.S. Air Force)



(a)



(b)

Figure 2

Cone Penetrometer of U.S. Army Corps of Engineers

(a) field instrument

(b) laboratory instrument

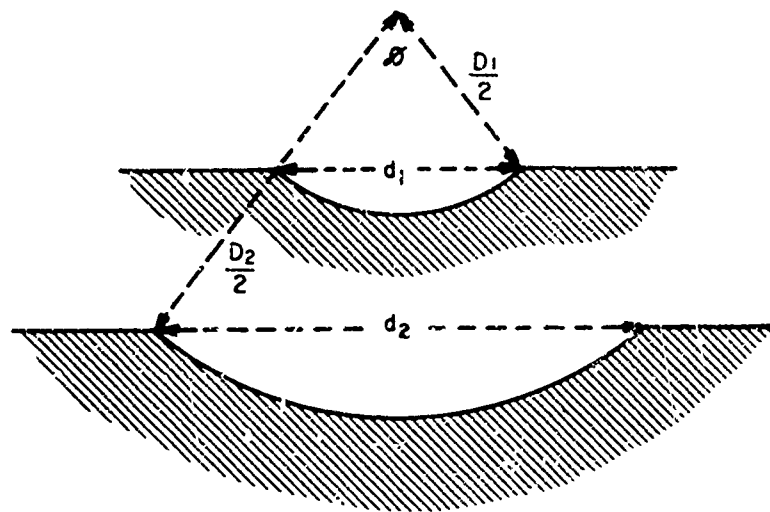


Figure 3(a)

Geometric Similarity of Indentation  
for the Hardness Test

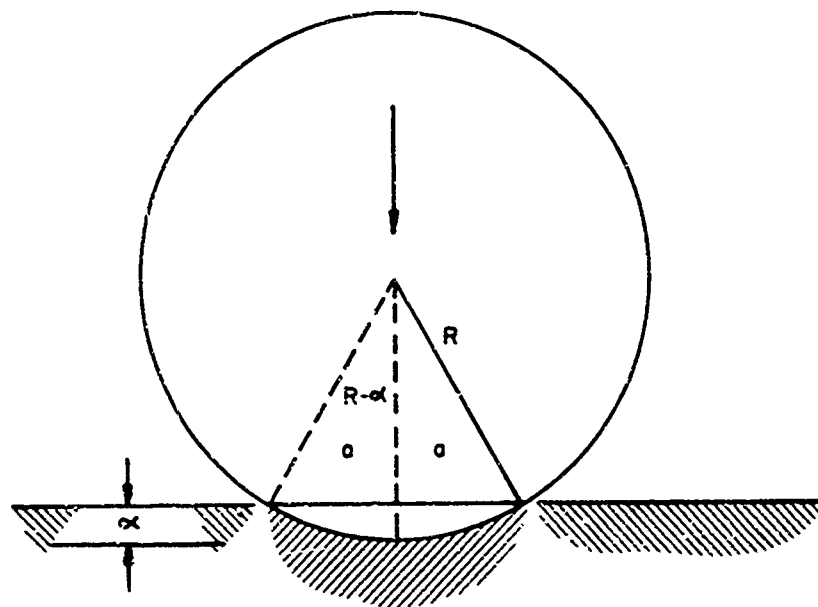


Figure 3(b)

Definition of Deformation Parameters  
for Hertz Contact Problem

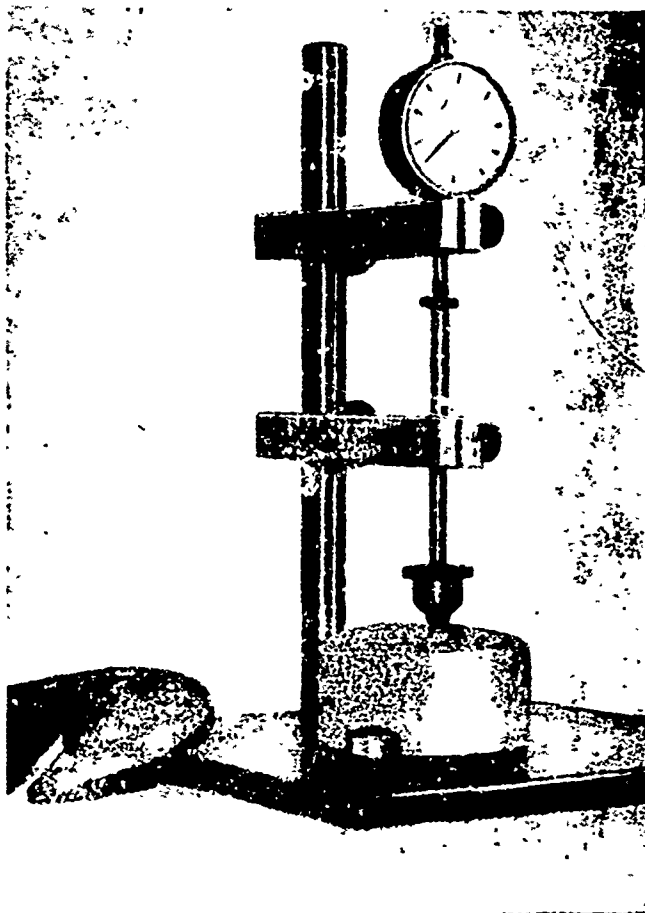


Figure 4

Spherical Penetrometer of Tsyrovich

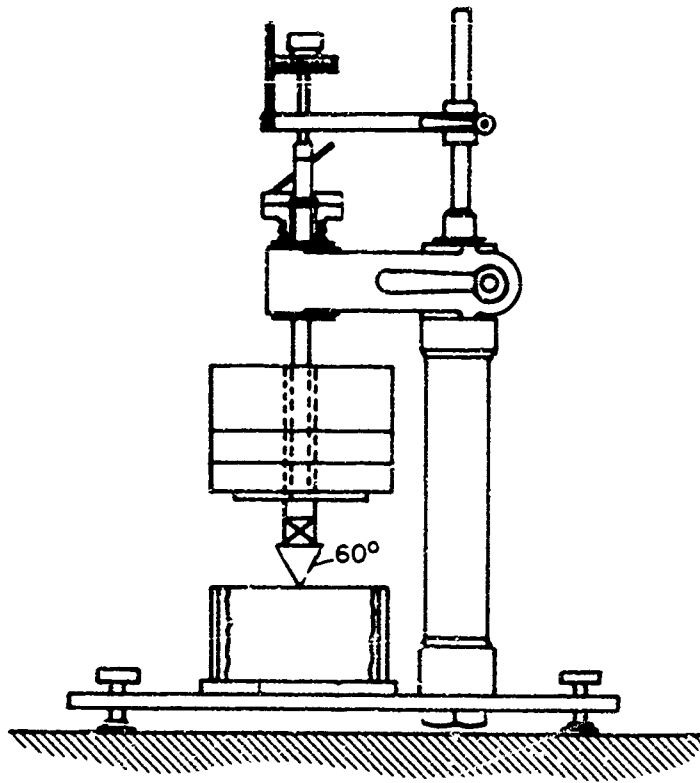


Figure 5

Swedish Cone Penetrometer

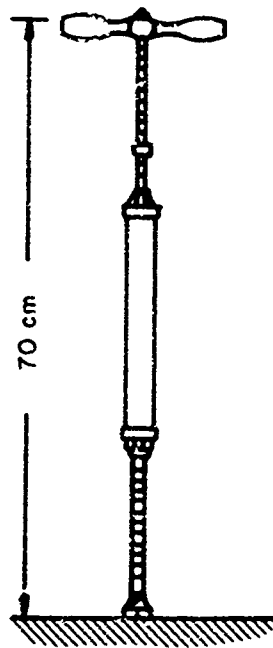
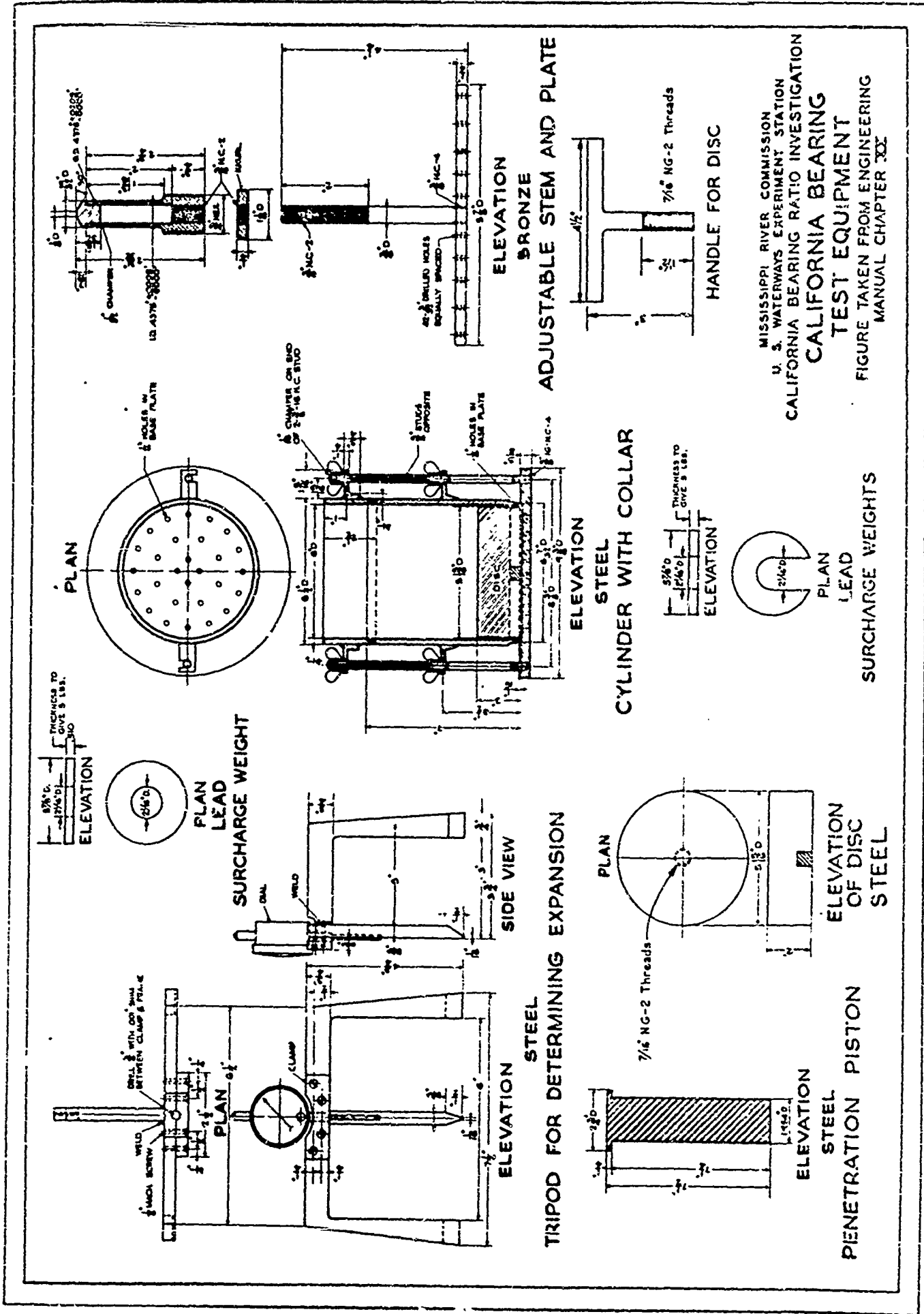


Figure 6

Proctor Plasticity Needle



MISSISSIPPI RIVER COMMISSION  
 U. S. WATERWAYS EXPERIMENT STATION  
**CALIFORNIA BEARING RATIO INVESTIGATION**  
**TEST EQUIPMENT**  
 FIGURE TAKEN FROM ENGINEERING  
 MANUAL CHAPTER XXX

Figure 7  
 California Bearing Test Equipment

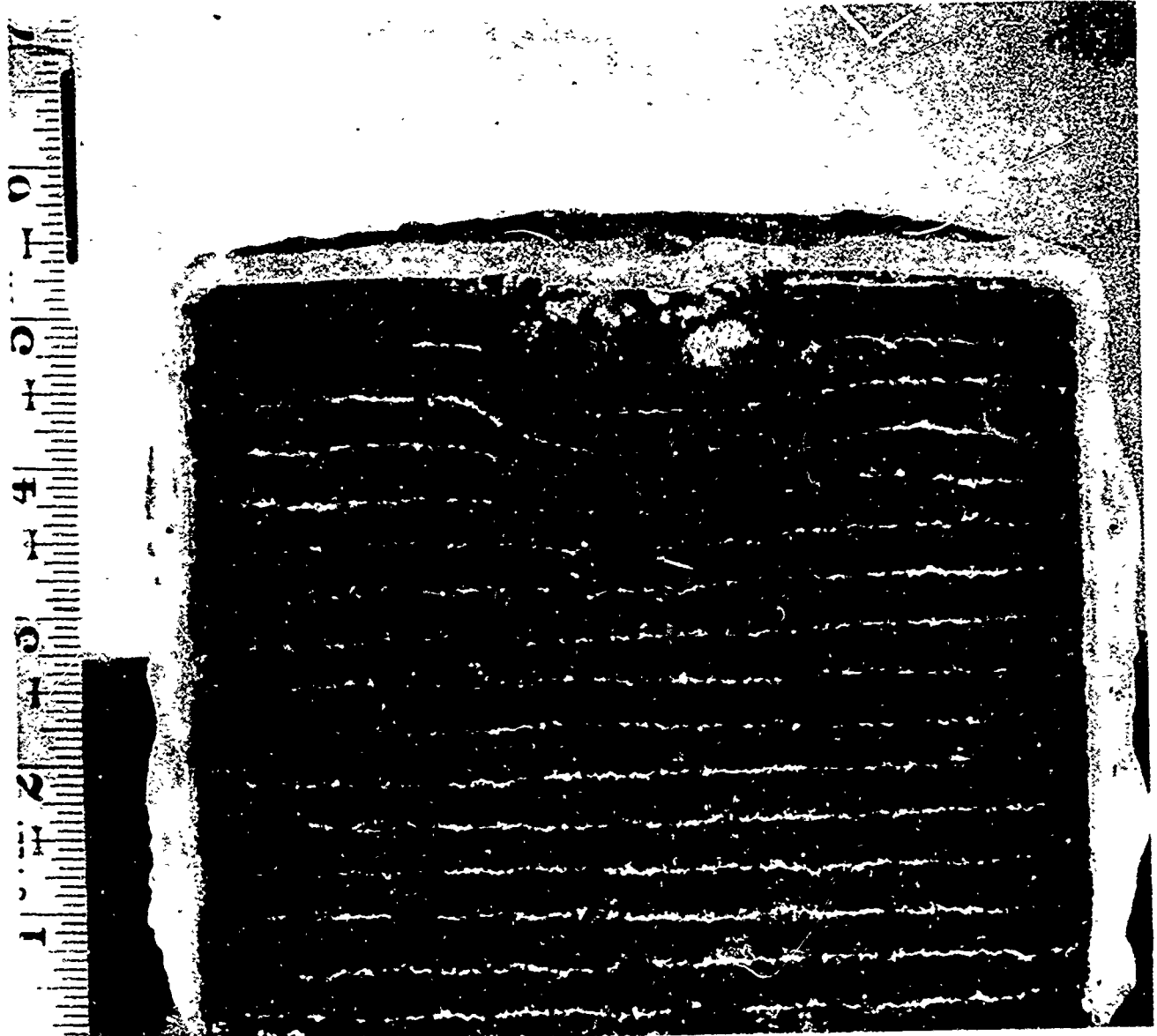


Figure 8

Deformations in the Soil after CBR Test



Figure 9  
U.S. Army CREEL Ram Penetrometer

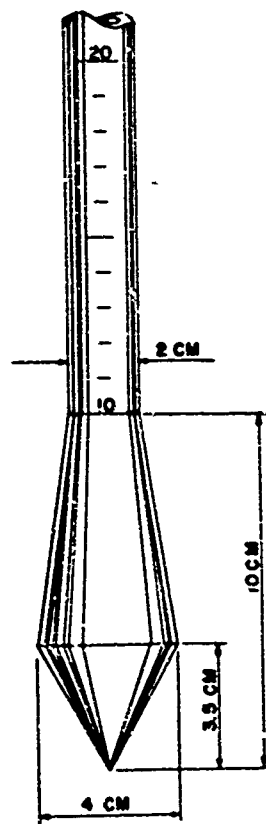


Figure 10  
Point of Ram Penetrometer

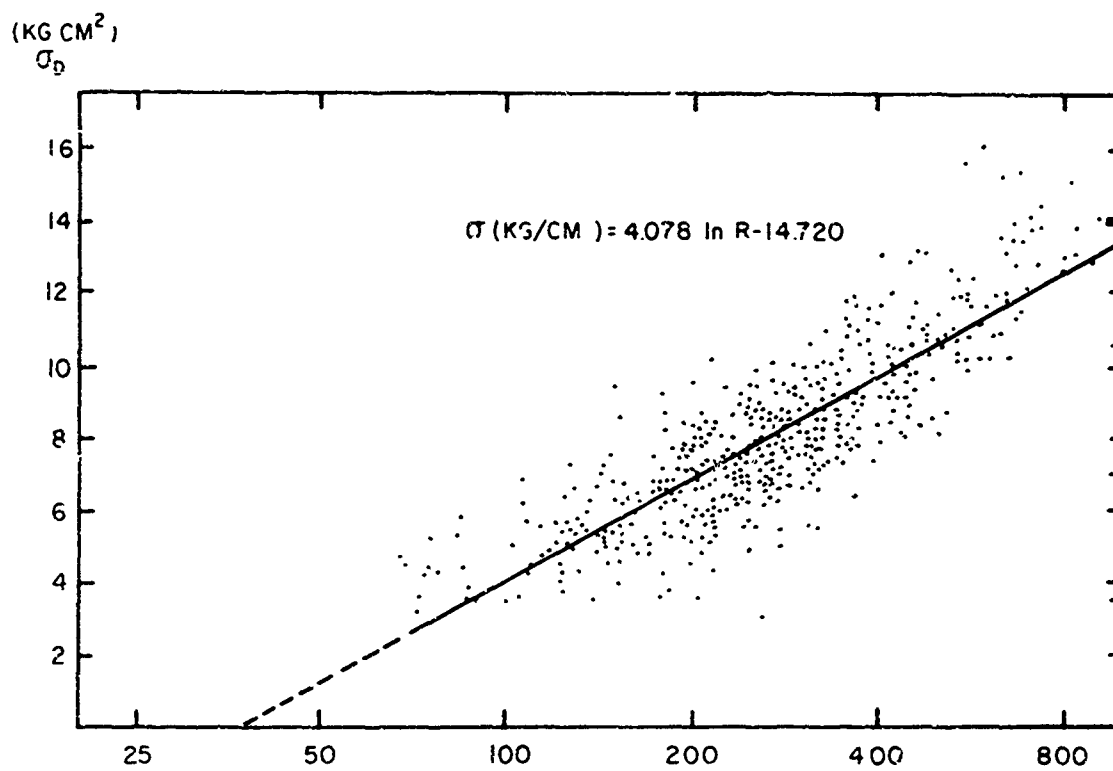


Figure 11  
Ram Hardness versus Compressive Strength

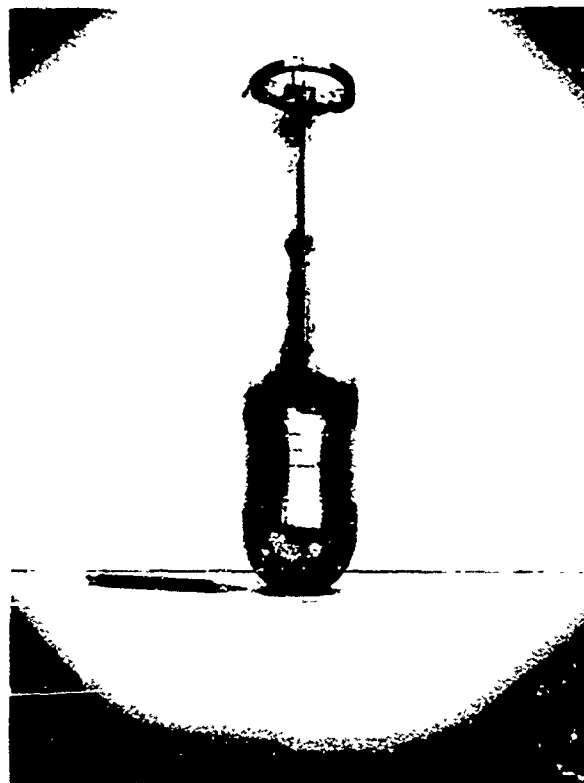


Figure 12  
Picture of Impact Penetrometer

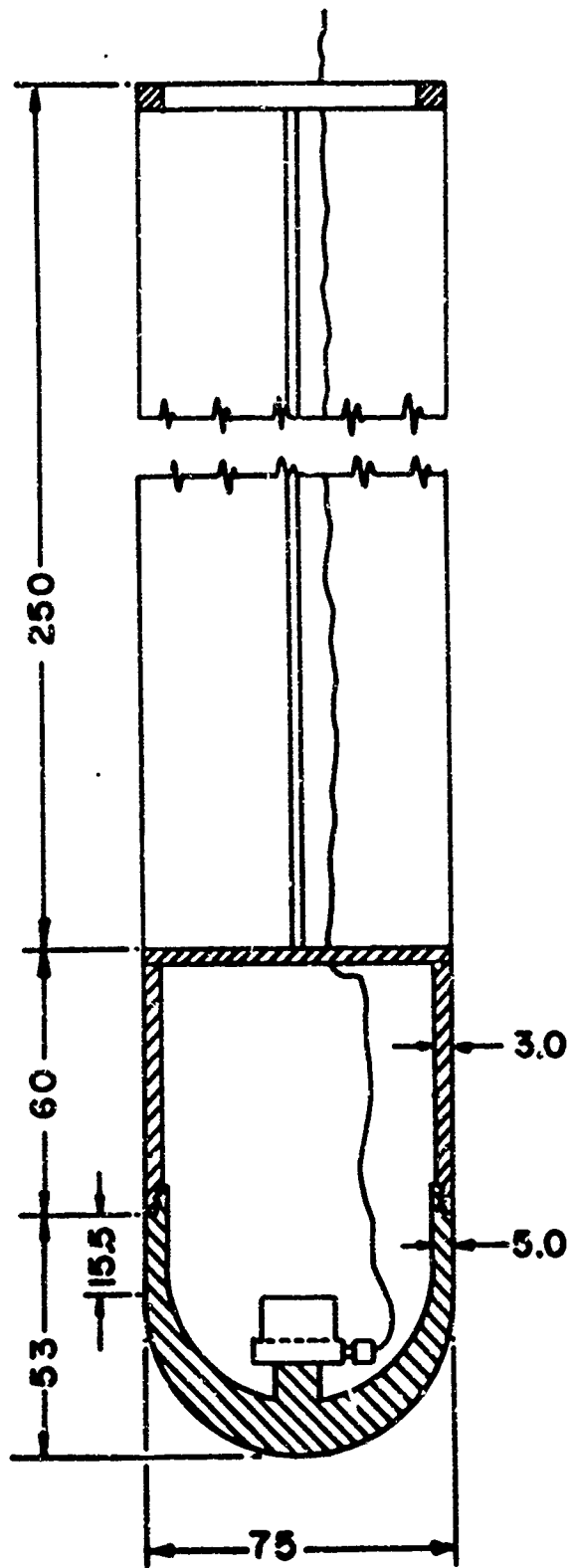


Figure 13

Section through Impact Penetrometer  
 (Numbers are dimensions in millimeters)

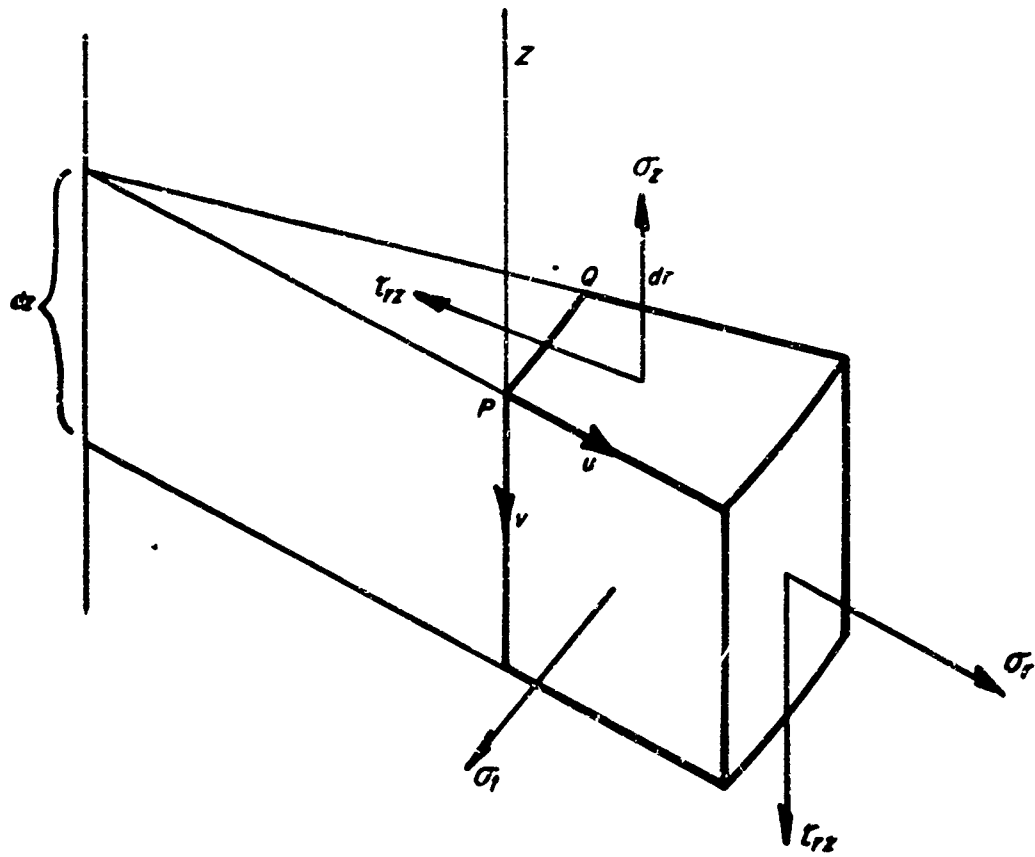


Figure 14  
Volume Element in Cylindrical Coordinate System

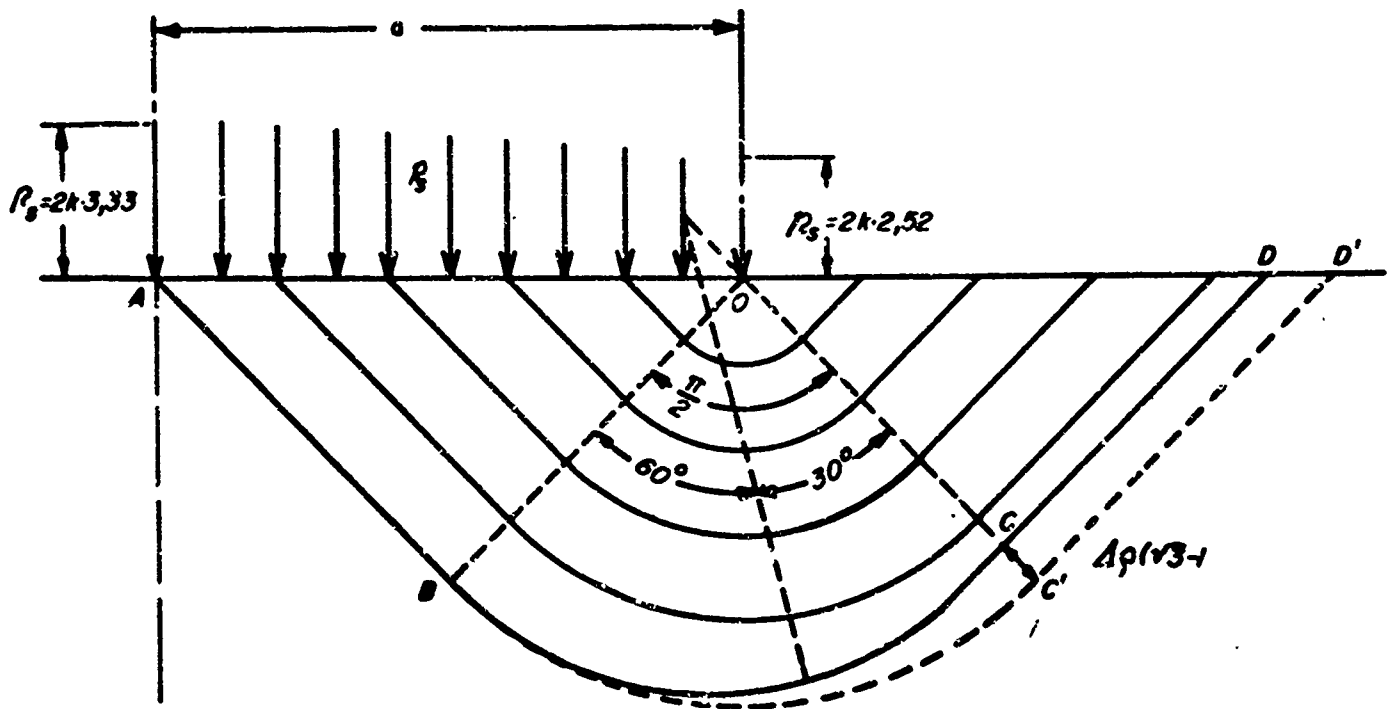


Figure 15  
Plastic Flow Lines for Hencky Contact Problem

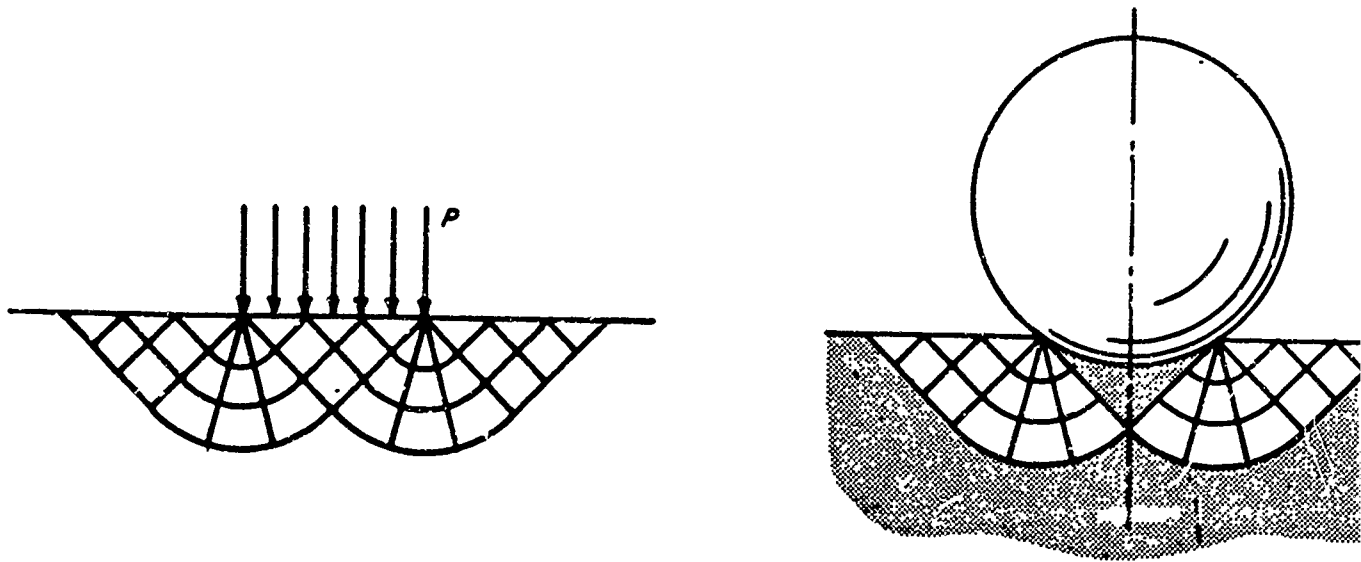


Figure 16  
Yield Lines for Plane and Spherical Punch

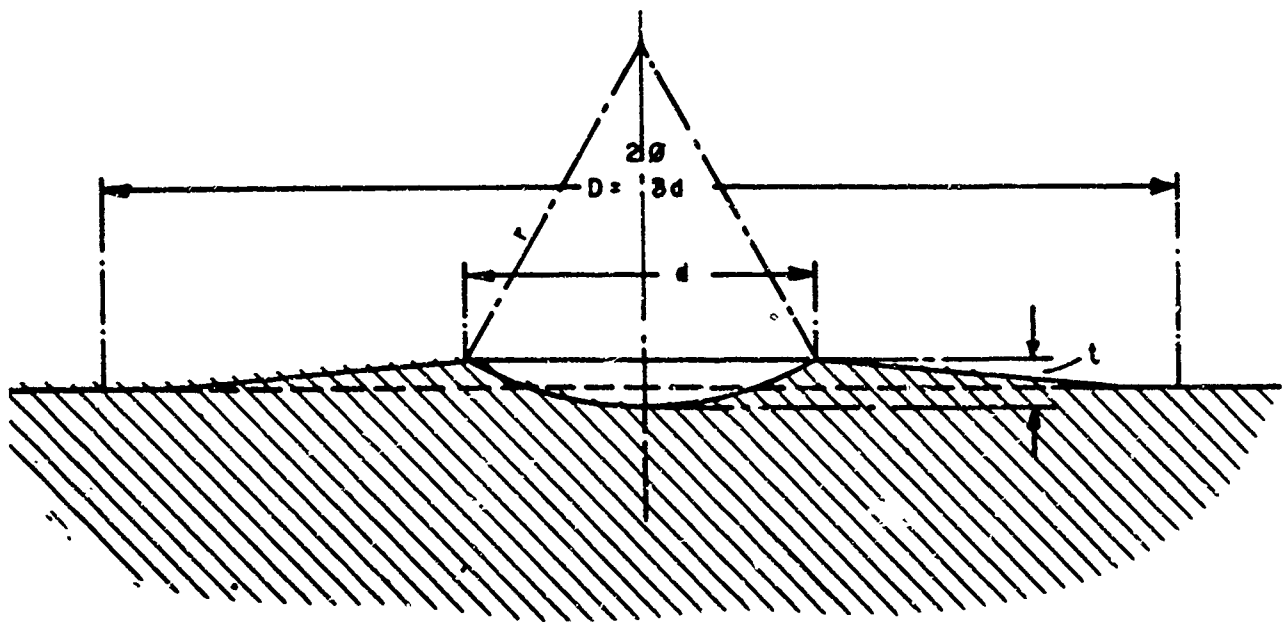
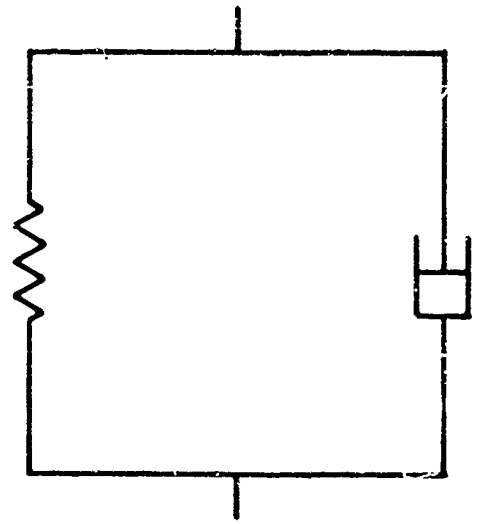


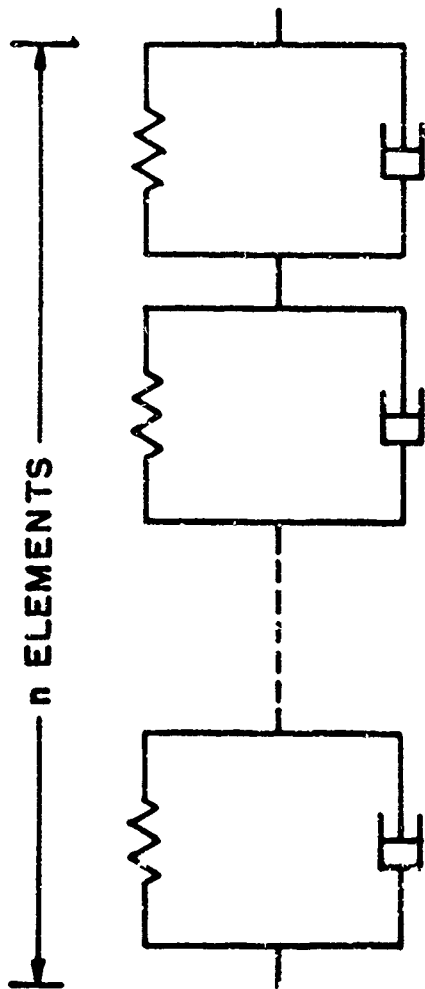
Figure 17  
Plasticized Region after Iterson



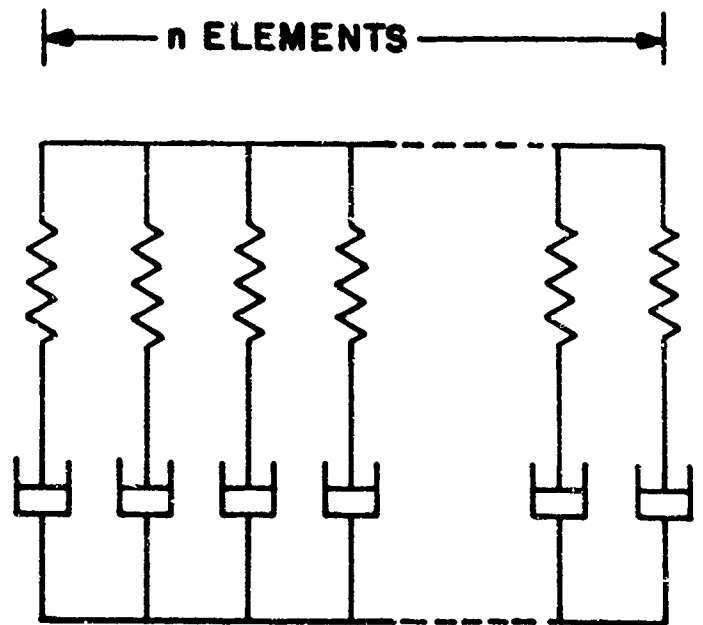
(A) MAXWELL ELEMENT



(B) VOIGT-KELVIN ELEMENT



(C) VOIGT ELEMENTS  
IN SERIES



(D) MAXWELL ELEMENTS  
PARALLEL

Figure 18  
Rheological Models

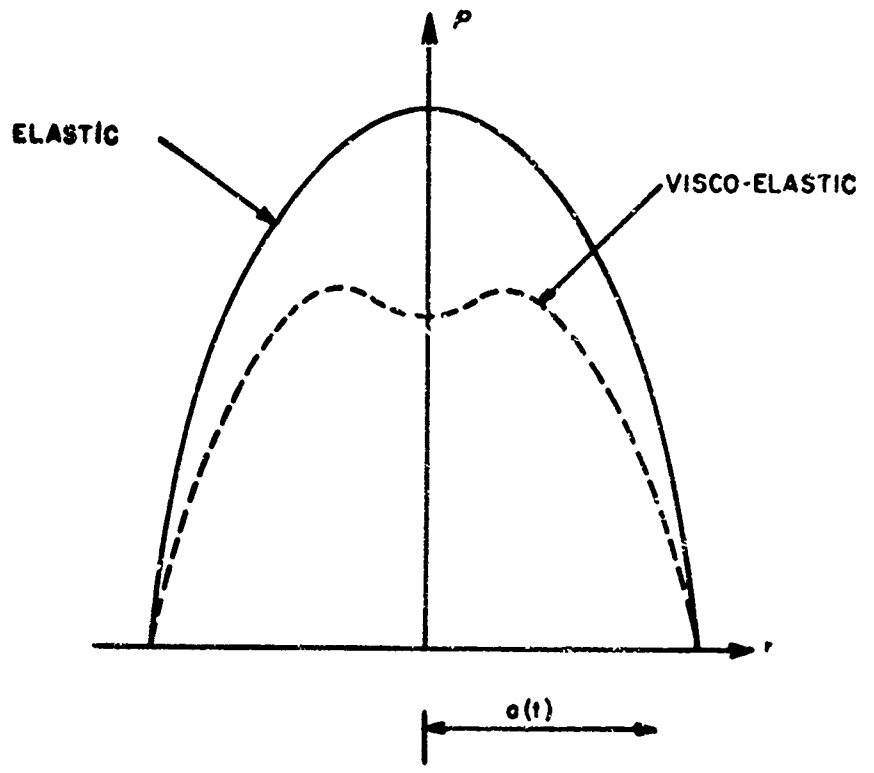


Figure 19  
Contact Stress Distribution after Lee

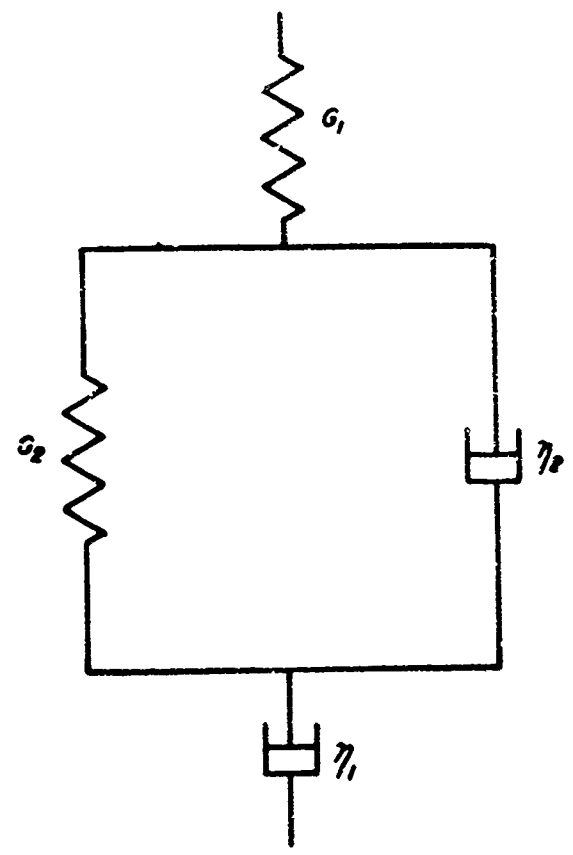


Figure 20  
Four Parameter Model

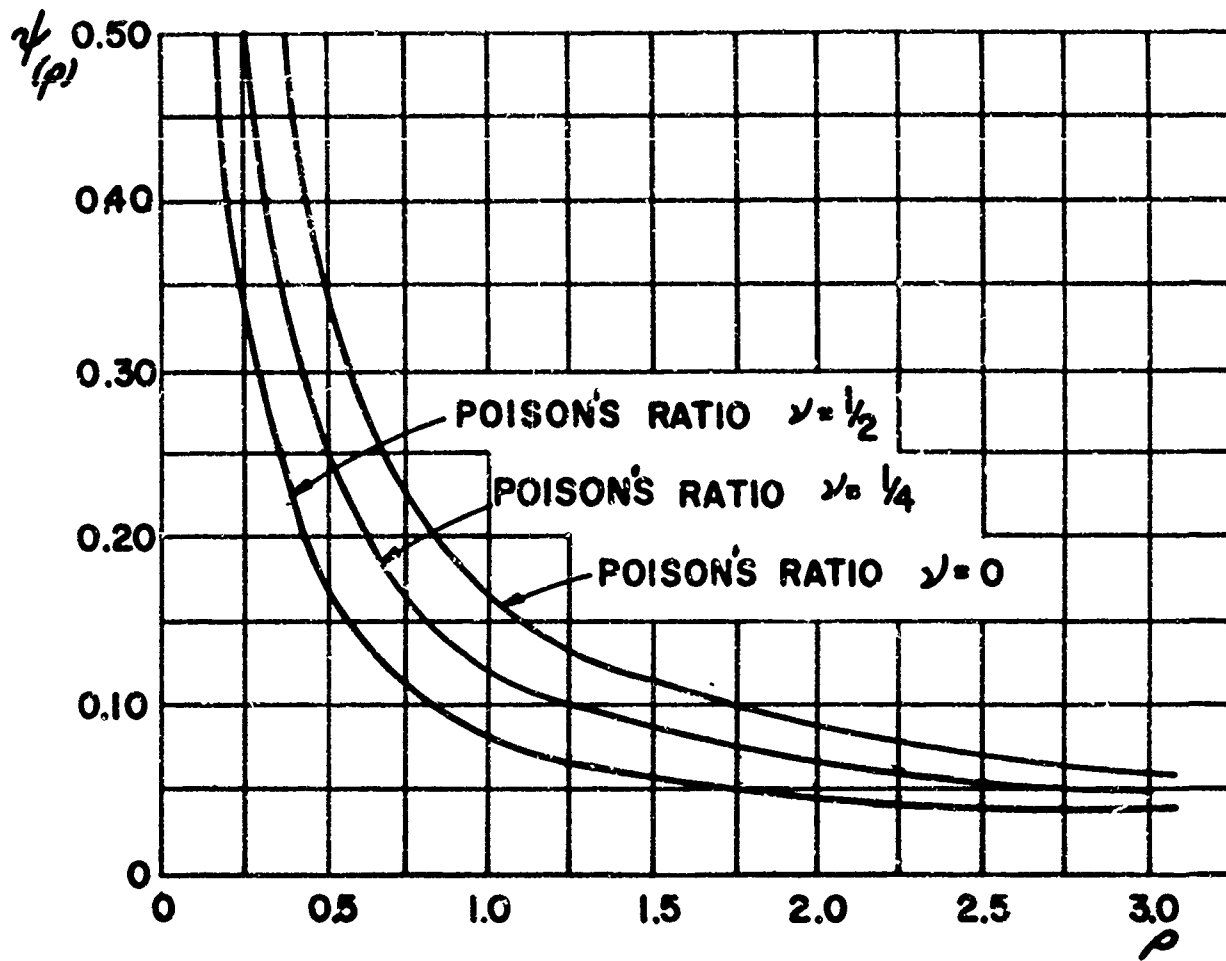


Figure 21  
 $\psi$  Versus  $\rho$

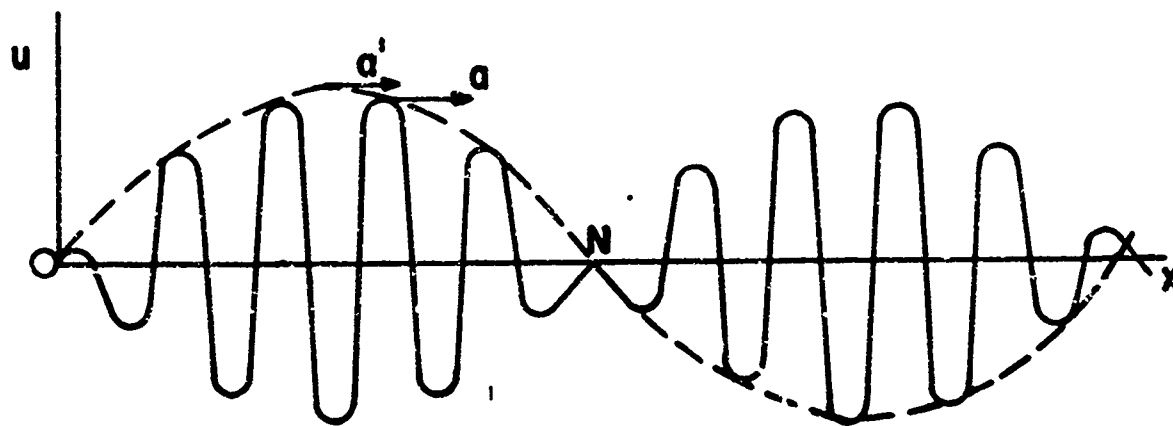


Figure 22  
 Group Velocity of Wave Trains

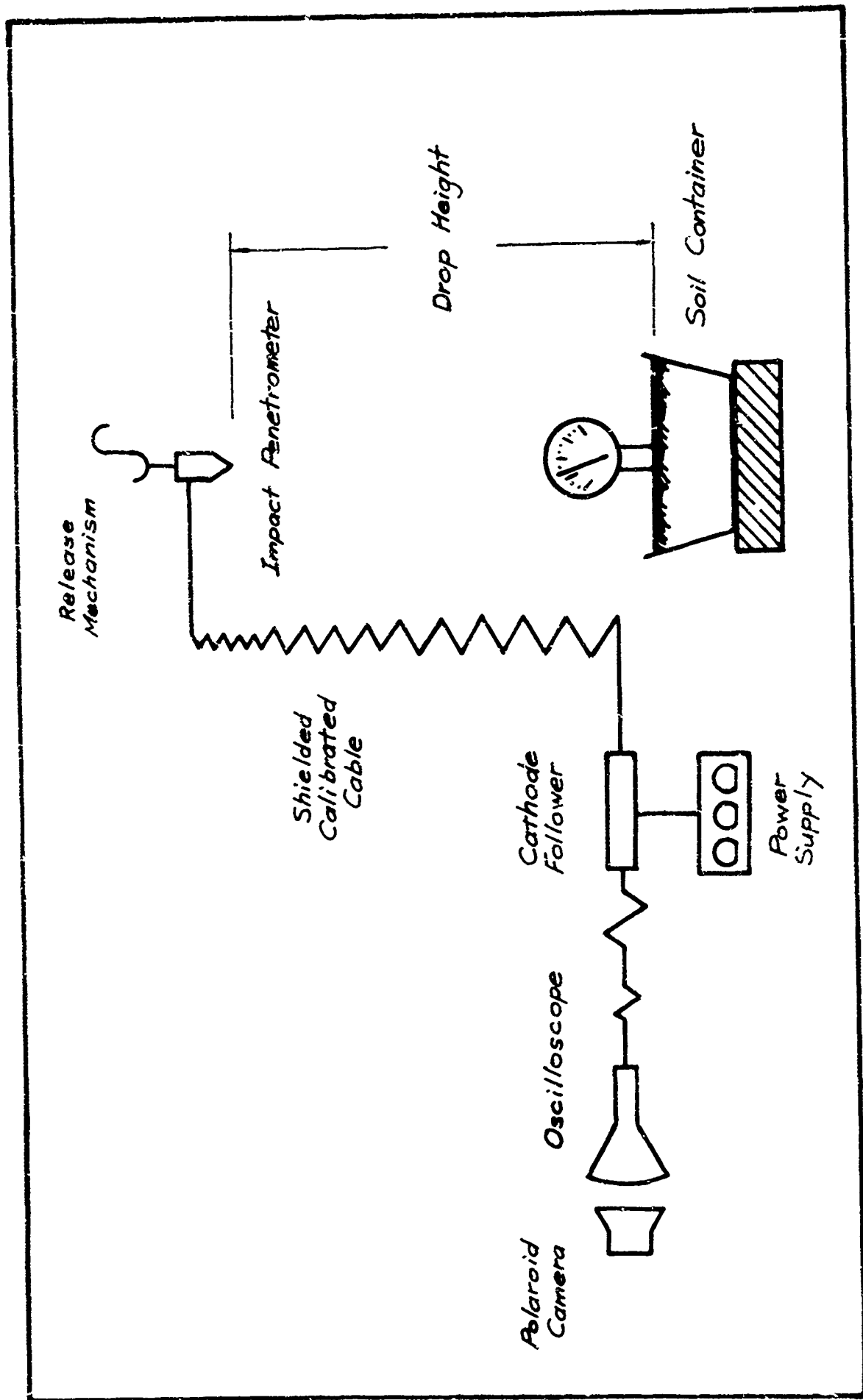


Figure 23: Schematic Test Setup



Figure 24  
Penetrometer before Impact on Paraffin



Figure 25  
Penetration into Estan 3



Figure 26  
Deformation produced by 920 cm/sec Impact  
on Cambar M-348

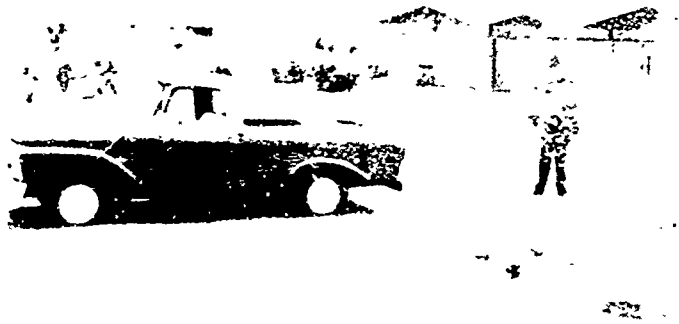


Figure 27  
Test Setup for Series No. 41

T e s t   S e r i e s   N o .   3 1

Target Material: Cambar Wax M-348 at 31°C.

Calibration Factor of Accelerometer:  $K = 8.6 \text{ mV/g}$

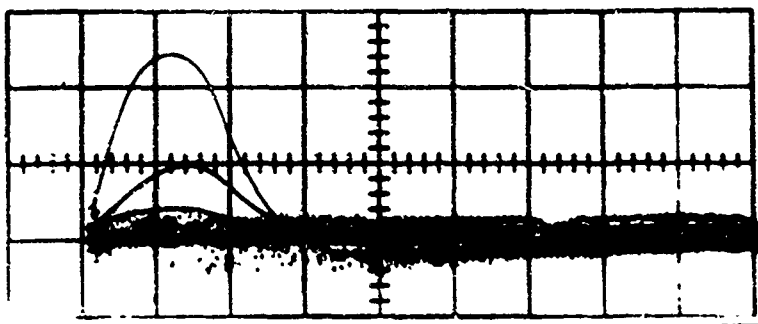
Drop Height:  $H = 61 \text{ cm}$

Oscilloscope Calibration:

$M_a = 200 \text{ mV/cm}$

$M_t = 5 \text{ msec/cm}$

$t = 0.16 \text{ cm}$



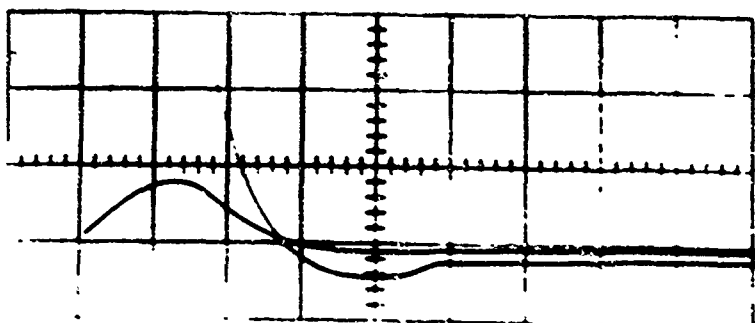
Drop Height:  $H = 122 \text{ cm}$

Oscilloscope Calibration:

$M_a = 200 \text{ mV/cm}$

$M_t = 5 \text{ msec/cm}$

$t = 0.64 \text{ cm}$



T e s t   S e r i e s   N o . 3 1

Target Material: Cambar Wax M-349 at 31°C.

Calibration Factor of Accelerometer:  $K = 8.6 \text{ mV/g}$

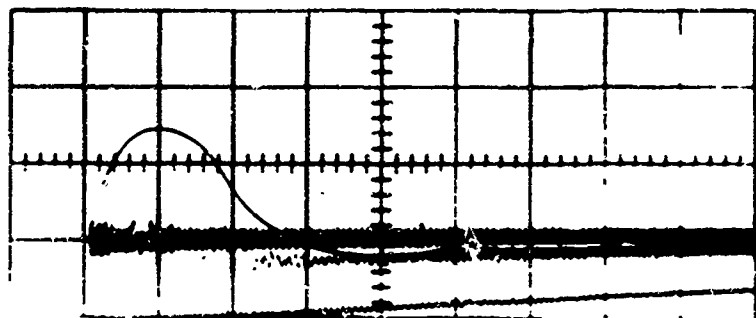
Drop Height:  $H = 183 \text{ cm}$

Oscilloscope Calibration:

$M_a = 500 \text{ mV/cm}$

$M_t = 5 \text{ msek/cm}$

$t = 0.8 \text{ cm}$



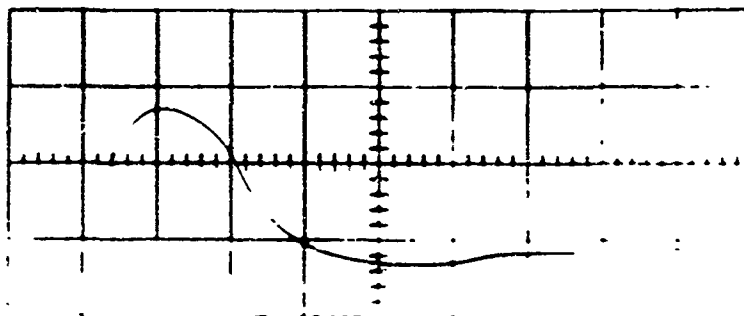
Drop Height:  $H = 305 \text{ cm}$

Oscilloscope Calibration:

$M_a = 500 \text{ mV/cm}$

$M_t = 5 \text{ msek/cm}$

$t = 3.2 \text{ cm}$



T e s t   S e r i e s   N o . 31

Target Material: Cambar Wax M-348 at 31°C.

Calibration Factor of Accelerometer:  $K = 8.6 \text{ mV/g}$

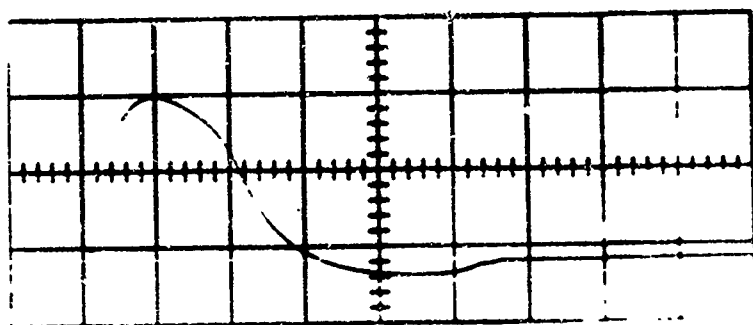
Drop Height:  $H = 425 \text{ cm}$

Oscilloscope Calibration:

$M_a = 500 \text{ mV/cm}$

$M_t = 5 \text{ msec/cm}$

$t = 3.8 \text{ cm}$



T e s t   S e r i e s   N o . 3 2

Target Material: Lubricating Grease Estan 3 at 28°C.

Calibration Factor of Accelerometer:  $K = 8.6 \text{ mV/g}$

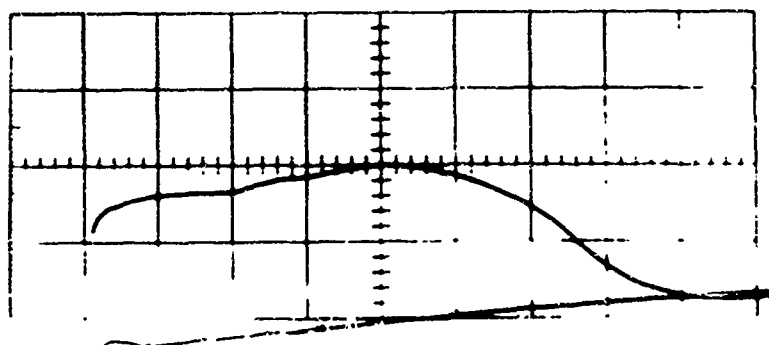
Drop Height:  $H = 61 \text{ cm}$

Oscilloscope Calibration:

$M_a = 50 \text{ mV/cm}$

$M_t = 10 \text{ msec/cm}$

$t = 12.8 \text{ cm}$



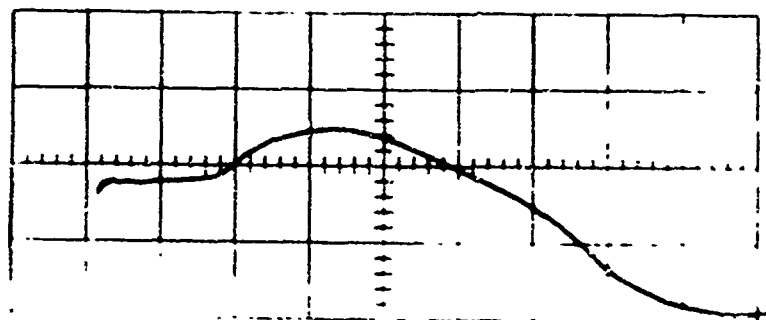
Drop Height:  $H = 122 \text{ cm}$

Oscilloscope Calibration:

$M_a = 50 \text{ mV/cm}$

$M_t = 5 \text{ msec/cm}$

$t = 19.0 \text{ cm}$



T e s t   S e r i e s   N o .   3 2

Target Material: Lubricating Grease Estan 3 at 28°C.

Calibration Factor of Accelerometer:  $K = 8.6 \text{ mV/g}$

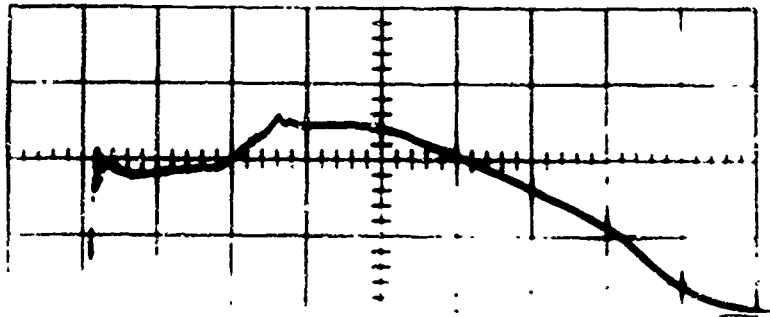
Drop Height:  $H = 183 \text{ cm}$

Oscilloscope Calibration:

$M_a = 50 \text{ mV/cm}$

$M_t = 10 \text{ msek/cm}$

$t = 24.0 \text{ cm}$



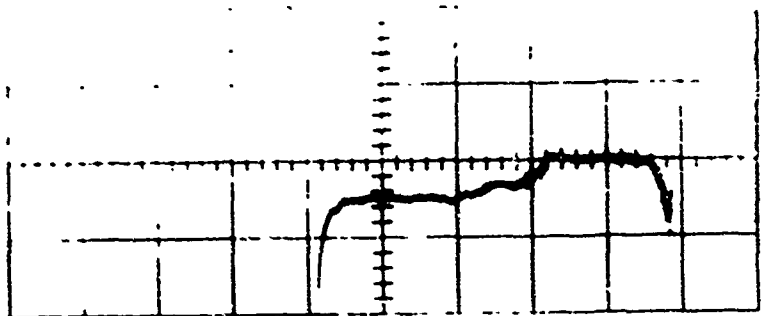
Drop Height:  $H = 305 \text{ cm}$

Oscilloscope Calibration:

$M_a = 50 \text{ mV/cm}$

$M_t = 10 \text{ msek/cm}$

$t = 30.0 \text{ cm}$



Test Series No. 34

Target Material: Paraffin at 28°C.

Calibration Factor of Accelerometer:  $K = 8.6 \text{ mV/g}$

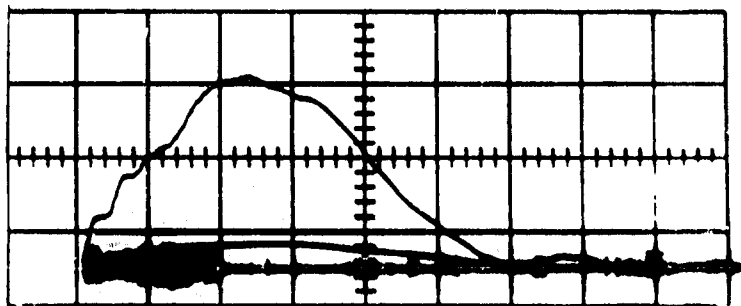
Drop Height:  $H = 61 \text{ cm}$

Oscilloscope Calibration:

$M_a = 2,000 \text{ mV/cm}$

$M_t = 0.2 \text{ msec/cm}$

$t = 0.1 \text{ cm}$



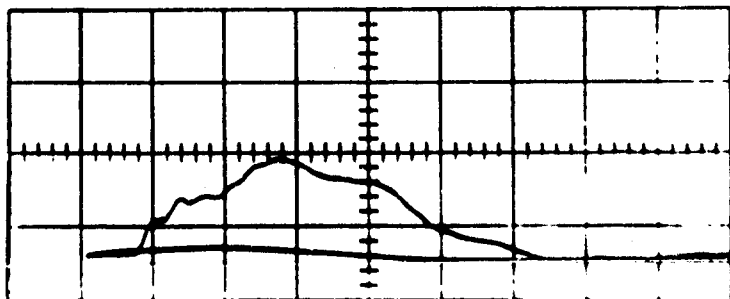
Drop Height:  $H = 122 \text{ cm}$

Oscilloscope Calibration:

$M_a = 5,000 \text{ mV/cm}$

$M_t = 0.2 \text{ msec/cm}$

$t = 0.1 \text{ cm}$



Test Series No. 34

Target Material: Paraffin at 28°C.

Calibration Factor of Accelerometer:  $K = 8.6 \text{ mV/g}$

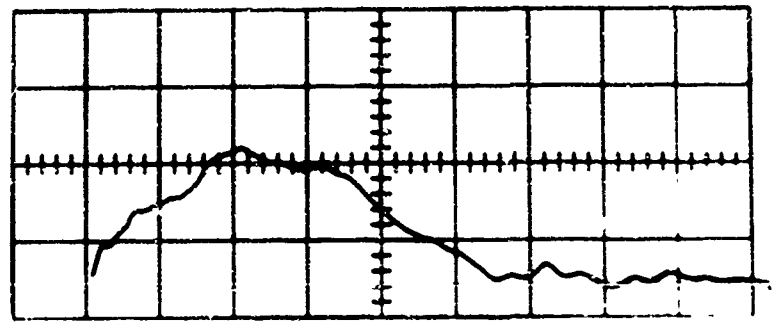
Drop Height:  $H = 183 \text{ cm}$

Oscilloscope Calibration:

$M_a = 5,000 \text{ mV/cm}$

$M_t = 0.2 \text{ msek/cm}$

$t = 1.4 \text{ cm}$



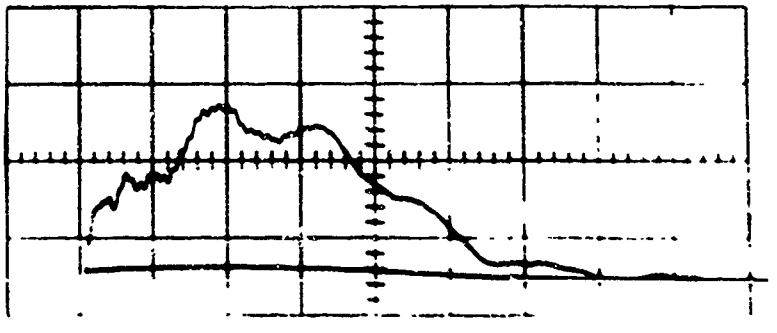
Drop Height:  $H = 305 \text{ cm}$

Oscilloscope Calibration:

$M_a = 5,000 \text{ mV/cm}$

$M_t = 0.2 \text{ msek/cm}$

$t = 0.3 \text{ cm}$



T e s t   S e r i e s   N o .   3 7

Target Material: Undisturbed Clay Soil

Calibration Factors: Penetrometer:  $K = 8.6 \text{ mV/g}$

$r_1$ :  $K = 34 \text{ mV/g}$ ;  $r_2$ :  $K = 56 \text{ mV/g}$

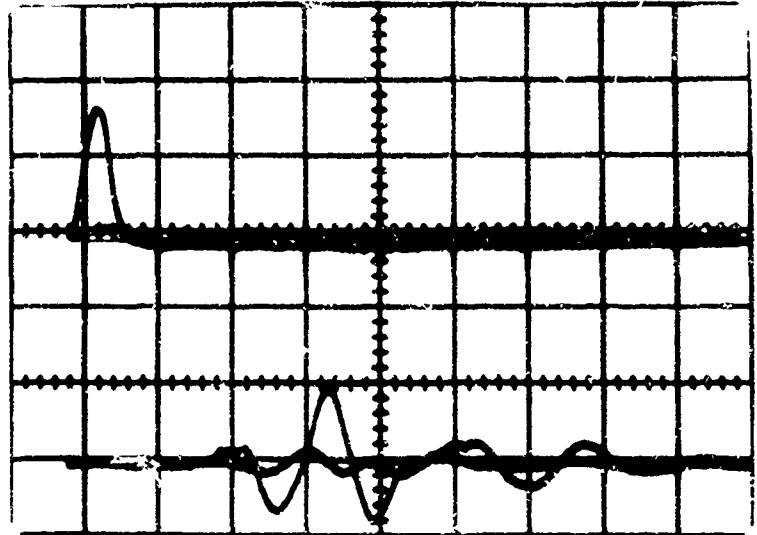
Drop Height:  $H = 275 \text{ cm}$

Oscilloscope Calibration:

Penetrometer:

$M_a = 1000 \text{ mV/cm}$

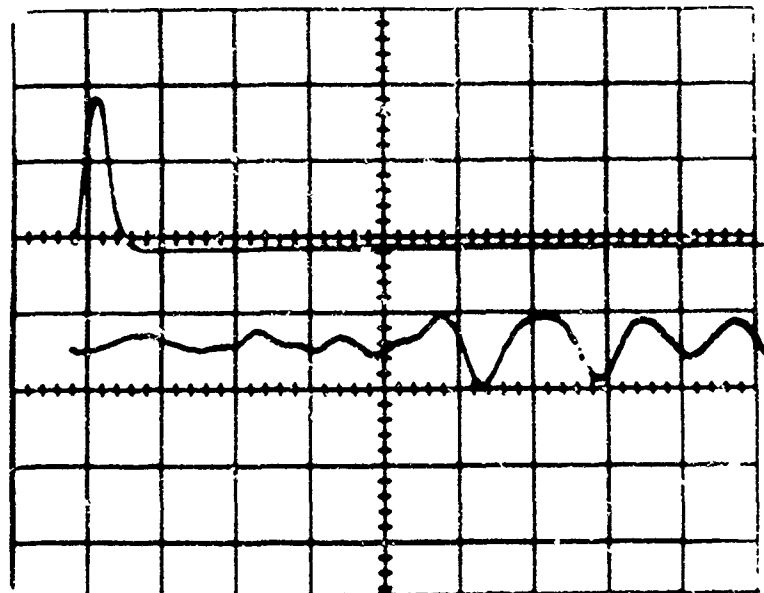
$M_t = 10 \text{ msec/cm}$



$r_1 = 283 \text{ cm}$

$M_a = 0.5 \text{ mV/cm}$

$M_t = 10 \text{ msec/cm}$



$r_2 = 482 \text{ cm}$

$M_a = 0.5 \text{ mV/cm}$

$M_t = 10 \text{ msec/cm}$

T e s t   S e r i e s   N o .   3 7

Target Material: Undisturbed Clay Soil

Calibration Factors: Penetrometer:  $K = 8.6 \text{ mV/g}$

$r_1$ :  $K = 34 \text{ mV/g}$ ;  $r_2$ :  $K = 56 \text{ mV/g}$

Drop Height:  $H = 520 \text{ cm}$

Oscilloscope Calibration:

Penetrometer:

$M_a = 1000 \text{ mV/cm}$

$M_t = 10 \text{ msec/cm}$

$r_1 = 290 \text{ cm}$

$M_a = 0.5 \text{ mV/cm}$

$M_t = 10 \text{ msec/cm}$

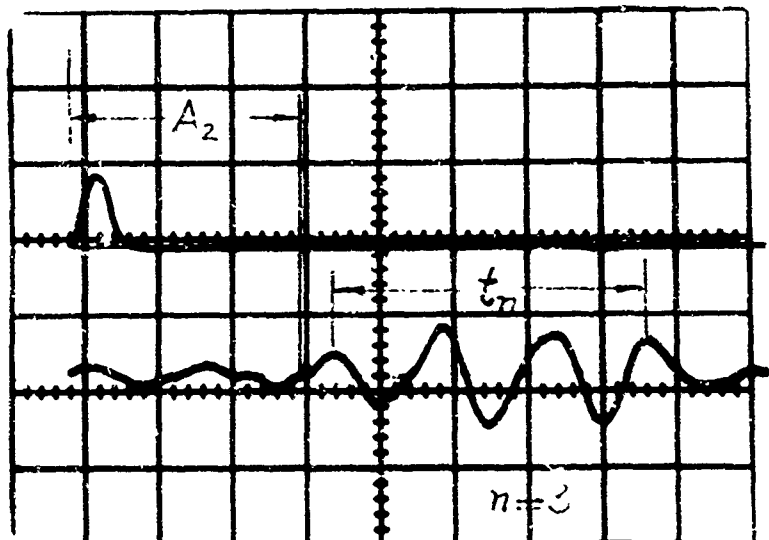
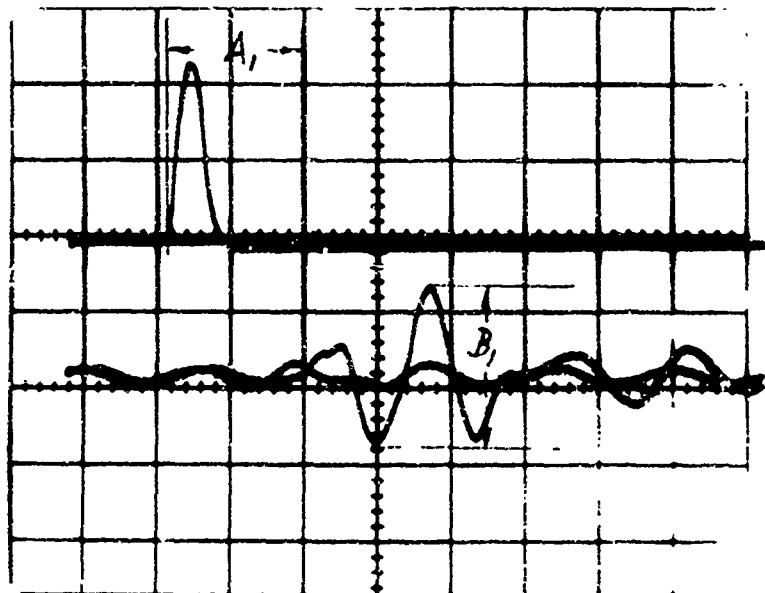
$r_2 = 510 \text{ cm}$

$M_a = 0.5 \text{ mV/cm}$

$M_t = 10 \text{ msec/cm}$

Penetrometer:

$M_a = 2000 \text{ mV/cm}$



Test Series No. 38

Target Material: Clayey, Sandy Silt, Undisturbed

Calibration Factors: Penetrometer:  $K = 8.6 \text{ mV/g}$

$r_1$ :  $K = 31 \text{ mV/g}$ ;  $r_2$ :  $K = 34 \text{ mV/g}$

Drop Height:  $H = 275 \text{ cm}$

Oscilloscope Calibration:

Penetrometer:

$M_a = 200 \text{ mV/cm}$

$M_t = 2 \text{ msec/cm}$

$r_1 = 680 \text{ cm}$

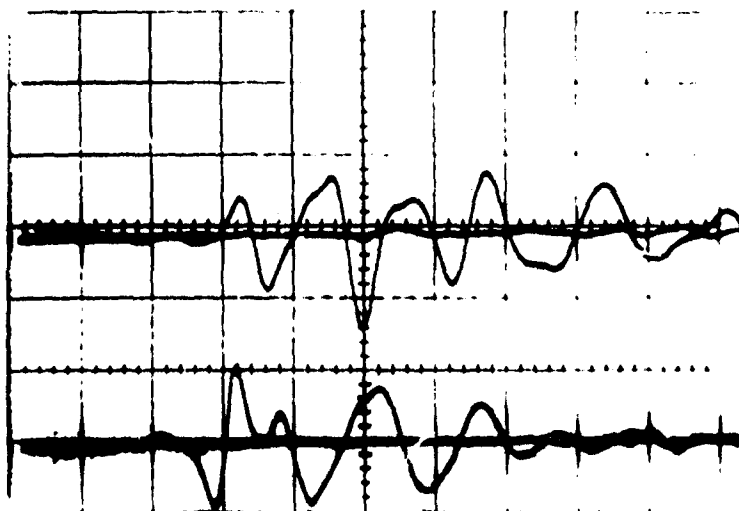
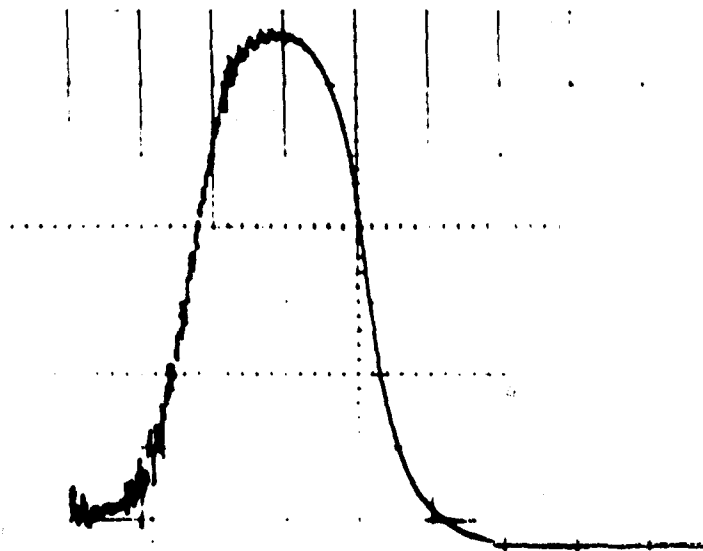
$M_a = 1 \text{ mV/cm}$

$M_t = 10 \text{ msec/cm}$

$r_2 = 1000 \text{ cm}$

$M_a = 500 \text{ mV/cm}$

$M_t = 10 \text{ msec/cm}$



Test Series No. 38

Target Material: Clayey, Sandy Silt, Undisturbed

Calibration Factors: Penetrometer:  $K = 8.6 \text{ mV/g}$

$r_1$ :  $K = 31 \text{ mV/g}$ ;  $r_2$ :  $K = 34 \text{ mV/g}$

Drop Height:  $H = 275 \text{ cm}$

Oscilloscope Calibration:

Penetrometer:

$M_a = 200 \text{ mV/cm}$

$M_t = 2 \text{ msec/cm}$

$r_1 = 680 \text{ cm}$

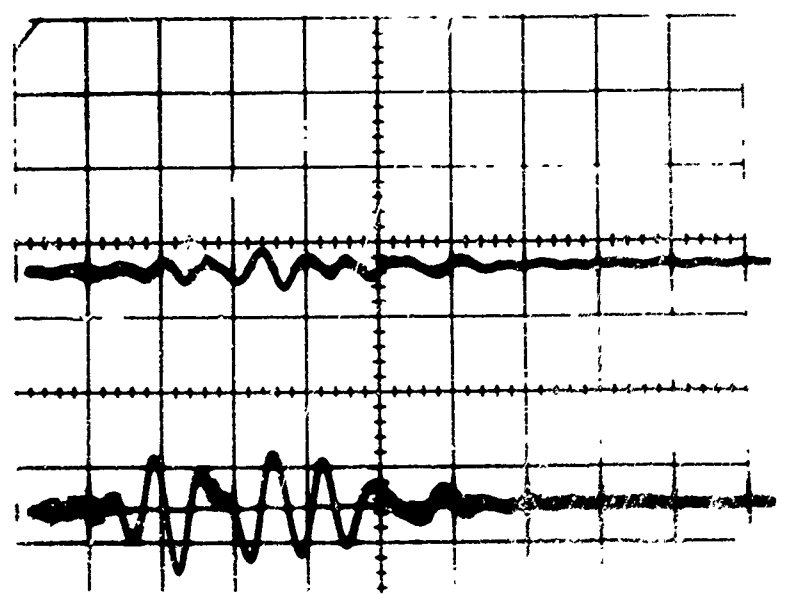
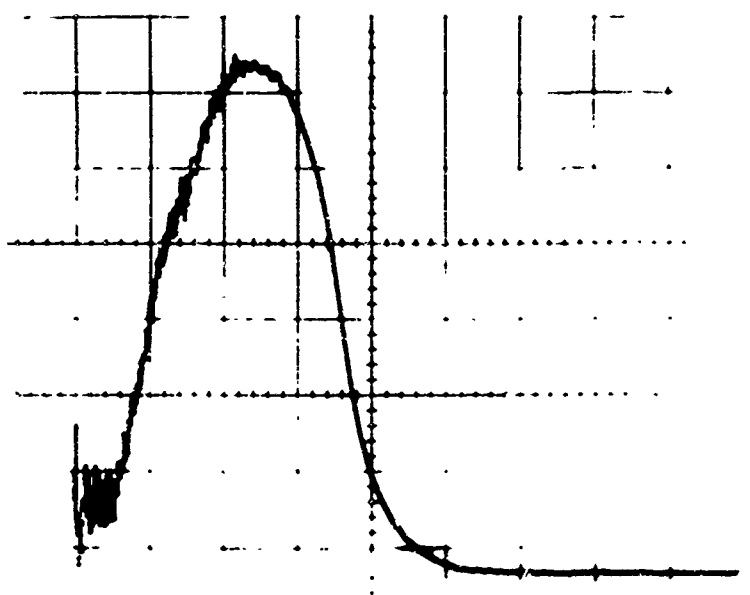
$M_a = 500 \text{ mV/cm}$

$M_t = 20 \text{ msec/cm}$

$r_2 = 1000 \text{ cm}$

$M_a = 500 \text{ mV/cm}$

$M_t = 20 \text{ msec/cm}$



Test Series No. 38

Target Material: Clayey, Sandy Silt, Undisturbed

Calibration Factors: Penetrometer:  $K = 8.6 \text{ mV/g}$

$r_1$ :  $K = 31 \text{ mV/g}$ ;  $r_2$ :  $K = 34 \text{ mV/g}$

Drop Height:  $H = 275 \text{ cm}$

Oscilloscope Calibration:

Penetrometer:

$M_a = 200 \text{ mV/cm}$

$M_t = 10 \text{ msec/cm}$

$r_1 = 680 \text{ cm}$

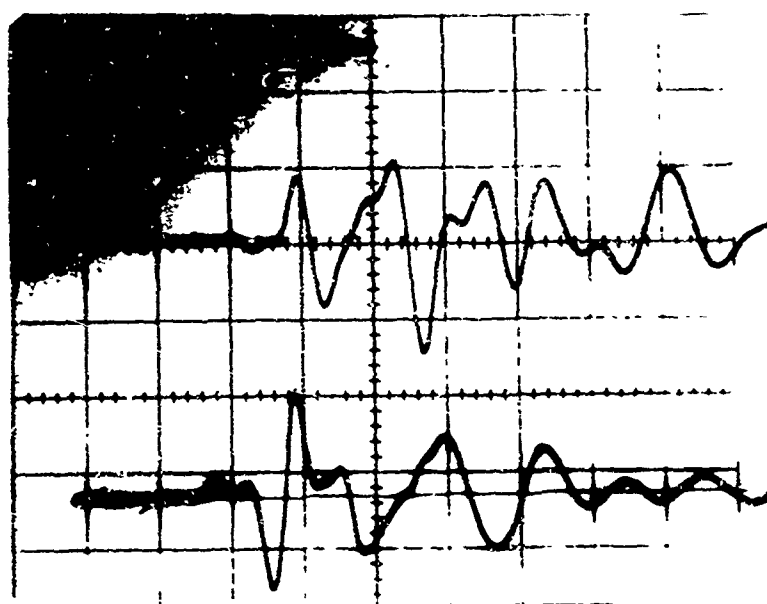
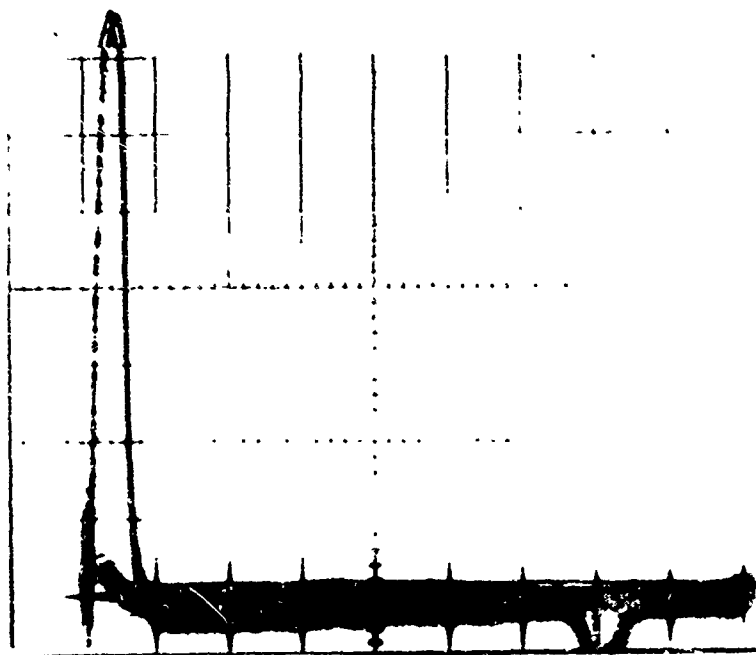
$M_a = 1 \text{ mV/cm}$

$M_t = 10 \text{ msec/cm}$

$r_2 = 1000 \text{ cm}$

$M_a = 500 \text{ mV/cm}$

$M_t = 10 \text{ msec/cm}$



T e s t   S e r i e s   N o . 3 8

Target Material: Clayey, Sandy Silt, Undisturbed

Calibration Factors: Penetrometer:  $K = 8.6 \text{ mV/g}$

$r_1$ :  $K = 31 \text{ mV/g}$ ;  $r_2$ :  $K = 34 \text{ mV/g}$

Drop Height:  $H = 275 \text{ cm}$

Oscilloscope Calibration:

Penetrometer:

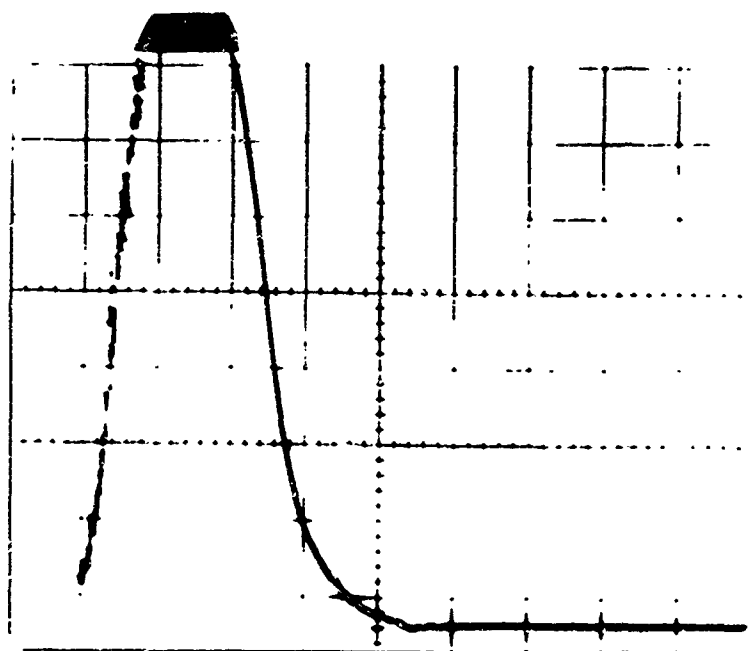
$M_a = 200 \text{ mV/cm}$

$M_t = 2 \text{ msek/cm}$

$r_1 = 580 \text{ cm}$

$M_a = 500 \text{ mV/cm}$

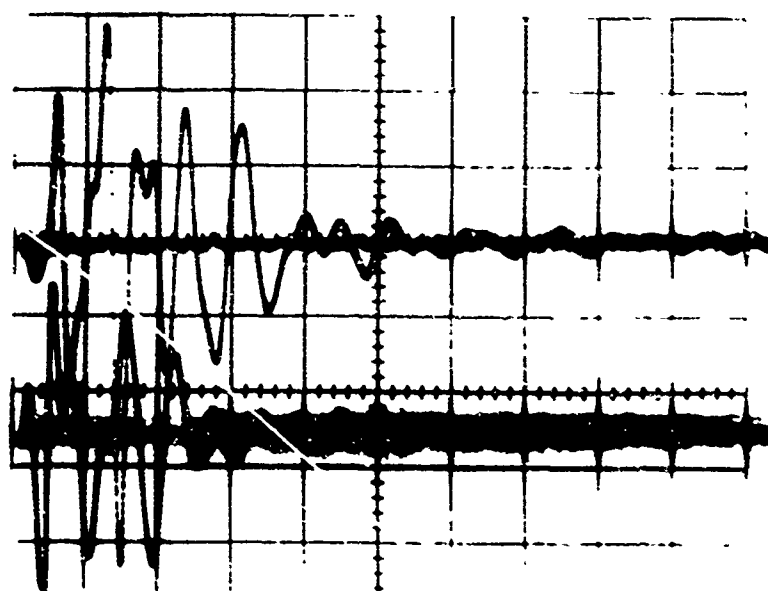
$M_t = 200 \text{ msek/cm}$



$r_2 = 1000 \text{ cm}$

$M_a = 200 \text{ mV/cm}$

$M_t = 200 \text{ msek/cm}$



T e s t   S e r i e s   N o .   3 8

Target Material: Clayey, Sandy Silt, Undisturbed

Calibration Factors: Penetrometer:  $K = 8.6 \text{ mV/g}$

$r_1$ :  $K = 31 \text{ mV/g}$ ;  $r_2$ :  $K = 34 \text{ mV/g}$

Drop Height:  $H = 520 \text{ cm}$

Oscilloscope Calibration:

Penetrometer:

$M_a = 500 \text{ mV/cm}$

$M_t = 2 \text{ msek/cm}$

$r_1 = 680 \text{ cm}$

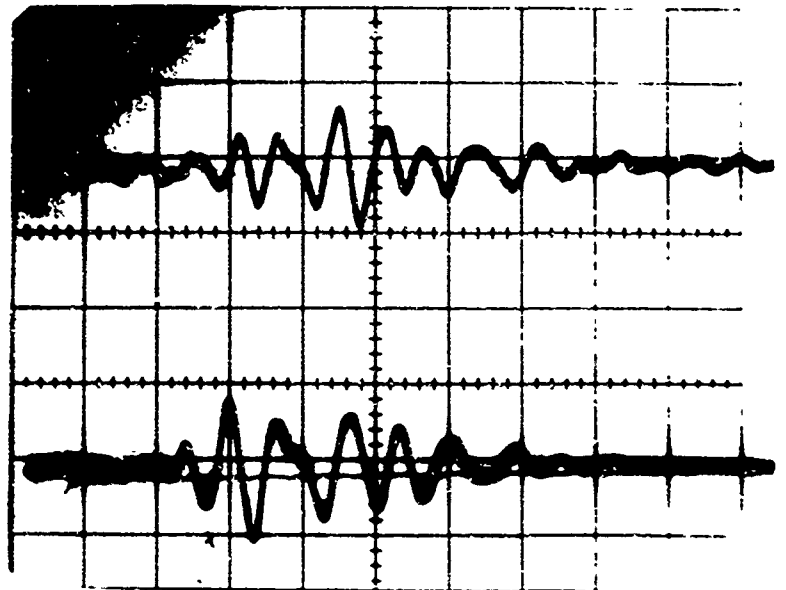
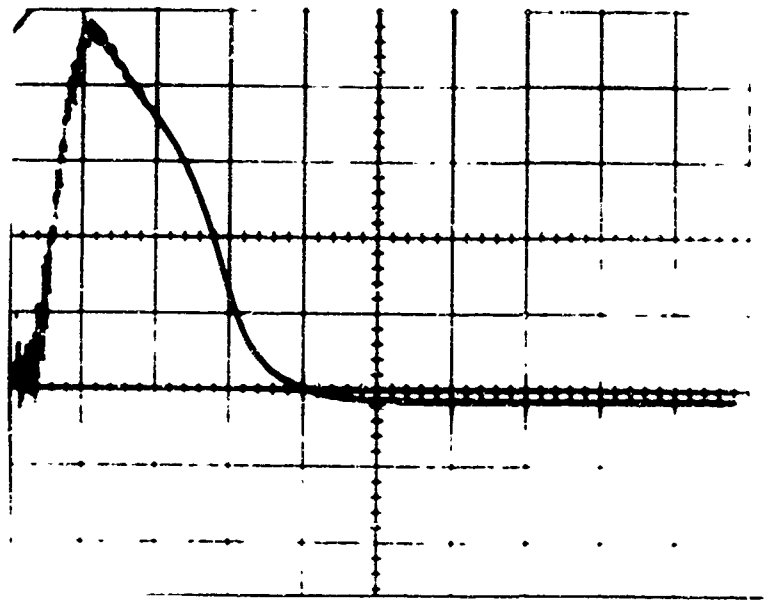
$M_a = 500 \text{ mV/cm}$

$M_t = 20 \text{ msek/cm}$

$r_2 = 1000 \text{ cm}$

$M_a = 200 \text{ mV/cm}$

$M_t = 20 \text{ msek/cm}$



T e s t   S e r i e s   N o .   3 9

Target Material: Beach Sand, Freely Deposited

Calibration Factors: Penetrometer:  $K = 8.6 \text{ mV/g}$

$r_1$ :  $K = 31 \text{ mV/g}$ ;  $r_2$ :  $K = 34 \text{ mV/g}$

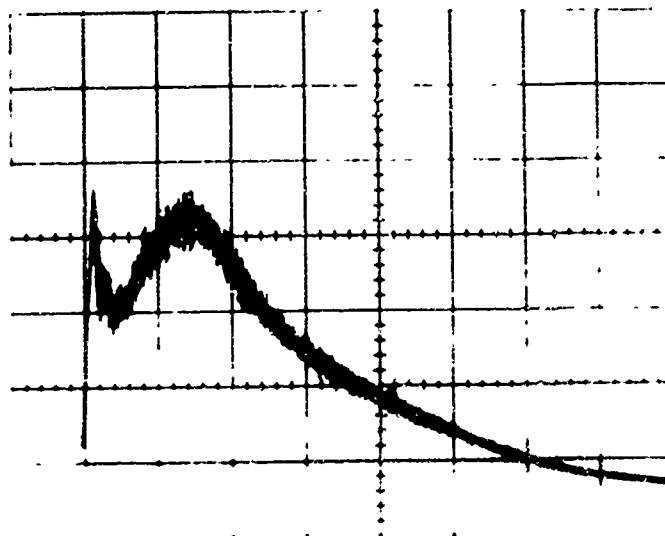
Drop Height:  $H = 275 \text{ cm}$

Oscilloscope Calibration:

Penetrometer:

$M_a = 100 \text{ mV/cm}$

$M_t = 5 \text{ msek/cm}$



$r_1 = 140 \text{ cm}$

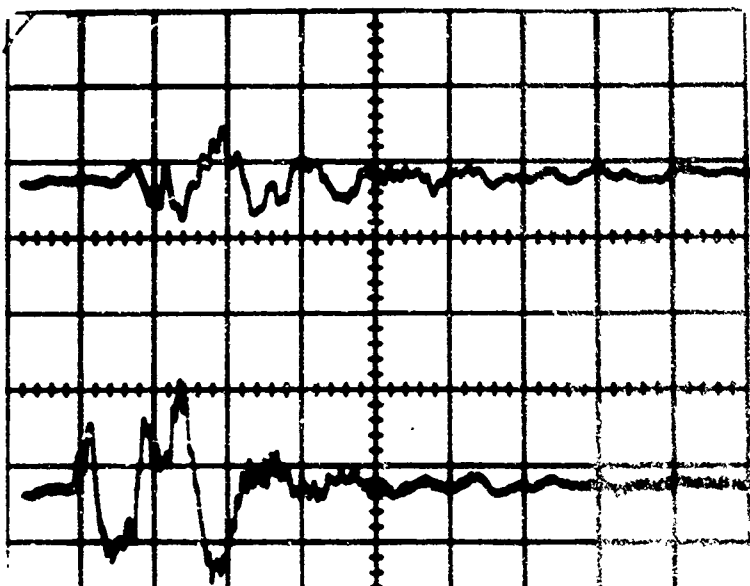
$M_a = 500 \text{ mV/cm}$

$M_t = 10 \text{ msek/cm}$

$r_2 = 280 \text{ cm}$

$M_a = 500 \text{ mV/cm}$

$M_t = 10 \text{ msek/cm}$



Test Series No. 39

Target Material: Beach Sand, Freely Deposited

Calibration Factors: Penetrometer:  $K = 8.6 \text{ mV/g}$

$r_1$ :  $K = 31 \text{ mV/g}$ ;  $r_2$ :  $K = 34 \text{ mV/g}$

Drop Height:  $H = 275 \text{ cm}$

Oscilloscope Calibration:

Penetrometer:

$M_a = 100 \text{ mV/cm}$

$M_t = 10 \text{ msec/cm}$

$r_1 = 140 \text{ cm}$

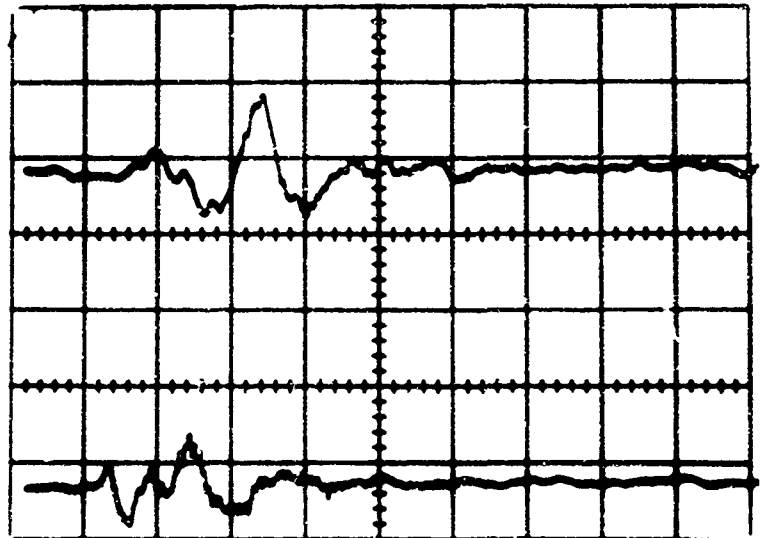
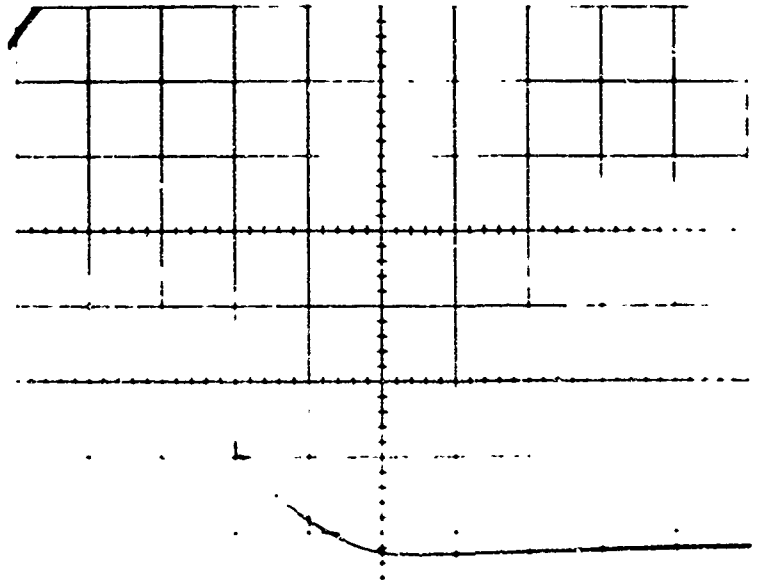
$M_a = 1 \text{ mV/cm}$

$M_t = 10 \text{ msec/cm}$

$r_2 = 280 \text{ cm}$

$M_a = 500 \text{ mV/cm}$

$M_t = 10 \text{ msec/cm}$



T e s t   S e r i e s   N o .   3 9

Target Material: Beach Sand, Freely Deposited

Calibration Factors: Penetrometer:  $K = 8.6 \text{ mV/g}$

$r_1$ :  $K = 31 \text{ mV/g}$ ;  $r_2$ :  $K = 34 \text{ mV/g}$

Drop Height:  $H = 520 \text{ cm}$

Oscilloscope Calibration:

Penetrometer:

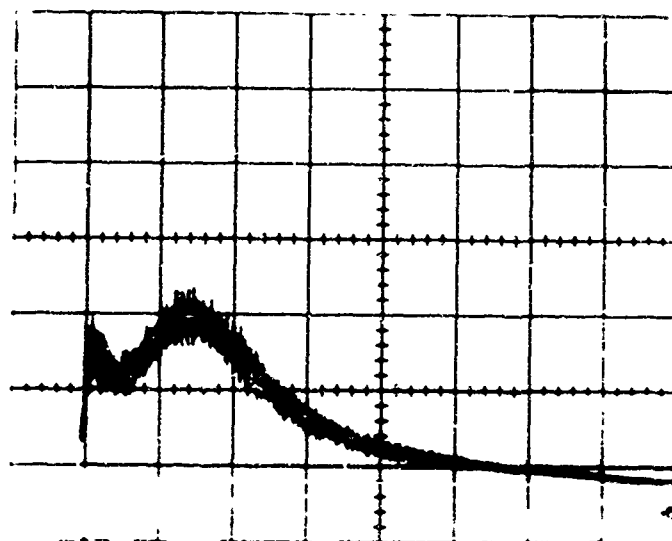
$M_a = 200 \text{ mV/cm}$

$M_t = 5 \text{ msek/cm}$

$r_1 = 140 \text{ cm}$

$M_a = 2 \text{ mV/cm}$

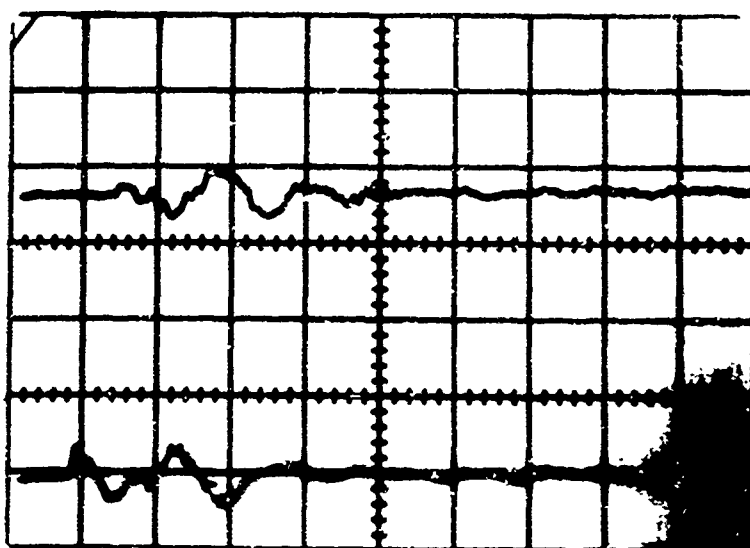
$M_t = 10 \text{ msek/cm}$



$r_2 = 280 \text{ cm}$

$M_a = 1 \text{ mV/cm}$

$M_t = 10 \text{ msek/cm}$



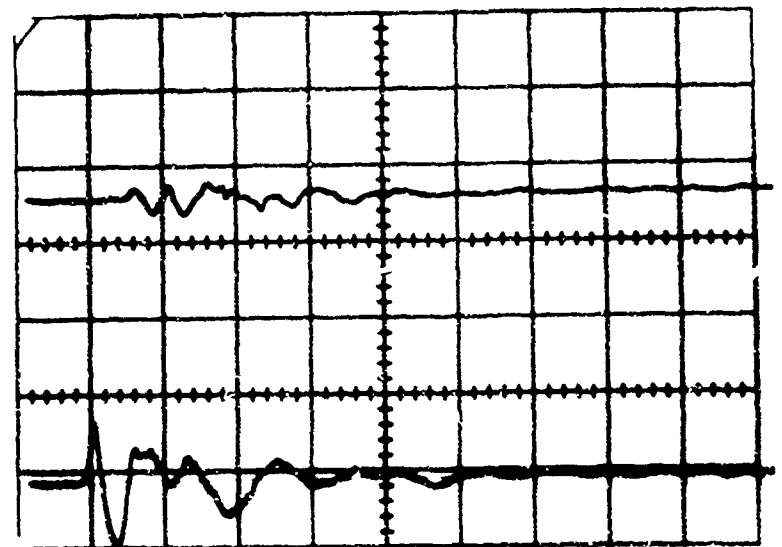
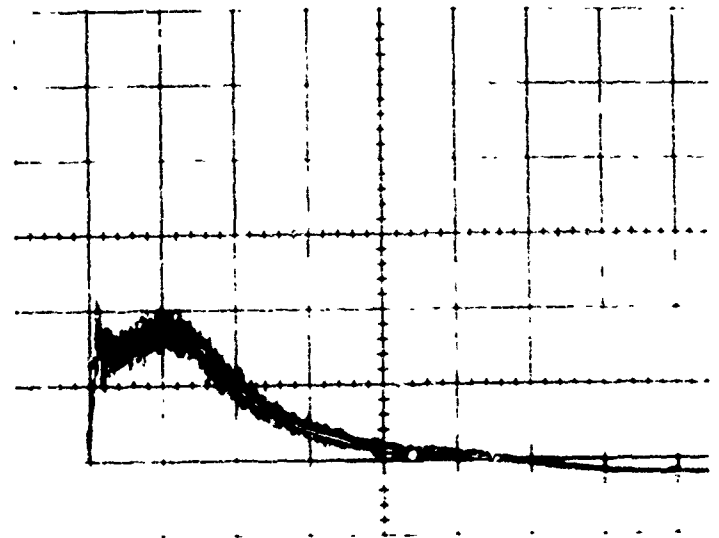
## T e s t   S e r i e s   N o . 3 9

Target Material: Beach Sand, Freely Deposited

Calibration Factors: Penetrometer:  $K = 8.6 \text{ mV/g}$  $r_1$ :  $K = 31 \text{ mV/g}$ ;  $r_2$ :  $K = 34 \text{ mV/g}$ Drop Height:  $H = 520 \text{ cm}$ 

Oscilloscope Calibration:

Penetrometer:

 $M_a = 200 \text{ mV/cm}$  $M_t = 5 \text{ msec/cm}$  $r_1 = 140 \text{ cm}$  $M_a = 2 \text{ mV/cm}$  $M_t = 10 \text{ msec/cm}$  $r_2 = 280 \text{ cm}$  $M_a = 2 \text{ mV/cm}$  $M_t = 10 \text{ msec/cm}$ 

Test Series No. 41

Target Material: Princeton Red Clay

Calibration Factors: Penetrometer:  $K = 8.6 \text{ mV/g}$

$r_1$ :  $K = 34 \text{ mV/g}$ ;  $r_2$ :  $K = 34 \text{ mV/g}$ ;

$r_3$ :  $K = 170 \text{ mV/g}$

Drop Height:  $H = 275 \text{ cm}$

Scilloscope Calibration:

Penetrometer:

$M_a = 500 \text{ mV/cm}$

$M_t = 5 \text{ msec/cm}$

$r_1 = 244 \text{ cm}$

$M_a = 500 \text{ mV/cm}$

$M_t = 10 \text{ msec/cm}$

$r_2 = 490 \text{ cm}$

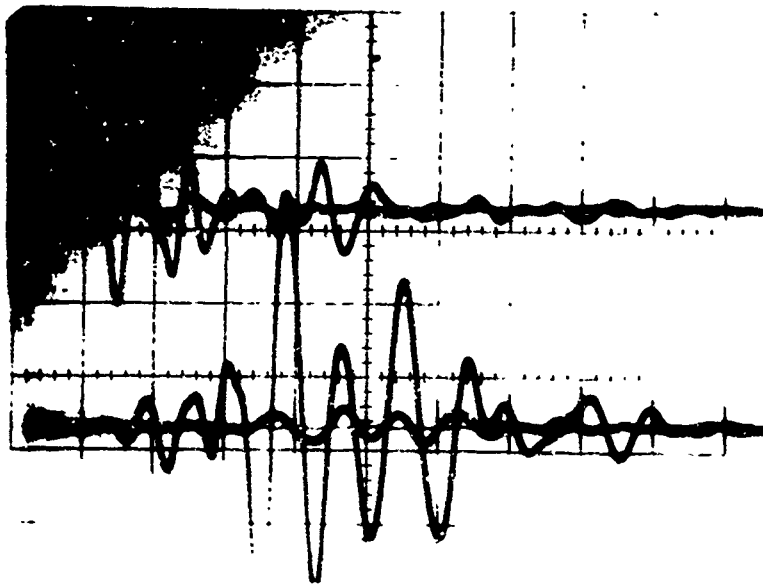
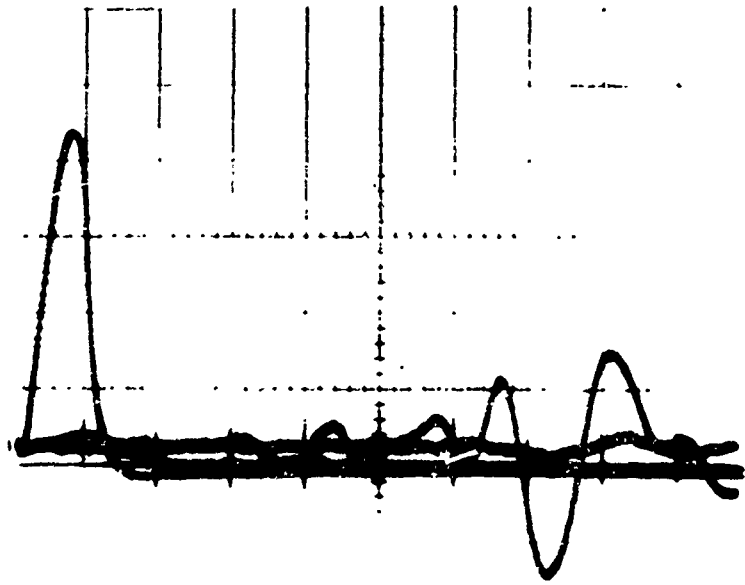
$M_a = 1 \text{ mV/cm}$

$M_t = 10 \text{ msec/cm}$

$r_3 = 850 \text{ cm}$

$M_a = 200 \text{ mV/cm}$

$M_t = 5 \text{ msec/cm}$



Test Series No. 41

Target Material: Princeton Red Clay

Calibration Factors: Penetrometer:  $K = 8.5 \text{ mV/g}$

$r_1$ :  $K = 34 \text{ mV/g}$ ;  $r_2$ :  $K = 34 \text{ mV/g}$ ;

$r_3$ :  $K = 170 \text{ mV/g}$

Drop Height:  $H = 275 \text{ cm}$

Oscilloscope Calibration:

Penetrometer:

$M_a = 500 \text{ mV/cm}$

$M_t = 5 \text{ msek/cm}$

$r_1 = 242 \text{ cm}$

$M_a = 500 \text{ mV/cm}$

$M_t = 10 \text{ msek/cm}$

$r_2 = 488 \text{ cm}$

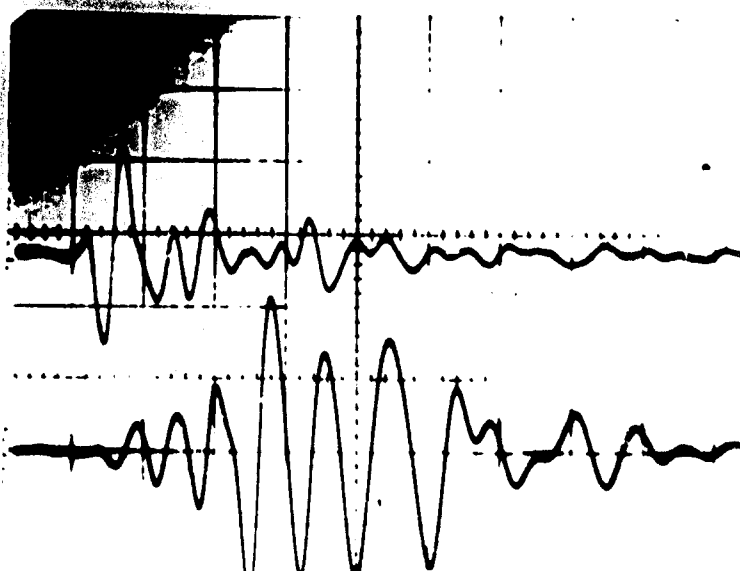
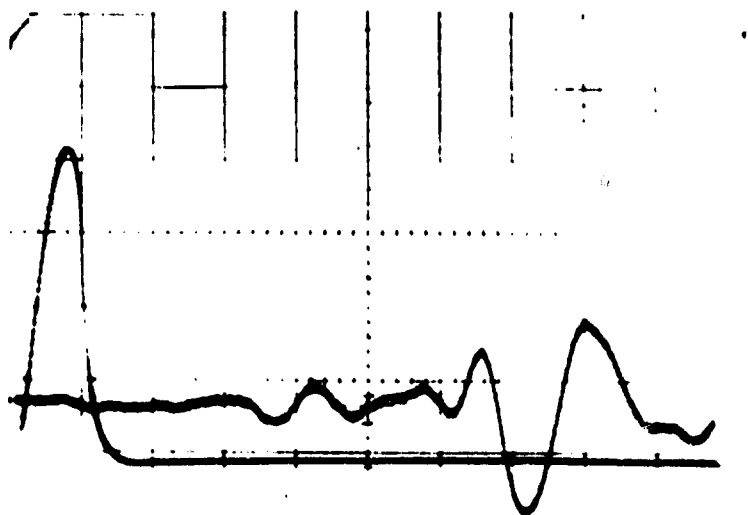
$M_a = 1 \text{ mV/cm}$

$M_t = 10 \text{ msek/cm}$

$r_3 = 825 \text{ cm}$

$M_a = 0.2 \text{ mV/cm}$

$M_t = 5 \text{ msek/cm}$



T e s t   S e r i e s   N o .   4 1

Target Material: Princeton Red Clay

Calibration Factors: Penetrometer:  $K = 8.6 \text{ mV/g}$

$r_1$ :  $K = 34 \text{ mV/g}$ ;  $r_2$ :  $K = 34 \text{ mV/g}$

$r_3$ :  $K = 170 \text{ mV/g}$

Drop Height:  $H = 275 \text{ cm}$

Oscilloscope Calibration:

Penetrometer:

$M_a = 500 \text{ mV/cm}$

$M_t = 5 \text{ msek/cm}$

$r_1 = 230 \text{ cm}$

$M_a = 500 \text{ mV/cm}$

$M_t = 10 \text{ msek/cm}$

$r_2 = 475 \text{ cm}$

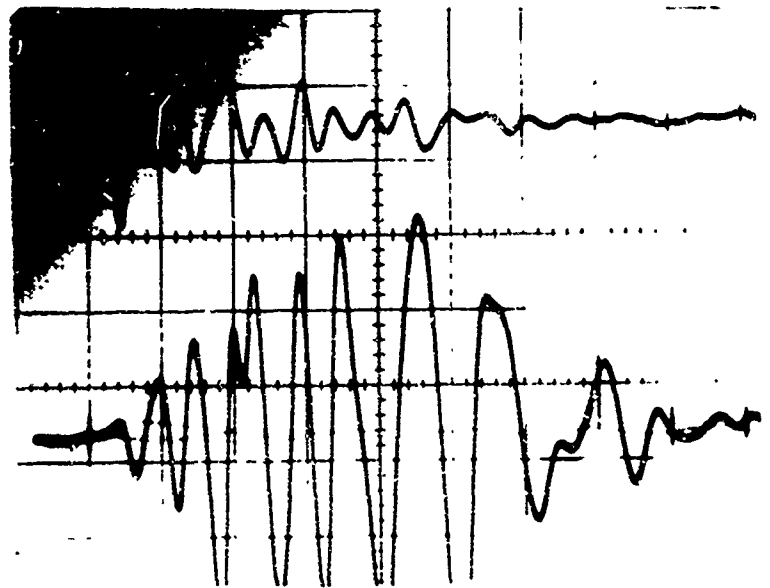
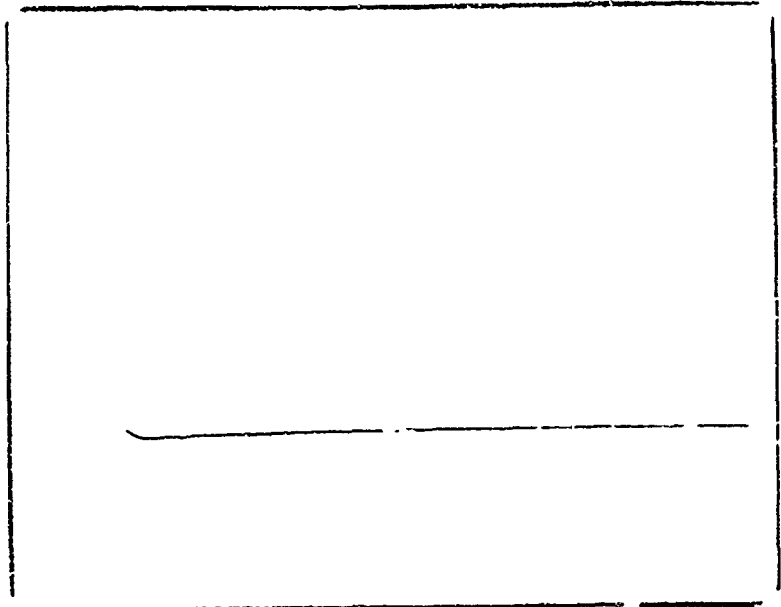
$M_a = 500 \text{ mV/cm}$

$M_t = 10 \text{ msek/cm}$

$r_3 = 815 \text{ cm}$

$M_a = 200 \text{ mV/cm}$

$M_t = 5 \text{ msek/cm}$



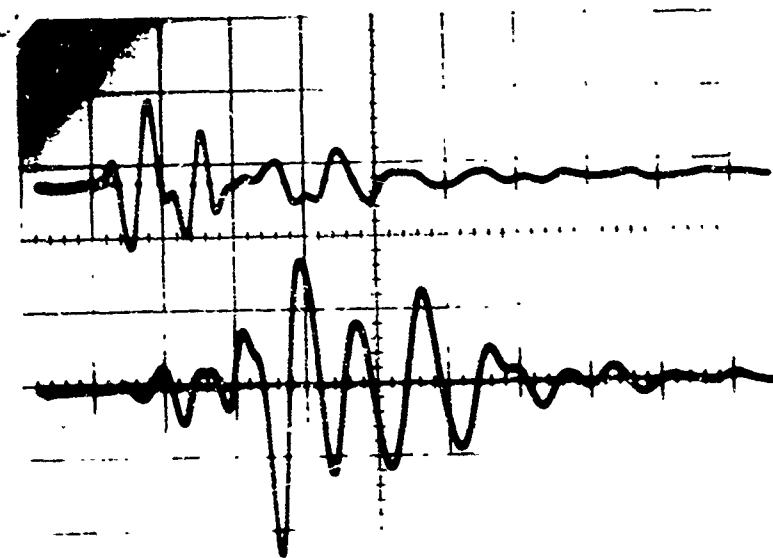
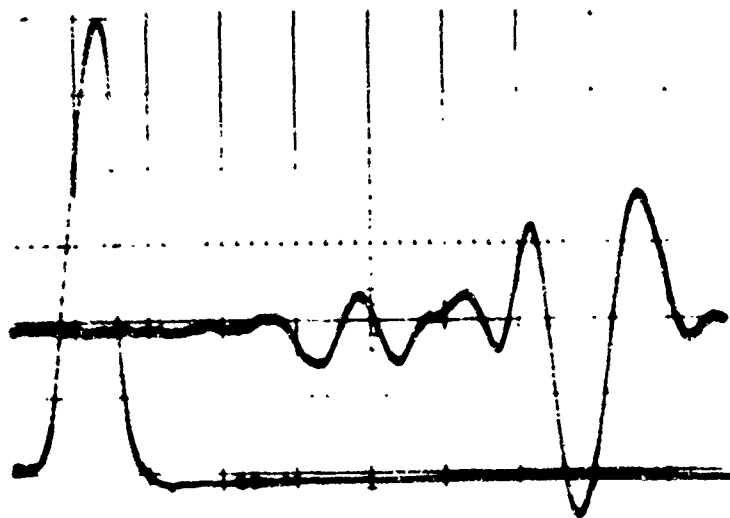
## T e s t   S e r i e s   N o . 4 1

Target Material: Princeton Red Clay

Calibration Factors: Penetrometer:  $K = 8.6 \text{ mV/g}$  $r_1$ :  $K = 34 \text{ mV/g}$ ;  $r_2$ :  $K = 34 \text{ mV/g}$ ; $r_3$ :  $K = 170 \text{ mV/g}$ Drop Height:  $H = 520 \text{ cm}$ 

Oscilloscope Calibration:

Penetrometer:

 $M_a = 500 \text{ mV/cm}$  $M_t = 5 \text{ msec/cm}$  $r_1 = 244 \text{ cm}$  $M_a = 1 \text{ mV/cm}$  $M_t = 10 \text{ msec/cm}$  $r_2 = 491 \text{ cm}$  $M_a = 2 \text{ mV/cm}$  $M_t = 10 \text{ msec/cm}$  $r_3 = 830 \text{ cm}$  $M_a = 0.2 \text{ mV/cm}$  $M_t = 5 \text{ msec/cm}$ 

T e s t   S e r i e s   N o .   4 2

Target Material: Silty Sand (Plowed Field)

Calibration Factors: Penetrometer:  $K = 8.6 \text{ mV/g}$

$r_1$ :  $K = 34 \text{ mV/g}$ ;  $r_2$ :  $K = 34 \text{ mV/g}$

Drop Height:  $H = 275 \text{ cm}$

Oscilloscope Calibration:

Penetrometer:

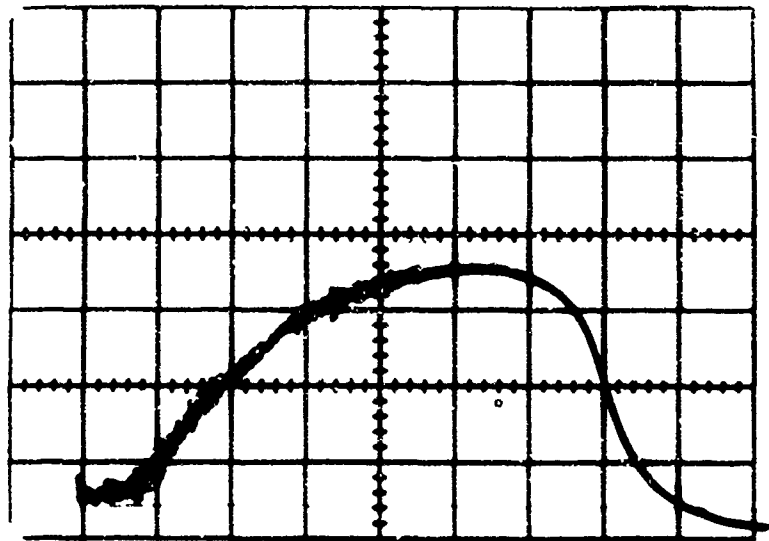
$M_a = 200 \text{ mV/cm}$

$M_t = 2 \text{ msec/cm}$

$r_1 = 198 \text{ cm}$

$M_a = 1 \text{ mV/cm}$

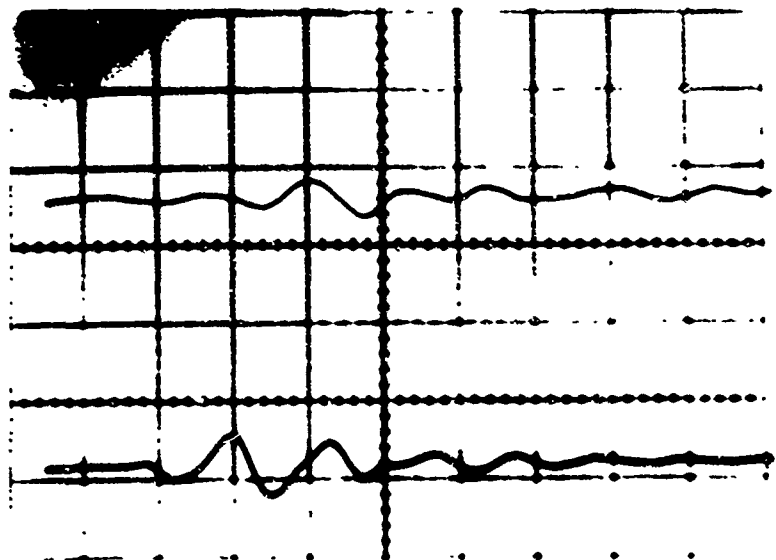
$M_t = 10 \text{ msec/cm}$



$r_2 = 415 \text{ cm}$

$M_a = 500 \text{ mV/cm}$

$M_t = 10 \text{ msec/cm}$



T e s t   S e r i e s   N o . 4 2

Target Material: Silty Sand (Plowed Field)

Calibration Factors: Penetrometer:  $K = 8.6 \text{ mV/g}$

$r_1$ :  $K = 34 \text{ mV/g}$ ;  $r_2$ :  $K = 34 \text{ mV/g}$

Drop Height:  $H = 275 \text{ cm}$

Oscilloscope Calibration:

Penetrometer:

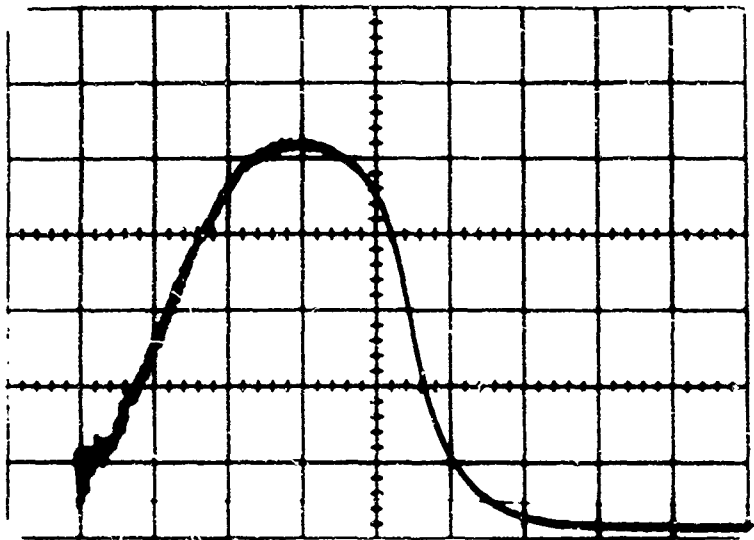
$M_a = 200 \text{ mV/cm}$

$M_t = 2 \text{ msek/cm}$

$r_1 = 178 \text{ cm}$

$M_a = 500 \text{ mV/cm}$

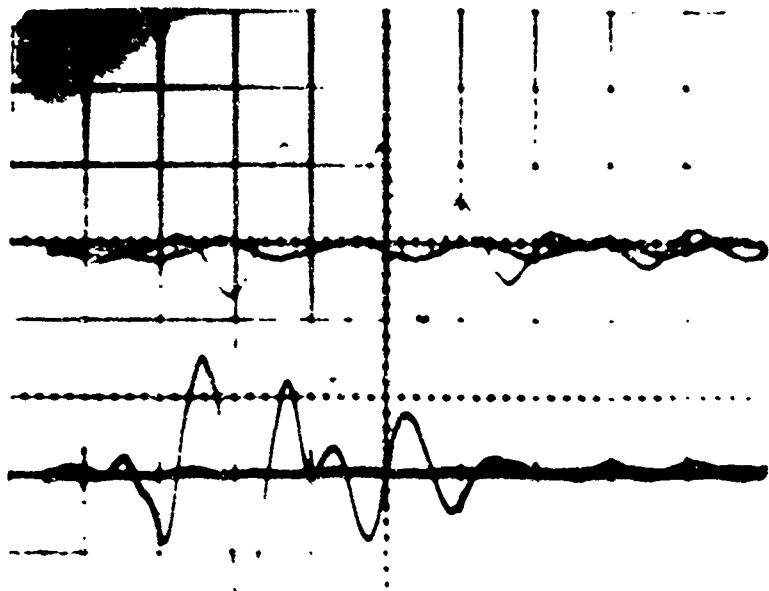
$M_t = 10 \text{ msek/cm}$



$r_2 = 396 \text{ cm}$

$M_a = 200 \text{ mV/cm}$

$M_t = 10 \text{ msek/cm}$



Test Series No. 42

Target Material: Silty Sand (Flowed Field)

Calibration Factors: Penetrometer:  $K = 8.6 \text{ mV/g}$

$r_1$ :  $K = 34 \text{ mV/g}$ ;  $r_2$ :  $K = 34 \text{ mV/g}$

Drop Height:  $H = 520 \text{ cm}$

Oscilloscope Calibration:

Penetrometer:

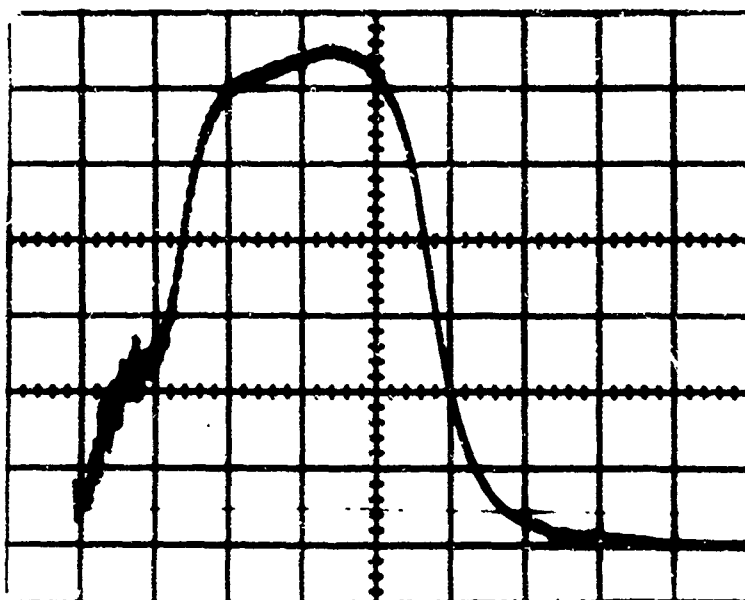
$M_a = 200 \text{ mV/cm}$

$M_t = 2 \text{ msek/cm}$

$r_1 = 178 \text{ cm}$

$M_a = 1 \text{ mV/cm}$

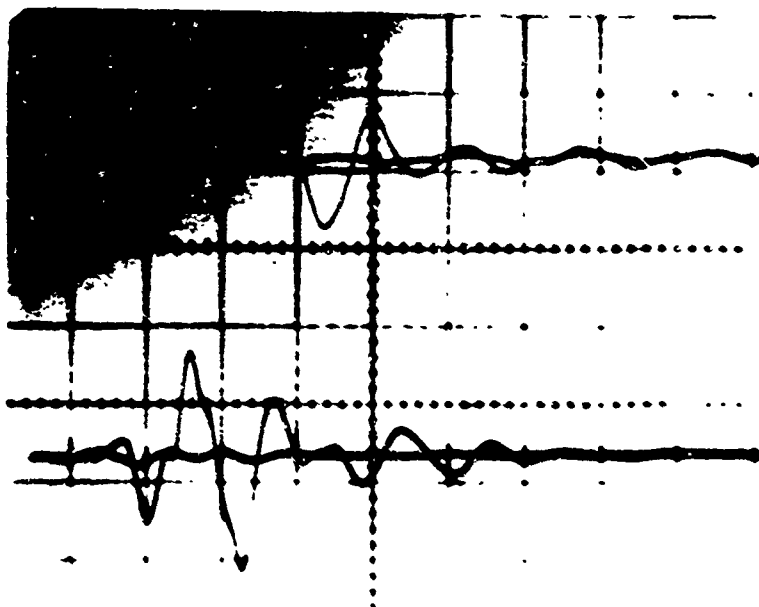
$M_t = 10 \text{ msek/cm}$



$r_2 = 396 \text{ cm}$

$M_a = 500 \text{ mV/cm}$

$M_t = 10 \text{ msek/cm}$



T e s t   S e r i e s   N o .   43

Target Material: Crushed Rock, Compacted

Calibration Factors: Penetrometer:  $K = 8.6 \text{ mV/g}$

$r_1$ :  $K = 34 \text{ mV/g}$ ;  $r_2$ :  $K = 34 \text{ mV/g}$

Drop Height:  $H = 275 \text{ cm}$

Oscilloscope Calibration:

Penetrometer:

$M_a = 500 \text{ mV/cm}$

$M_t = 1 \text{ msek/cm}$

$r_1 = 112 \text{ cm}$

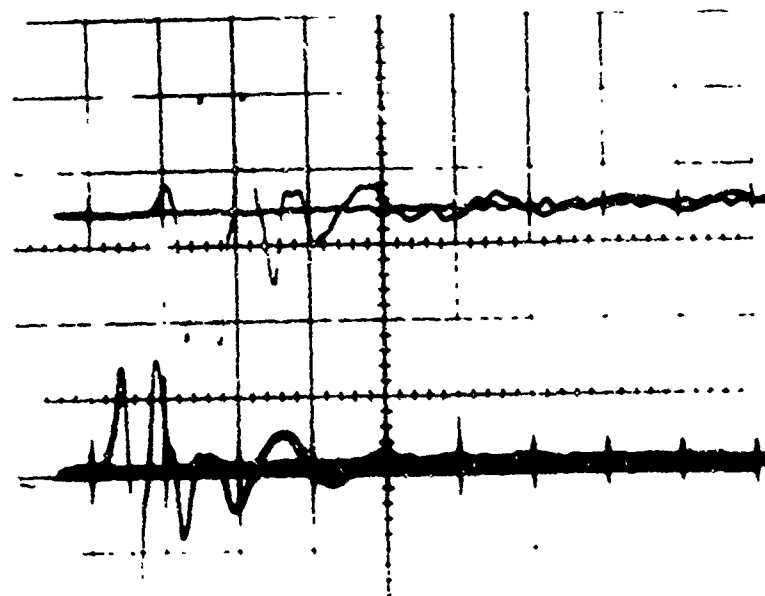
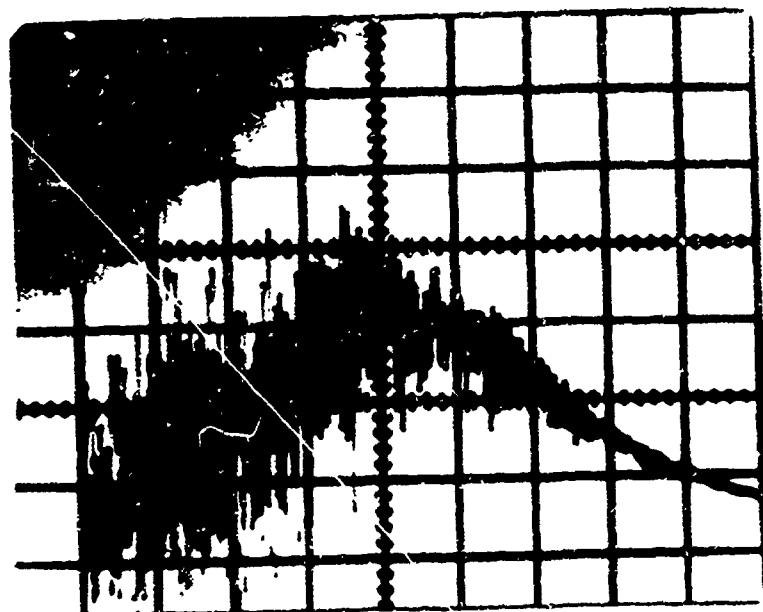
$M_a = 2 \text{ mV/cm}$

$M_t = 10 \text{ msek/cm}$

$r_2 = 233 \text{ cm}$

$M_a = 1 \text{ mV/cm}$

$M_t = 10 \text{ msek/cm}$



Test Series No. 43

Target Material: Crushed Rock, Compacted

Calibration Factors: Penetrometer:  $K = 8.6 \text{ mV/g}$

$r_1$ :  $K = 34 \text{ mV/g}$ ;  $r_2$ :  $K = 34 \text{ mV/g}$

Drop Height:  $H = 520 \text{ cm}$

Oscilloscope Calibration:

Penetrometer:

$M_a = 500 \text{ mV/cm}$

$M_t = 1 \text{ msec/cm}$

$r_1 = 107 \text{ cm}$

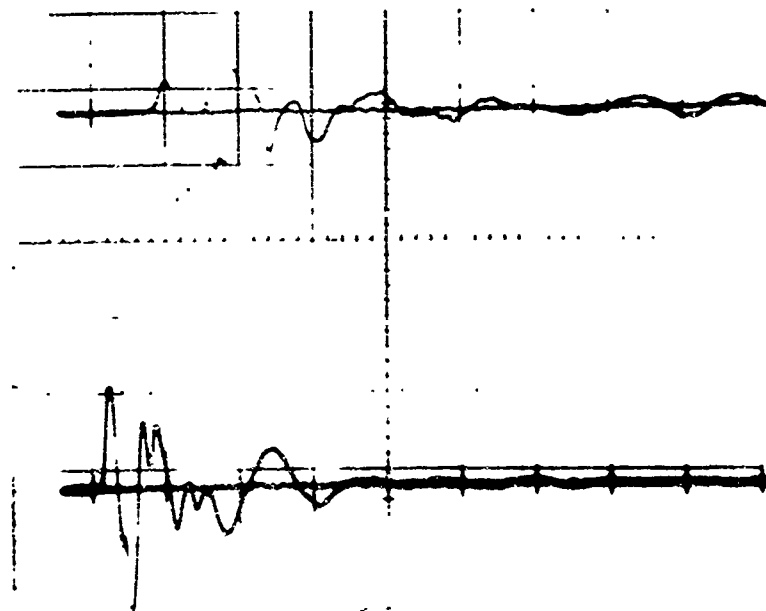
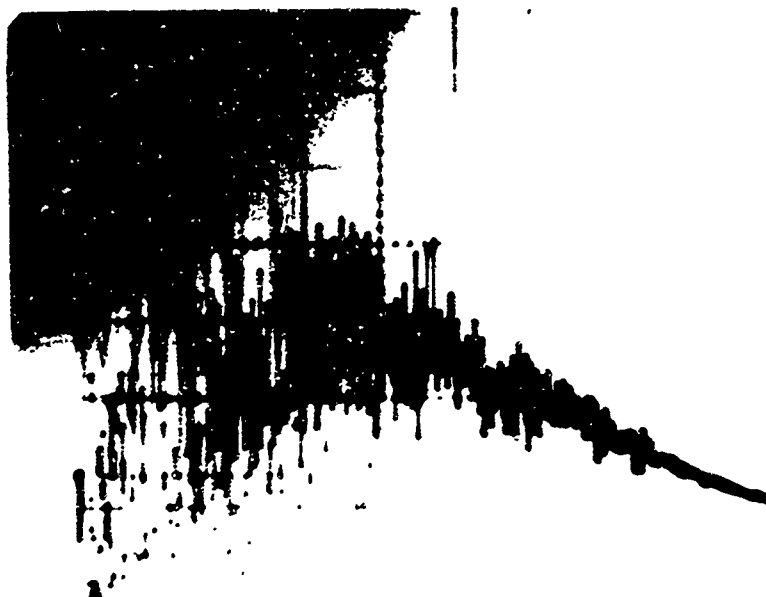
$M_a = 2 \text{ mV/cm}$

$M_t = 10 \text{ msec/cm}$

$r_2 = 238 \text{ cm}$

$M_a = 1 \text{ V/cm}$

$M_t = 10 \text{ msec/cm}$



Test Series No. 43

Target Material: Crushed Rock, Compacted

Calibration Factors: Penetrometer:  $K = 8.6 \text{ mV/g}$

$r_1$ :  $K = 34 \text{ mV/g}$ ;  $r_2$ :  $K = 34 \text{ mV/g}$

Drop Height:  $H = 520 \text{ cm}$

Oscilloscope Calibration:

Penetrometer:

$M_a = 1000 \text{ mV/cm}$

$M_t = 1 \text{ msec/cm}$

$r_1 = 107 \text{ cm}$

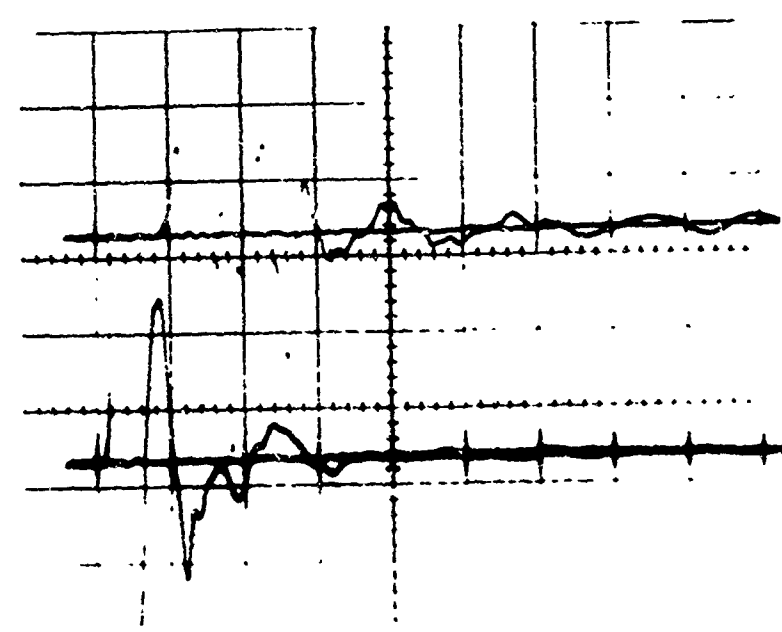
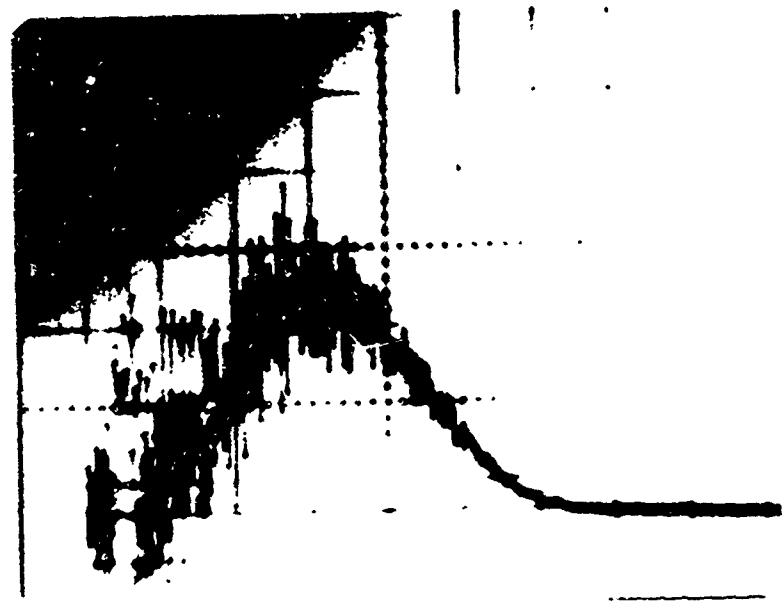
$M_a = 2 \text{ mV/cm}$

$M_t = 10 \text{ msec/cm}$

$r_2 = 238 \text{ cm}$

$M_a = 1 \text{ mV/cm}$

$M_t = 10 \text{ msec/cm}$



Test Series No. 44

Target Material: Uniform, Fine Sand, Natural Deposit

Calibration Factors: Penetrometer:  $K = 8.6 \text{ mV/g}$

$r_1$ :  $K = 34 \text{ mV/g}$ ;  $r_2$ :  $K = 34 \text{ mV/g}$

Drop Height:  $H = 275 \text{ cm}$

Oscilloscope Calibration:

Penetrometer:

$M_a = 200 \text{ mV/cm}$

$M_t = 2 \text{ msec/cm}$

$r_1 = 151 \text{ cm}$

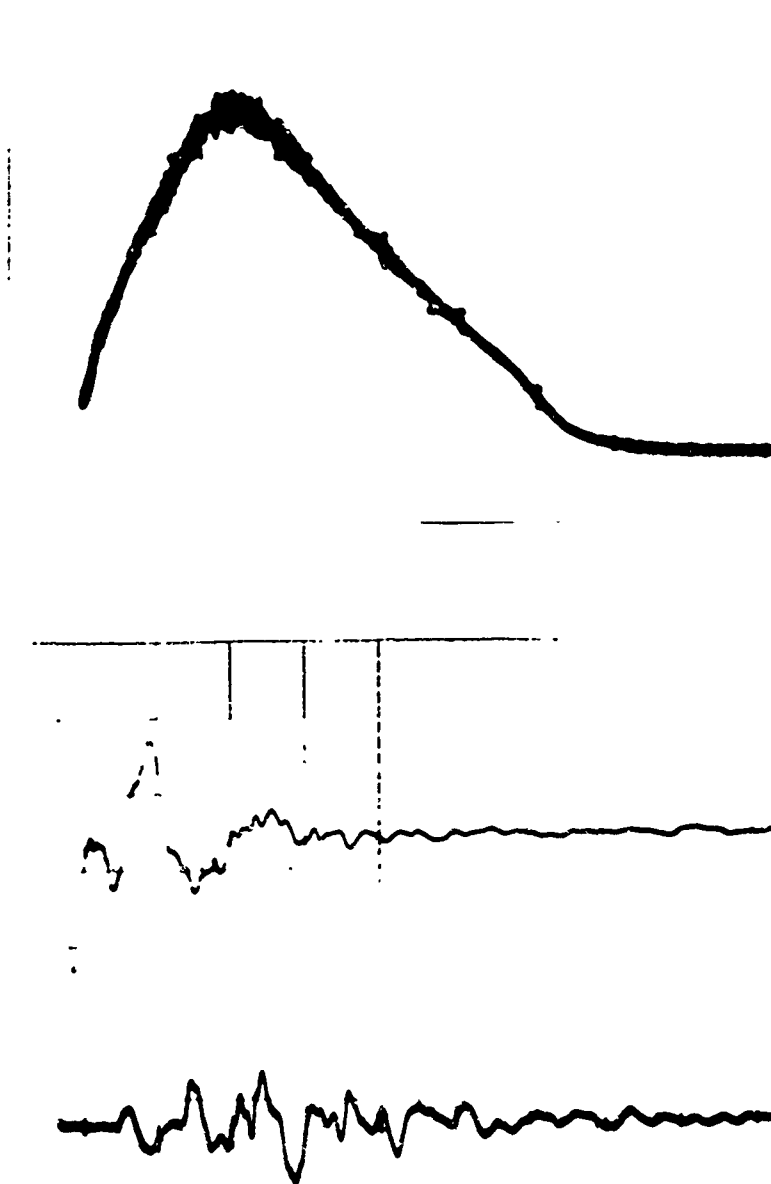
$M_a = 1 \text{ mV/cm}$

$M_t = 10 \text{ msec/cm}$

$r_2 = 375 \text{ cm}$

$M_a = 500 \text{ mV/cm}$

$M_t = 10 \text{ msec/cm}$



T e s t   S e r i e s   N o   44

Target Material: Uniform, Fine Sand, Natural Deposit

Calibration Factors: Penetrometer:  $K = 8.6 \text{ mV/g}$

$r_1$ :  $K = 34 \text{ mV/g}$ ;  $r_2$ :  $K = 34 \text{ mV/g}$

Drop Height:  $H = 520 \text{ cm}$

Oscilloscope Calibration:

Penetrometer:

$M_a = 500 \text{ mV/cm}$

$M_t = 2 \text{ msek/cm}$

$r_1 = 160 \text{ cm}$

$M_a = 2 \text{ mV/cm}$

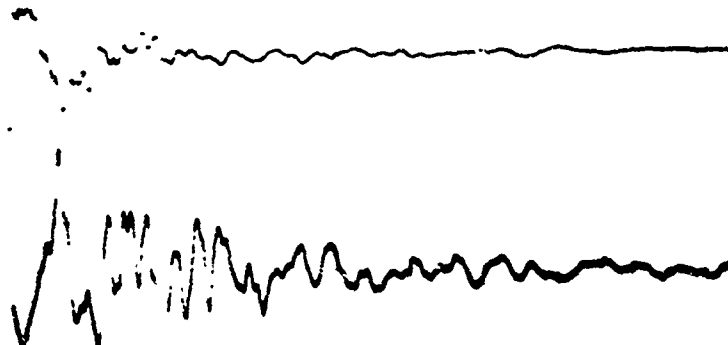
$M_t = 10 \text{ msek/cm}$



$r_2 = 387 \text{ cm}$

$M_a = 5 \text{ mV/cm}$

$M_t = 10 \text{ msek/cm}$



T e s t   S e r i e s   N o .   4 4

Target Material: Uniform, Fine Sand, Natural Deposit

Calibration Factors: Penetrometer:  $K = 8.6 \text{ mV/g}$

$r_1$ :  $K = 34 \text{ mV/g}$ ;  $r_2$ :  $K = 34 \text{ mV/g}$

Drop Height:  $H = 520 \text{ cm}$

Oscilloscope Calibration:

Penetrometer:

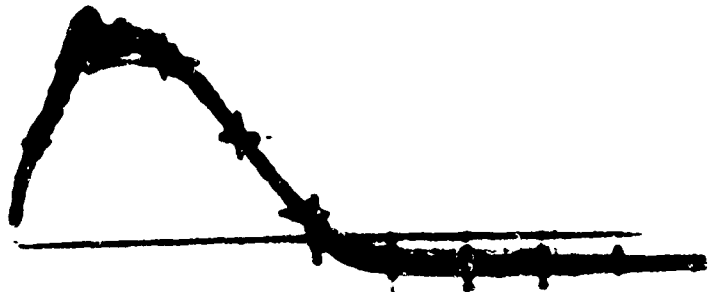
$M_a = 500 \text{ mV/cm}$

$M_t = 2 \text{ msec/cm}$

$r_1 = 166 \text{ cm}$

$M_a = 1 \text{ mV/cm}$

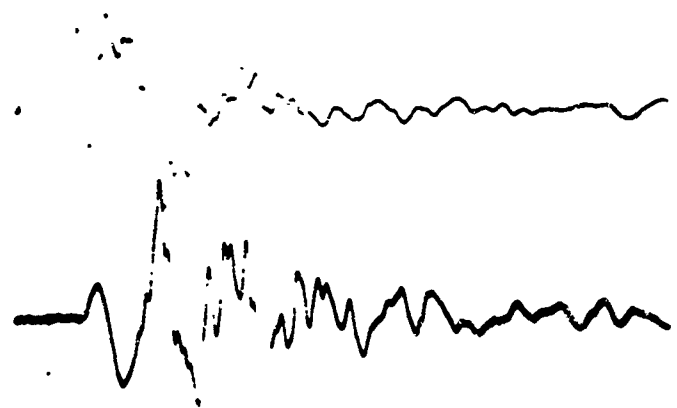
$M_t = 10 \text{ msec/cm}$



$r_2 = 394 \text{ cm}$

$M_a = 500 \text{ mV/cm}$

$M_t = 10 \text{ msec/cm}$



Test Series No. 45

Target Material: Swamp

Calibration Factors: Penetrometer:  $K = 8.6 \text{ mV/g}$

$r_1$ :  $K = 34 \text{ mV/g}$ ;  $r_2$ :  $K = 34 \text{ mV/g}$

Drop Height:  $H = 275 \text{ cm}$

Oscilloscope Calibration:

Penetrometer:

$M_a = 50 \text{ mV/cm}$

$M_t = 20 \text{ msec/cm}$

$r_1 = 76 \text{ cm}$

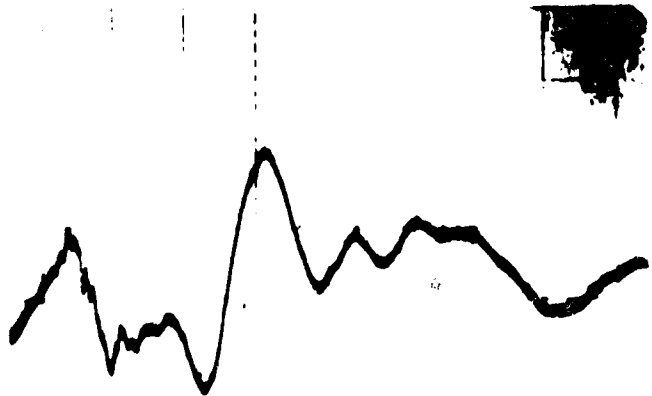
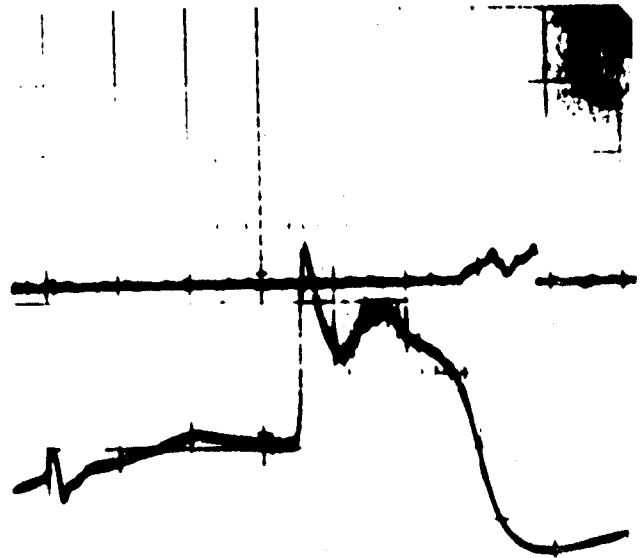
$M_a = 500 \text{ mV/cm}$

$M_t = 20 \text{ msec/cm}$

$r_2 = 76 \text{ cm}$

$M_a = 500 \text{ mV/cm}$

$M_t = 20 \text{ msec/cm}$



Test Series No. 12

Target Material: Sandy Silt with some Clay;  
Natural Surface Deposit

Calibration Factor of Accelerometer:  $K = 8.6 \text{ mV/g}$

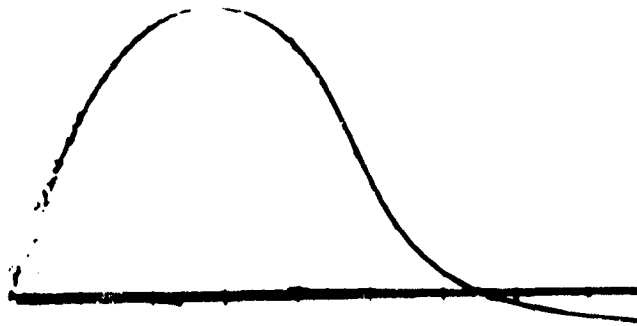
Drop Height:  $H = 61 \text{ cm}$

Oscilloscope Calibration:

$M_a = 100 \text{ mV/cm}$

$M_t = 2 \text{ msec/cm}$

$t = 1.8 \text{ cm}$



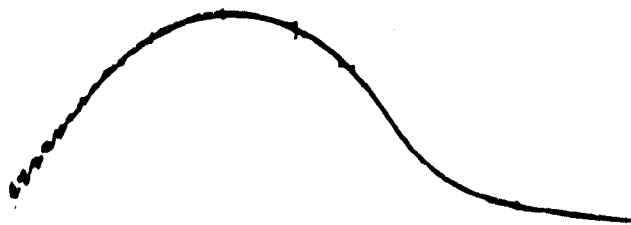
Drop Height:  $H = 122 \text{ cm}$

Oscilloscope Calibration:

$M_a = 200 \text{ mV/cm}$

$M_t = 2 \text{ msec/cm}$

$t = 2.1 \text{ cm}$



T e s t   S e r i e s   N o . 1 2

Target Material:   Sandy Silt with some Clay;  
                            Natural Surface Deposit

Calibration Factor of Accelerometer:    $K = 8.6 \text{ mV/g}$

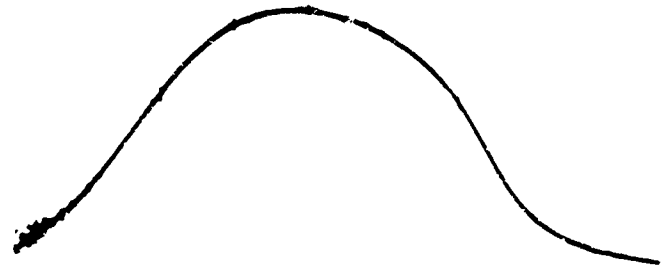
Drop Height:    $H = 183 \text{ cm}$

Oscilloscope Calibration:

$M_a = 200 \text{ mV/cm}$

$M_t = 2 \text{ msec/cm}$

$t = 3.7 \text{ cm}$



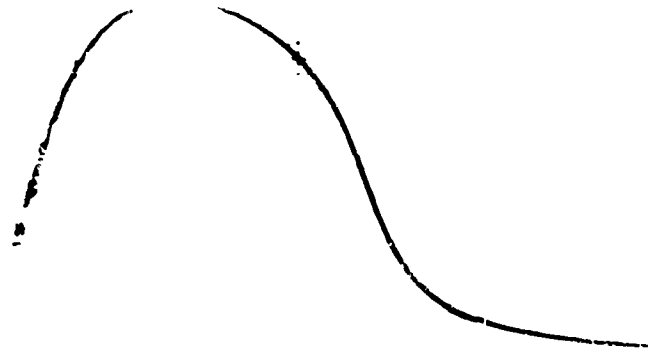
Drop Height:    $H = 305 \text{ cm}$

Oscilloscope Calibration:

$M_a = 200 \text{ mV/cm}$

$M_t = 2 \text{ msec/cm}$

$t = 4.5 \text{ cm}$





T e s t   S e r i e s   N o . 1 5

Target Material: Ottawa Sand, U.S. Sieve Size No. 30-40

Calibration Factor of Accelerometer:  $K = 8.6 \text{ mV/g}$

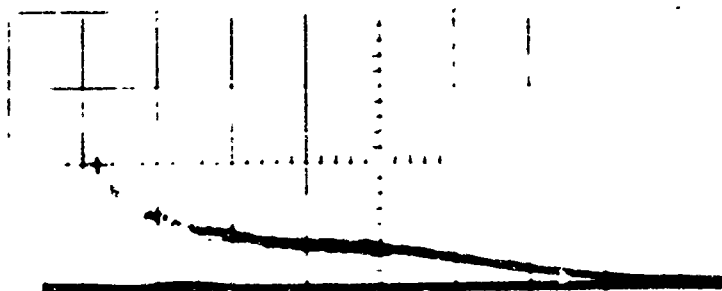
Drop Height:  $H = 61 \text{ cm}$

Oscilloscope Calibration:

$M_a = 100 \text{ mV/cm}$

$M_t = 5 \text{ msec/cm}$

$t = 4.8 \text{ cm}$



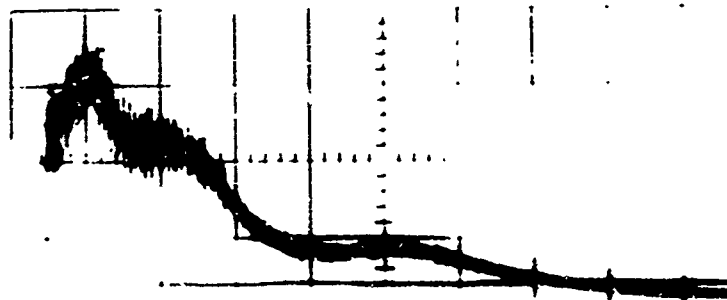
Drop Height:  $H = 122 \text{ cm}$

Oscilloscope Calibration:

$M_a = 100 \text{ mV/cm}$

$M_t = 5 \text{ msec/cm}$

$t = 5.2 \text{ cm}$



T e s t   S e r i e s   N o .   1 5

Target Material: Ottawa Sand, U.S. Sieve Size No. 30-40

Calibration Factor of Accelerometer:  $K = 8.6 \text{ mV/g}$

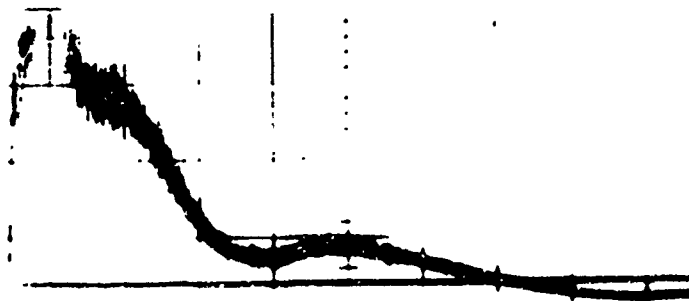
Drop Height:  $H = 183 \text{ cm}$

Oscilloscope Calibration:

$M_a = 100 \text{ mV/cm}$

$M_t = 5 \text{ msec/cm}$

$t = 5.7 \text{ cm}$



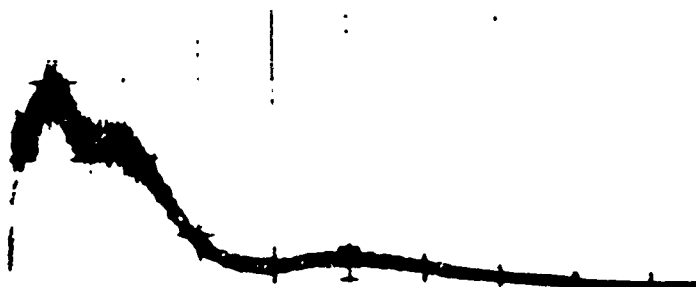
Drop Height:  $H = 305 \text{ cm}$

Oscilloscope Calibration:

$M_a = 200 \text{ mV/cm}$

$M_t = 5 \text{ msec/cm}$

$t = 6.4 \text{ cm}$

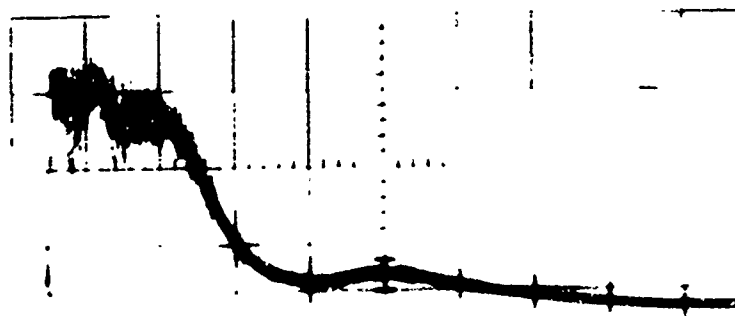


## T e s t   S e r i e s   N o .   1 5

Target Material: Ottawa Sand, U.S. Sieve Size No. 30-40

Calibration Factor of Accelerometer:  $K = 8.6 \text{ mV/g}$ Drop Height:  $H = 425 \text{ cm}$ 

Oscilloscope Calibration:

 $M_a = 200 \text{ mV/cm}$  $M_t = 5 \text{ msec/cm}$  $t = 6.8 \text{ cm}$ 

T e s t   S e r i e s   N o .   1 9

Target Material: Beach Sand, Natural Deposit

Calibration Factor of Accelerometer:  $K = 8.6 \text{ mV/g}$

Drop Height:  $H = 61 \text{ cm}$

Oscilloscope Calibration:

$M_a = 50 \text{ mV/cm}$

$M_t = 5 \text{ msec/cm}$

$t = 6.8 \text{ cm}$



Drop Height:  $H = 122 \text{ cm}$

Oscilloscope Calibration:

$M_a = 50 \text{ mV/cm}$

$M_t = 5 \text{ msec/cm}$

$t = 7.0 \text{ cm}$



T e s t   S e r i e s   N o . 19

Target Material: Beach Sand, Natural Deposit

Calibration Factor of Accelerometer:  $K = 8.6 \text{ mV/g}$

Drop Height:  $H = 183 \text{ cm}$

Oscilloscope Calibration:

$M_a = 100 \text{ mV/cm}$

$M_t = 10 \text{ msec/cm}$

$t = 7.0 \text{ cm}$



Drop Height:  $H = 305 \text{ cm}$

Oscilloscope Calibration:

$M_a = 200 \text{ mV/cm}$

$M_t = 5 \text{ msec/cm}$

$t = 7.5 \text{ cm}$



T e s t   S e r i e s   N o . 19

Target Material: Beach Sand, Natural Deposit

Calibration Factor of Accelerometer:  $K = 8.6 \text{ mV/g}$

Drop Height:  $H = 425 \text{ cm}$

Oscilloscope Calibration:

$M_a = 200 \text{ mV/cm}$

$M_t = 5 \text{ msec/cm}$

$t = 7.8 \text{ cm}$



Drop Height:  $H = 700 \text{ cm}$

Oscilloscope Calibration:

$M_a = 200 \text{ mV/cm}$

$M_t = 5 \text{ msec/cm}$

$t = 8.0 \text{ cm}$



T e s t   S e r i e s   N o . 2 2

Target Material: Princeton Red Clay;  
Moisture Content = 2.65%,  $w = 86.8 \text{ lb/ft}^3$

Calibration Factor of Accelerometer:  $K = 8.6 \text{ mV/g}$

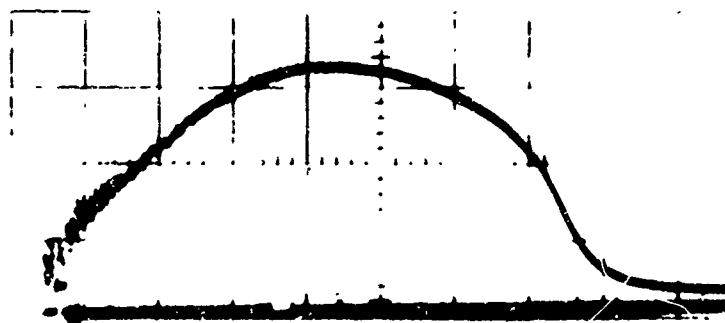
Drop Height:  $H = 61 \text{ cm}$

Oscilloscope Calibration:

$M_a = 100 \text{ mV/cm}$

$M_t = 2 \text{ msek/cm}$

$t = 2.3 \text{ cm}$



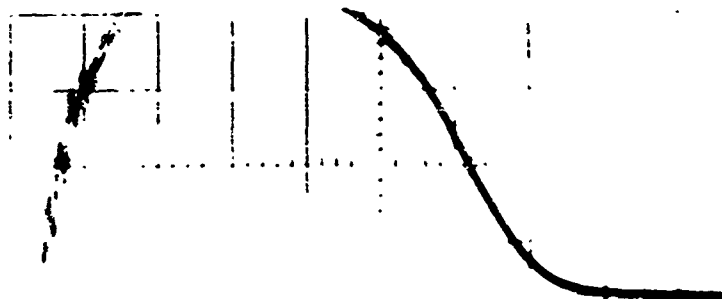
Drop Height:  $H = 122 \text{ cm}$

Oscilloscope Calibration:

$M_a = 100 \text{ mV/cm}$

$M_t = 2 \text{ msek/cm}$

$t = 3.0 \text{ cm}$



T e s t   S e r i e s   N o . 22

Target Material: Princeton Red Clay;  
Moisture Content = 2.65%,  $w = 86.8 \text{ lb/ft}^3$

Calibration Factor of Accelerometer:  $K = 8.6 \text{ mV/g}$

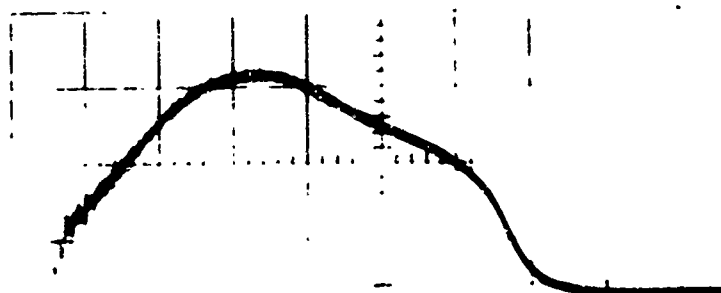
Drop Height:  $H = 183 \text{ cm}$

Oscilloscope Calibration:

$M_a = 200 \text{ mV/cm}$

$M_t = 2 \text{ msec/cm}$

$t = 4.0 \text{ cm}$



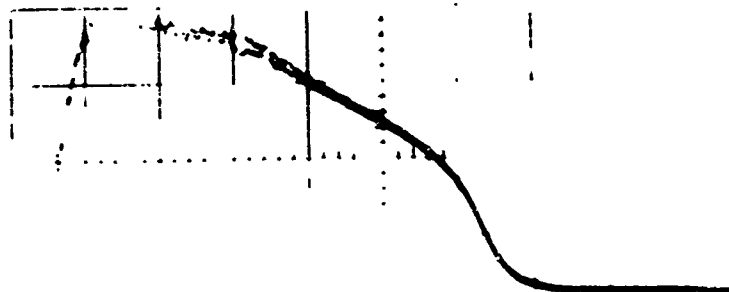
Drop Height:  $H = 305 \text{ cm}$

Oscilloscope Calibration:

$M_a = 200 \text{ mV/cm}$

$M_t = 2 \text{ msec/cm}$

$t = 4.2 \text{ cm}$



Test Series No. 22

Target Material: Princeton Red Clay;  
 Moisture Content = 2.65%,  $w = 86.8 \text{ lb/ft}^3$   
 Calibration Factor of Accelerometer:  $K = 8.6 \text{ mV/g}$

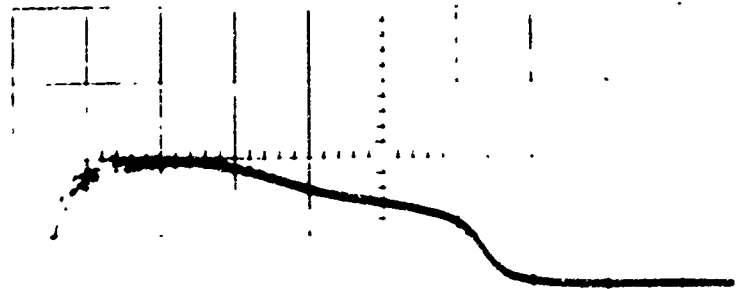
Drop Height:  $H = 425 \text{ cm}$

Oscilloscope Calibration:

$M_a = 500 \text{ mV/cm}$

$M_t = 2 \text{ msec/cm}$

$t = 4.8 \text{ cm}$



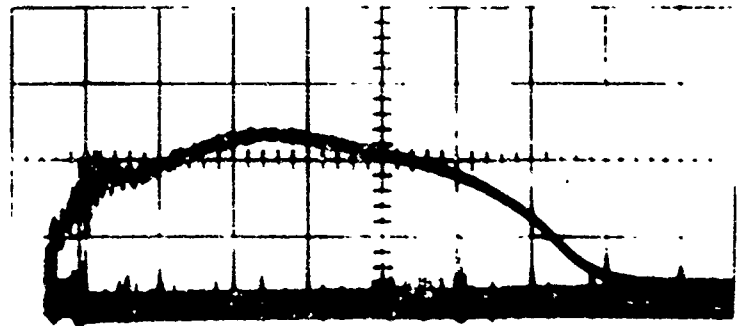
Drop Height:  $H = 122 \text{ cm}$

Oscilloscope Calibration:

$M_a = 200 \text{ mV/cm}$

$M_t = 2 \text{ msec/cm}$

$t = 3.0 \text{ cm}$



Unclassified  
Security Classification

AD 134043

AD634043

DOCUMENT CONTROL DATA - R&D

(Security classification of title, body of abstract and indexing annotation must be entered when the overall report is classified)

1. ORIGINATING ACTIVITY (Corporate author) Department of Civil Engineering School of Engineering and Applied Science Princeton University, Princeton, N. J. 08540		2a. REPORT SECURITY CLASSIFICATION Unclassified	
		2b. GROUP	
3. REPORT TITLE The Determination of Soil Properties in Situ by an Impact Penetrometer			
4. DESCRIPTIVE NOTES (Type of report and inclusive dates) Scientific Interim Report No. 1			
5. AUTHOR(S) (Last name, first name, initials) Schmid, Werner E.			
6. REPORT DATE January 1966		7a. TOTAL NO. OF PAGES 192	7b. NO. OF REFS 66
8a. CONTRACT OR GRANT NO. AF 19(628)-2427		9a. ORIGINATOR'S REPORT NUMBER(S) Princeton Soil Engineering Research Series No. 3 Scientific Report No. 1	
b. PROJECT NO. 7628 - 762804		9b. OTHER REPORT NO(S) (Any other numbers that may be assigned this report) AFCRL 66-43	
c. DOD Element: 624 05394			
d. DOD Subelement 681000			
10. AVAILABILITY/LIMITATION NOTICES Distribution of this document is unlimited. Extra copies available from author upon request.			
11. SUPPLEMENTARY NOTES		12. SPONSORING MILITARY ACTIVITY Hq., AFCRL OAR (CRJ) USAF, L. G. Hanscom Field Bedford, Massachusetts 01730	
13. ABSTRACT The report presents part of the scientific investigations carried out under a task program related to the determination and assessment of surface dynamic soil properties by laboratory instrumentation. It first reviews the historical development of the hardness-penetrometer concept and presents a pilot model for a new aerial penetrometer. Basic theoretical considerations are then advanced regarding the stress-strain relationships in axial symmetry and the dynamic loads associated with the drop-impact penetrometer. The existing theory of elasticity solutions are then reviewed and the solutions for a sphere impacting on an ideally plastic and on an elasto-plastic semi-infinite solid are presented. The Hertz solution of an elastic sphere impacting on an elastic half-space is modified by using the elastic-viscoelastic analogy to find a solution for a sphere dropping onto a four parameter viscoelastic half space. The problem of energy transfer during impact by vibrations is discussed shortly. The data for 15 test series carried out with the pilot model penetrometer on natural soils and on some artificial materials are presented and evaluated. It is concluded that the principle of the drop impact-penetrometer is applicable in experiments for assessing the mechanical properties of a natural soil surface. The proposed modification of a prototype penetrometer should also increase its capability and reliability as a remote sensor for operational applications. The instrument as envisaged will not only permit determination of mechanical surface properties on terrestrial soils but should also be extremely useful for the exploration, by remoted techniques, of lunar and other extraterrestrial surfaces.			

14. KEY WORDS	LINK A		LINK B		LINK C	
	ROLE	WT	ROLE	WT	ROLE	WT
Aerial penetrometer; spherical impact; properties of soil surfaces; mobility and trafficability, aerospace operations from unprepared surfaces, remote sensing, impact of sphere on viscoelastic half-space.						
					CFSTI	FEB 17 1967
						RECEIVED

**INSTRUCTIONS**

1. **ORIGINATING ACTIVITY:** Enter the name and address of the contractor, subcontractor, grantee, Department of Defense activity or other organization (*corporate author*) issuing the report.
- 2a. **REPORT SECURITY CLASSIFICATION:** Enter the overall security classification of the report. Indicate whether "Restricted Data" is included. Marking is to be in accordance with appropriate security regulations.
- 2b. **GROUP:** Automatic downgrading is specified in DoD Directive 5200.10 and Armed Forces Industrial Manual. Enter the group number. Also, when applicable, show that optional markings have been used for Group 3 and Group 4 as authorized.
3. **REPORT TITLE:** Enter the complete report title in all capital letters. Titles in all cases should be unclassified. If a meaningful title cannot be selected without classification, show title classification in all capitals in parenthesis immediately following the title.
4. **DESCRIPTIVE NOTES:** If appropriate, enter the type of report, e.g., interim, progress, summary, annual, or final. Give the inclusive dates when a specific reporting period is covered.
5. **AUTHOR(S):** Enter the name(s) of author(s) as shown on or in the report. Enter last name, first name, middle initial. If military, show rank and branch of service. The name of the principal author is an absolute minimum requirement.
6. **REPORT DATE:** Enter the date of the report as day, month, year, or month, year. If more than one date appears on the report, use date of publication.
- 7a. **TOTAL NUMBER OF PAGES:** The total page count should follow normal pagination procedures, i.e., enter the number of pages containing information.
- 7b. **NUMBER OF REFERENCES:** Enter the total number of references cited in the report.
- 8a. **CONTRACT OR GRANT NUMBER:** If appropriate, enter the applicable number of the contract or grant under which the report was written.
- 8b, 8c, & 8d. **PROJECT NUMBER:** Enter the appropriate military department identification, such as project number, subproject number, system numbers, task number, etc.
- 9a. **ORIGINATOR'S REPORT NUMBER(S):** Enter the official report number by which the document will be identified and controlled by the originating activity. This number must be unique to this report.
- 9b. **OTHER REPORT NUMBER(S):** If the report has been assigned any other report numbers (*either by the originator or by the sponsor*), also enter this number(s).
10. **AVAILABILITY/LIMITATION NOTICES:** Enter any limitations on further dissemination of the report, other than those

imposed by security classification, using standard statements such as:

- (1) "Qualified requesters may obtain copies of this report from DDC."
- (2) "Foreign announcement and dissemination of this report by DDC is not authorized."
- (3) "U. S. Government agencies may obtain copies of this report directly from DDC. Other qualified DDC users shall request through \_\_\_\_\_."
- (4) "U. S. military agencies may obtain copies of this report directly from DDC. Other qualified users shall request through \_\_\_\_\_."
- (5) "All distribution of this report is controlled. Qualified DDC users shall request through \_\_\_\_\_."

If the report has been furnished to the Office of Technical Services, Department of Commerce, for sale to the public, indicate this fact and enter the price, if known.

11. **SUPPLEMENTARY NOTES:** Use for additional explanatory notes.

12. **SPONSORING MILITARY ACTIVITY:** Enter the name of the departmental project office or laboratory sponsoring (*paying for*) the research and development. Include address.

13. **ABSTRACT:** Enter an abstract giving a brief and factual summary of the document indicative of the report, even though it may also appear elsewhere in the body of the technical report. If additional space is required, a continuation sheet shall be attached.

It is highly desirable that the abstract of classified reports be unclassified. Each paragraph of the abstract shall end with an indication of the military security classification of the information in the paragraph, represented as (TS), (S), (C), or (U).

There is no limitation on the length of the abstract. However, the suggested length is from 150 to 225 words.

14. **KEY WORDS:** Key words are technically meaningful terms or short phrases that characterize a report and may be used as index entries for cataloging the report. Key words must be selected so that no security classification is required. Identifiers, such as equipment model designation, trade name, military project code name, geographic location, may be used as key words but will be followed by an indication of technical context. The assignment of links, roles, and weights is optional.